INSIGHTS INTO MARINE BACTERIAL COMMUNITY INTERACTIONS USING NOVEL FITNESS AND CHEMOTAXIS ASSAYS

by

JEREMY ETHAN SCHREIER

(Under the Direction of Mary Ann Moran)

ABSTRACT

Labile organic matter released by phytoplankton in the surface ocean supports diverse communities of heterotrophic bacteria. Interactions between bacteria within the substrate-rich region directly surrounding a phytoplankton known as the phycosphere are largely mediated by metabolites bacteria consume and excrete. This dissertation addresses how bacterial communities assemble and interact in ecological hot-spots such as phycospheres. To untangle the complexity of interactions between marine heterotrophic bacteria, we used novel fitness and chemotaxis assays featuring organic matter either provided by living co-cultured phytoplankton, or as single metabolites previously identified to be components of phytoplankton exometabolomes. In the first and second study, we measured the fitness of genes advantageous to the success of focal bacterium *Ruegeria pomeroyi* when sharing resources in phycospheres generated by the diatom *Thalassiosira pseudonana.* Bacteria were found to compete for phytoplankton metabolites and inorganic nutrients. We found that flexibility of a bacterium to utilize a wide variety of available metabolites not only supports coexistence but allows for plasticity as the landscape of competition changes with varying bacterial membership. In addition to competition, bacteria exchanged metabolites at concentrations sufficient to alleviate auxotrophies. Finally,

phycosphere bacteria were found to alter the physiochemical properties of their local environment through respiration and detoxification of reactive oxygen species. In the third study, we determined the roles of metabolites as signals directing bacterial foraging strategies, and as substrates enabling growth after arrival at an ecological hot-spot. We quantitatively separated the effects that these roles play in community assembly using pairs of bacterial strains competing in a model hotspot environment. We found that a single metabolite can vary in its role as a signal or substrate for a bacterial strain, and that each bacterial strain can respond differently to the same metabolite, underscoring the complex nature of microbial foraging strategies and interactions in simple communities. Collectively, these studies elucidated interactions driving the assembly of bacterial communities within ecological hot-spots in the surface ocean.

INDEX WORDS: Community assembly, Bacterial interactions, Phycosphere, Phytoplankton, Marine bacteria, Mutant fitness assays, Chemotaxis, Ocean hot-spots

INSIGHTS INTO MARINE BACTERIAL COMMUNITY INTERACTIONS USING NOVEL FITNESS AND CHEMOTAXIS ASSAYS

by

JEREMY ETHAN SCHREIER

B.S., Rutgers, 2014

A Dissertation Submitted to the Graduate Faculty of The University of Georgia in Partial Fulfillment of the Requirements for the Degree

DOCTOR OF PHILOSOPHY

ATHENS, GEORGIA

2023

INSIGHTS INTO MARINE BACTERIAL COMMUNITY INTERACTIONS USING NOVEL FITNESS AND CHEMOTAXIS ASSAYS

by

JEREMY ETHAN SCHREIER

Major Professor:	Mary Ann Moran
Committee:	Elizabeth Harvey
	Ford Ballantyne IV
	Adrienne Hoarfrost
	Adrian Burd

Electronic Version Approved:

Ron Walcott
Vice Provost for Graduate Education and Dean of the Graduate School
The University of Georgia
August 2023

DEDICATION

To my parents, for their love, support, and guidance.

ACKNOWLEDGEMENTS

During my time in graduate school, I have been privileged to work with individuals who drive science forward, and more importantly, show kindness towards others, curiosity to the unknown, and give without expectation. Research functions best in an environment where kindness and respect are the norm, and I can truly say this has been my experience in the Moran lab. Mary Ann, your support, guidance, drive, and creativity has pushed me to grow as a scientist, to ask sophisticated questions, and to think deeply. Thank you for all you have taught me. You have set the highest example of what it means to be a truly amazing mentor. I want to thank my mentors: Patricia, for teaching me that a work-life balance can be a healing and healthy practice; Chuck, Damon, Emyln, and Merryl, for giving me the opportunity to design lectures and labs, and for demonstrating the components of great teachers. I'd like to acknowledge those who started as lab mates, colleagues, and fellow grad students, and became climbing and foraging buddies, housemates, and life-long friends. I've been so lucky to be a part of your lives, and you have all helped me grow into the doctor I am today. Finally, I would like to thank my family and partner Demi for your encouragement always.

TABLE OF CONTENTS

Page

CHAPTER 1

LITERATURE REVIEW AND INTRODUCTION

Half of the photosynthesis on Earth is carried out by phytoplankton in the surface ocean, resulting in the fixation of approximately 63 Pg C yr^{-1} (1) from the atmospheric reservoir of CO_2. Of this, an estimated 33 – 39 Pg C yr^{-1} makes its way into the pool of labile organic compounds within hours to days, where it is subsequently processed by heterotrophic marine bacteria (2, 3). The rapid flux of metabolites between phytoplankton and bacteria creates a quantitatively important link in global carbon and nutrient cycles (4, 5). Processes and mechanisms dictating the flux of primary production available to heterotrophic microbes are still being understood (2), stemming from the challenge of studying interactions between surface ocean microorganisms that occur on the microscale, yet influence processes at the global scale.

Heterotrophic marine bacterial communities assemble from regional pools of high biodiversity to interact as local communities (6) centered around hot-spots of labile organic molecules released by living phytoplankton. Ecological interactions between phytoplankton and bacteria are believed to occur within a narrow diffusive boundary layer surrounding a phytoplankton cell coined the phycosphere (7, 8). This microscale physiochemical realm is characterized by elevated metabolite concentrations relative to bulk seawater due to extracellular release by phytoplankton cells. Phytoplankton release extracellular metabolites through both active and passive mechanisms, representing a flux of 15 Pg C yr^{-1} and accounting for approximately half of the labile organic carbon supporting bacterial heterotrophy (2, 9).

Phytoplankton shape their phycosphere-associated bacterial community by the composition of the organic matter they release (10-12). Characterized by a diversity of carbohydrates, amino acids, osmolytes, organic sulfur compounds, nucleobases, signaling compounds, and antimicrobials, this pool of shared organic metabolites attracts and shapes local communities of heterotrophic bacteria (4, 5, 8, 12-15). The reliance of bacteria on phytoplankton-released compounds as a source of carbon, energy, and nutrients leads to interactions such as competition and cooperation between diverse lineages of bacteria sharing the same resource pool (7). Studies of the ecological principles guiding heterotrophic bacteria community assembly processes within the phycosphere are still in their infancy (11, 16-19). Nonetheless, recent investigation of synthetic phycospheres observed that bacterial communities assemble as sets of guilds linked to individual metabolites, suggestive of a resource-based model of community assembly (20). Within this model, interactions between bacteria are driven by preference for specific resources out of the complex milieu present in seawater.

To begin untangling the complexity of interactions between phycosphere bacteria, we used novel fitness and chemotaxis assays in experiments provisioned by organic matter released from living co-cultured phytoplankton, or as specific metabolites previously identified to be components of diatom or dinoflagellate exometabolomes. In chapters 2 and 3 of this dissertation, transposon sequencing provided measures of the fitness of individual mutants in a saturated transposon mutant library of the model marine heterotrophic bacterium *Ruegeria pomeroyi* DSS-3. Transposon sequencing is used in microbiological contexts to characterize the function of unknown genes (21, 22), determine genes essential for bacterial growth (23, 24), and explore metabolic exchanges between organisms (25, 26). Here, this technique provided insights into ecological interactions that occur between heterotrophic bacteria that coexist in the phycosphere.

In chapter 2, we used transposon sequencing to detect interactions occurring among phycosphere bacteria through identification of genes influencing fitness. In a model phycosphere containing diatom *Thalassiosira pseudonana* CCMP1335 as the phytoplankton host, *Rhodobacteraceae* bacterium *Ruegeria pomeroyi* DSS-3 was inoculated in the form of a random transposon mutant pool either alone or sharing the coculture with one or both of two other bacteria, *Vibrio hepatarius* HF70 and *Marivivens donghaensis* HF1. The bacteria selected for this study were abundant members of a coastal microbial community that had been subject to enrichment with diatom metabolites (20). Fitness effects of *R. pomeroyi* single-gene transposon insertion mutants were determined after 8 days of culture in the model system. Mutants with lower growth rates in multibacterial communities were regarded as having disruptions in genes that would have been beneficial in coculture with other species if remaining functional. Those with higher growth rates in multibacterial communities were regarded as having disruptions in genes that would have been costly in the presence of other species if remaining functional.

In chapter 3, we expanded the scope of the mutant fitness assay to provide insights into the benefits and challenges of living in increasingly species-rich communities. We again used the diatom *T. pseudonana* to create an ecologically relevant phycosphere, where substrate supply rate and composition results in a phycosphere environment with microbial densities and organic matter supply rates comparable to natural ocean environments. The diatom model systems were inoculated with up to eight heterotrophic bacteria in a pattern that allowed comparison of more species-rich communities to their simpler component parts. *R. pomeroyi* was present in all communities and inoculated in the form of a transposon mutant library. Fitness of individual mutants were assessed using transposon sequencing, and mutants with fitness significantly altered in coalescent communities relative to the component communities were explored using

the genetic concept of epistasis. This concept quantifies the effect of one gene mutation in the presence of another, asking whether or not phenotype effects are additive (27). Epistasis-like patterns have been observed in ecological communities, for example non-additive effects of increasing substrate diversity on bacterial community composition (28).

In chapter 4, novel chemotaxis assays were performed using the microfluidics device known as the *in situ* chemotaxis assay (ISCA). The ISCA contains wells independently connected to the external environment by a port through which metabolites diffuse out and bacteria swim in (29). The strength of the chemotactic response of bacteria, or chemotactic index, is determined by normalizing the concentration of cells in ISCA wells filled with metabolites to the mean concentration of cells in wells containing only seawater (29). The ISCA has been used in both laboratory and field experiments to characterize the chemotactic strength of marine bacteria to complex medium (29) and to phytoplankton-derived dissolved organic matter (12, 30).

Here, the ISCA enabled understanding of how the ability of bacteria to chemotax towards phytoplankton metabolites (i.e., using the metabolites as a *signal* of a favorable environment) and subsequently consume them (i.e., using the metabolites as a *substrate* to support growth) can influence community assembly. The growth and chemotactic performance of three marine Alphaproteobacteria and four marine Gammaproteobacteria were measured in response to ten representative phytoplankton metabolites spanning chemical classes including amino acids and derivatives, organic acids, and organic sulfur compounds. The bacteria selected for this study were abundant members of a coastal microbial community that had been subject to enrichment with diatom metabolites (20); the metabolites selected for this study had been identified in analyses of marine diatoms (31-33) or dinoflagellates (32). Competition experiments between

pairs of bacteria were performed to understand how chemotaxis and growth on a single metabolite shapes community composition. A null model of chemotaxis and growth (i.e., assuming bacteria respond independently even if other species are present) was generated using empirically measured parameters of chemotactic index and cell growth determined in monoculture. Any significant deviations from the null model in experimental tests of paired strains assembling into a two-member community suggested interactions between bacteria, such as competition or antagonism, can develop rapidly in the early phases of community assembly.

Phytoplankton-derived metabolites account for only a small fraction of Earth's marine dissolved organic carbon reservoir at any single point in time (34, 35), yet their short half-lives in surface seawater drives an enormous annual carbon flux through oceanic and atmospheric reservoirs (2, 3, 9). Our poor knowledge of interactions between microbes underlying processing of organic matter that drives this metabolite carbon flux suggests that more and better data are needed. Indeed, understanding climate–carbon feedback loops mediated by bacterial processing of microbially-derived metabolites depends on knowledge of this largely unconstrained metabolite-bacterial link (36). With ongoing advances in the chemical, biomolecular, and data sciences, more details of this network are emerging. Here, we contribute to this effort through an exploration of factors that control bacterial community assembly around marine phytoplankton, and rapidly process labile metabolites they release.

References

1. M. J. Behrenfeld, E. Boss, D. A. Siegel, D. M. Shea, Carbon-based ocean productivity and phytoplankton physiology from space. *Global Biogeochemical Cycles* **19** (2005).

2. M. A. Moran *et al.*, The Ocean's labile DOC supply chain. *Limnology and Oceanography* **67**, 1007-1021 (2022).
3. J. J. Cole, S. Findlay, M. L. Pace, Bacterial production in fresh and saltwater ecosystems: a cross-system overview. *Marine Ecology Progress Series* **43**, 1-10 (1988).
4. F. Azam, F. Malfatti, Microbial structuring of marine ecosystems. *Nature Reviews Microbiology* **5**, 782-791 (2007).
5. M. A. Moran *et al.*, Deciphering ocean carbon in a changing world. *Proceedings of the National Academy of Sciences* **113**, 3143-3151 (2016).
6. M. A. Leibold *et al.*, The metacommunity concept: a framework for multi-scale community ecology. *Ecology Letters* **7**, 601-613 (2004).
7. J. R. Seymour, S. A. Amin, J.-B. Raina, R. Stocker, Zooming in on the phycosphere: the ecological interface for phytoplankton–bacteria relationships. *Nature Microbiology* **2**, 1-12 (2017).
8. W. Bell, R. Mitchell, Chemotactic and growth responses of marine bacteria to algal extracellular products. *The Biological Bulletin* **143**, 265-277 (1972).
9. C. A. Carlson, D. A. Hansell, DOM sources, sinks, reactivity, and budgets. *Biogeochemistry of Marine Dissolved Organic Matter*, 65-126 (2015).
10. G. Behringer *et al.*, Bacterial communities of diatoms display strong conservation across strains and time. *Frontiers in Microbiology* **9**, 659 (2018).
11. J. Mönnich *et al.*, Niche-based assembly of bacterial consortia on the diatom *Thalassiosira rotula* is stable and reproducible. *The ISME Journal* **14**, 1614-1625 (2020).
12. J.-B. Raina *et al.*, Chemotaxis shapes the microscale organization of the ocean's microbiome. *Nature* **605**, 132-138 (2022).

13. S. A. Amin, M. S. Parker, E. V. Armbrust, Interactions between diatoms and bacteria. *Microbiology and Molecular Biology Reviews* **76**, 667-684 (2012).
14. M. Landa *et al.*, Sulfur metabolites that facilitate oceanic phytoplankton–bacteria carbon flux. *The ISME Journal* **13**, 2536-2550 (2019).
15. A. A. Shibl *et al.*, Diatom modulation of select bacteria through use of two unique secondary metabolites. *Proceedings of the National Academy of Sciences* **117**, 27445-27455 (2020).
16. J. E. Schreier, C. B. Smith, T. R. Ioerger, M. A. Moran, A mutant fitness assay identifies bacterial interactions in a model ocean hot spot. *Proceedings of the National Academy of Sciences* **120**, e2217200120 (2023).
17. J. A. Kimbrel *et al.*, Host selection and stochastic effects influence bacterial community assembly on the microalgal phycosphere. *Algal Research* **40**, 101489 (2019).
18. T. J. Samo *et al.*, Attachment between heterotrophic bacteria and microalgae influences symbiotic microscale interactions. *Environmental Microbiology* **20**, 4385-4400 (2018).
19. M. M. Barreto Filho, M. Walker, M. P. Ashworth, J. J. Morris, Structure and long-term stability of the microbiome in diverse diatom cultures. *Microbiology Spectrum* **9**, e00269-00221 (2021).
20. H. Fu, M. Uchimiya, J. Gore, M. A. Moran, Ecological drivers of bacterial community assembly in synthetic phycospheres. *Proceedings of the National Academy of Sciences* **117**, 3656-3662 (2020).
21. W. F. Schroer *et al.*, Functional annotation and importance of marine bacterial transporters of plankton exometabolites. *ISME communications* **3**, 37 (2023).

22. M. N. Price *et al.*, Mutant phenotypes for thousands of bacterial genes of unknown function. *Nature* **557**, 503-509 (2018).

23. M. A. DeJesus *et al.*, Comprehensive essentiality analysis of the *Mycobacterium tuberculosis* genome via saturating transposon mutagenesis. *mBio* **8**, e02133-02116 (2017).

24. B. E. Poulsen *et al.*, Defining the core essential genome of *Pseudomonas aeruginosa. Proceedings of the National Academy of Sciences* **116**, 10072-10080 (2019).

25. B. LaSarre, A. M. Deutschbauer, C. E. Love, J. B. McKinlay, Covert cross-feeding revealed by genome-wide analysis of fitness determinants in a synthetic bacterial mutualism. *Applied and Environmental Microbiology* **86**, e00543-00520 (2020).

26. H. E. Knights, B. Jorrin, T. L. Haskett, P. S. Poole, Deciphering bacterial mechanisms of root colonization. *Environmental Microbiology Reports* **13**, 428-444 (2021).

27. D. Segre, A. DeLuna, G. M. Church, R. Kishony, Modular epistasis in yeast metabolism. *Nature Genetics* **37**, 77-83 (2005).

28. A. R. Pacheco, M. L. Osborne, D. Segrè, Non-additive microbial community responses to environmental complexity. *Nature Communications* **12**, 2365 (2021).

29. B. S. Lambert *et al.*, A microfluidics-based in situ chemotaxis assay to study the behaviour of aquatic microbial communities. *Nature Microbiology* **2**, 1344-1349 (2017).

30. S. Hallstrøm *et al.*, Chemotaxis may assist marine heterotrophic bacterial diazotrophs to find microzones suitable for N2 fixation in the pelagic ocean. *The ISME Journal* **16**, 2525-2534 (2022).

31. F. X. Ferrer-González *et al.*, Resource partitioning of phytoplankton metabolites that support bacterial heterotrophy. *The ISME Journal* **15**, 762-773 (2021).

32. M. Landa, A. S. Burns, S. J. Roth, M. A. Moran, Bacterial transcriptome remodeling during sequential co-culture with a marine dinoflagellate and diatom. *The ISME Journal* **11**, 2677-2690 (2017).
33. M. Olofsson *et al.*, Growth-stage-related shifts in diatom endometabolome composition set the stage for bacterial heterotrophy. *ISME Communications* **2**, 28 (2022).
34. M. A. Moran *et al.*, Microbial metabolites in the marine carbon cycle. *Nature Microbiology* **7**, 508-523 (2022).
35. D. A. Hansell, Recalcitrant dissolved organic carbon fractions. *Annual Review of Marine Science* **5**, 421-445 (2013).
36. R. Cavicchioli *et al.*, Scientists' warning to humanity: microorganisms and climate change. *Nature Reviews Microbiology* **17**, 569-586 (2019).

CHAPTER 2

A MUTANT FITNESS ASSAY IDENTIFIES BACTERIAL INTERACTIONS IN A MODEL OCEAN HOT-SPOT [1]

[1] Schreier, JE, Smith, CB, Ioerger, TR, Moran, MA. 2023. *Proceedings of the National Academy of Sciences.* e2217200120. Reprinted here with permission of the publisher.

Abstract

Bacteria that assemble in phycospheres surrounding living phytoplankton cells metabolize a substantial proportion of ocean primary productivity. Yet the type and extent of interactions occurring among species that colonize these micron-scale 'hot-spot' environments are challenging to study. We identified genes that mediate bacterial interactions in phycosphere communities by culturing a transposon mutant library of copiotrophic bacterium *Ruegeria pomeroyi* DSS-3 with the diatom *Thalassiosira pseudonana* CCMP1335 as the sole source of organic matter in the presence or absence of other heterotrophic bacterial species. The function of genes having significant effects on *R. pomeroyi* fitness indicated explicit cell-cell interactions initiated in the multi-bacterial phycospheres. We found that *R. pomeroyi* simultaneously competed for shared substrates while increasing reliance on substrates that did not support the other species' growth. Fitness outcomes also indicated that the bacterium competed for nitrogen in the forms of ammonium and amino acids; obtained purines, pyrimidines, and cofactors via cross-feeding; both initiated and defended antagonistic interactions; and sensed an environment with altered oxygen and superoxide levels. The large genomes characteristic of copiotrophic marine bacteria are hypothesized to enable responses to dynamic ecological challenges occurring at the scale of microns. Here, we discover 209 non-essential genes implicated in the management of fitness costs and benefits of membership in a globally significant bacterial community.

Significance Statement

Ecological interactions that occur between phycosphere-associated bacteria at the micron scale have the potential to influence a major fraction of annual carbon flux at the global scale. Despite the importance of microbial carbon flow, studying the ecology of these

microenvironments remains challenging. Fitness measures of bacterial transposon mutants identified four primary classes of interactions among members of a model bacterial community provisioned by a co-growing diatom. This work advances our understanding of ecological associations in multi-species microbial environments.

Introduction

Of the ~63 Pg of atmospheric carbon converted into surface ocean organic matter by marine phytoplankton each year (1), approximately 20 Pg are released as metabolites from living cells (2, 3). These labile components of the dissolved organic carbon (DOC) pool are taken up by heterotrophic marine bacteria, initiating a process that results in a large and rapid flux between phytoplankton productivity and global carbon reservoirs (4, 5). The mechanisms governing this flux of dissolved primary production through heterotrophic microbes are still poorly understood, stemming from challenges of studying the ecology of micron-scale environments.

Organic compounds released by living phytoplankton accumulate in a region around the cell referred to as the phycosphere (6), one type of microbial hot-spot (4) where bacteria are concentrated to take advantage of higher carbon and nutrient availability (7). Phycosphere organic matter is diverse in its composition, characterized by compound classes that include carbohydrates, amino acids, osmolytes, organic sulfur, nucleobases, and signaling molecules, among others (8-10). Consequently, a diversity of bacteria able to benefit from phytoplankton metabolites colonize phycospheres, typically including members of the Alphaproteobacteria (frequently the *Rhodobacteraceae*), Gammaproteobacteria, and Bacteroidetes (11-13). The bacterial species colonizing phycospheres most likely compete for metabolites (14-16), inorganic nutrients, essential metals, and other resources (17, 18). Such competitive interactions have been

proposed to explain the dominance in phycosphere communities of copiotrophic bacteria, those having large, well-regulated genomes and capacity for rapid growth when conditions are favorable (19).

While ecological associations among phycosphere bacteria have the potential to influence rates and efficiencies of carbon flux at the global scale, the interactions themselves occur at the micron scale (20). Here we detect interactions occurring among phycosphere bacteria through the identification of genes influencing fitness. In a model phycosphere containing diatom *Thalassiosira pseudonana* CCMP1335 as the phytoplankton host, *Rhodobacteraceae* bacterium *Ruegeria pomeroyi* DSS-3 was inoculated in the form of a random transposon mutant pool either alone or sharing the co-culture with one or both of two other bacteria, *Vibrio hepatarius* HF70 and *Marivivens donghaensis* HF1. The bacteria selected for this study were the three most abundant members of a coastal community enriched on diatom metabolites (14, 21). In the case of *R. pomeroyi*, the bacterium had also been isolated previously from the same coastal location where the enrichment culture inoculum was obtained (14, 22) and is amenable to genetic manipulation (23, 24). In this study, *R. pomeroyi* mutant populations recovered from the model system after 8 d were analyzed by Transposon Sequencing (TnSeq) (25-27) to determine fitness effects of each single-gene knockout in the presence and absence of other bacteria. Those with lower growth rates in multi-bacterial communities were regarded as having disruptions in genes that would have been beneficial in co-culture with other species if remaining functional. Those with higher growth rates in multi-bacterial communities were regarded as having disruptions in genes that would have been unnecessary or costly in the presence of other species if remaining functional (Fig. 2.1a). Differential growth rates among the mutant pool (~ 60,000 distinct

mutants) provided insights into potential mechanisms of interspecies interactions in a model marine hot-spot of biogeochemical importance.

Results and discussion

We established four model bacterial communities reliant on the extracellular release of photosynthate continually generated by co-cultured diatom *T. pseudonana* in a medium replete with phosphate, nitrate, vitamins B_{12}, B_7, B_1, and trace metals. The *R. pomeroyi* transposon mutant pool was inoculated into the diatom cultures as the sole bacterial species (treatment referred to as *Rp*), or along with *V. hepatarius* (*Rp+V),* or *M. donghaensis* (*Rp+M*), or both (*Rp+V+M*) (Fig. 2.1b; Fig S2.1). The same number of *R. pomeroyi* cells was inoculated into all model communities to ensure equal mutant diversity, and therefore the total bacterial density in multi-bacterial communities was initially 1.4- to 3.7-fold greater than in the single-bacterium treatment. This difference, however, was not reflected in the mature cultures, likely representing the carrying capacity set by substrate release from the living diatom (Fig. 2.1b). The *R. pomeroyi* mutant pools experienced an average of 5.5 generations during the 8-d experiment as determined by colony forming units (CFUs). CFUs of *V. hepatarius* declined by ~2 – 4 orders of magnitude, with a more pronounced decline when both *R. pomeroyi* and *M. donghaensis* were present (*Rp+V+M*). *M. donghaensis* increased 2-fold and then gradually declined (Fig. 2.1b). Diatom growth (Fig. 2.1b) and photosynthetic physiology (F_v/F_m; Fig. S2.2) were indistinguishable across treatments.

Mutant fitness overview. Fitness was calculated for the 3,748 *R. pomeroyi* genes having at least one curated transposon insertion site (defined as insertions within the central 90% of a coding region); these represented 86% of the 4,293 total coding regions. To calculate fitness (*W*),

a mutant's change in abundance over 8 d was compared to that of the combined mutant pool (26). Thus, a mutant with a fitness of 1 had a growth rate equivalent to the combined mutant pool in the same treatment, whereas a mutant with a fitness of 0.5 was growing at half the average rate of all mutants. Although fitness of *R. pomeroyi* mutants was generally correlated between the single- and multi-bacteria cultures (Fig. 2.2a), those with significant differences revealed the specific genes for which loss of function affected *R. pomeroyi*'s ability to interact with the bacteria sharing the phycosphere. The magnitude of the treatment effect was represented by $\log_2$ fold-change of *R. pomeroyi* mutant fitness in multi-bacterial values relative to single-bacterium treatments (Fig. 2.2b).

When mutants having significant differences in fitness were analyzed based on function of the deleted gene and direction of fitness change, four phenomenological modes of ecological interactions emerged from the data: (i) vying for resources via competition (13% of significant mutants), (ii) obtaining resources via cross-feeding (11%), (iii) invoking chemically-mediated interactions via secondary metabolites (4%), and (iv) adapting to altered environmental conditions (10%) (Fig. 3a)**.** The remaining mutants had genes disrupted in central metabolism (12%), regulation (6%), mixed functions not well annotated or not clearly linked to bacterial interactions (25%), and hypothetical proteins (19%) (Dataset S2.1).

Competition. Twenty-six mutants with significant fitness differences had non-functional genes annotated for resource acquisition, encompassing several different arenas of bacterial competition in the *T. pseudonana* phycosphere. One of these was competition for substrates, as evidenced by fitness differences in 24 mutants disrupted in the transport or catabolism of organic molecules (Table 2.1). Most substrate mutants had lower fitness in multi-bacterial treatments (plotting below the 1:1 line in Fig. 2.2a); they included mutants for transport of dicarboxylic

acid-like molecules, and for catabolism of glycolate, dimethylsulfoniopropionate (DMSP), carnitine, taurine, threonine, and methylamine. The remaining five substrate mutants instead had higher fitness in multi-bacterial treatments (plotting above the 1:1 line in Fig. 2.2a); these included mutants for transport of sugars and a nitrogen rich amino acid (glutamine, glutamate, aspartate, and/or asparagine).

We considered a possible explanation for these two opposite fitness outcomes, hypothesizing that when substrates of disrupted genes are uncontested resources, available only to *R. pomeroyi*, they will be of increased importance for fitness in multi-bacterial communities and lead to lower fitness relative to the combined mutant pool. On the other hand, when substrates are communal resources and *R. pomeroyi* is less successful in attaining them when other bacteria are present, they will be of decreased importance to fitness in multi-bacterial communities and lead to higher relative fitness. Predictions following from this hypothesis are that in the first case, the substrates of the transporter/catabolic genes support growth of *R. pomeroyi* only, while in the second, the substrates support growth of *R. pomeroyi* plus at least one other species.

This hypothesis was tested by inoculating wild-type *R. pomeroyi*, *V. hepatarius*, and *M. donghaensis* individually into media containing one of six substrates selected based on well-annotated genes with known target molecules in the *R. pomeroyi* genome (Table 2.1). All organic compounds supported growth of *R. pomeroyi* (Fig. 2.3b). Glycolate and DMSP, whose catabolism mutants had lower fitness in multi-bacterial communities, indeed supported growth only of *R. pomeroyi*, consistent with roles as uncontested resources. However, glutamine, asparagine (Fig. 2.3c), aspartate, and glutamate (Fig. S2.3), whose transporter mutants had increased fitness in multi-bacterial communities, supported growth of *R. pomeroyi* and at least

one other species, consistent with roles as communal resources. This bacterium's fitness in the phycosphere thus appeared affected by its abilities to both compete for substrates that are shared, and have access to those that are less commonplace. *R. pomeroyi* devotes 12% of its genome to transporters, a high proportion compared to other Alphaproteobacteria (28); among these transporters are ~126 annotated for uptake of organic compounds.

A second group of mutants revealed a contest for phycosphere nutrients. First, *R. pomeroyi glnD* mutants had lower fitness phenotypes when in multi-bacterial communities. Bacteria with a disrupted *glnD* receive an artificial signal of nitrogen sufficiency (29), causing the downregulation of high-affinity ammonium assimilation; the fitness decreases were therefore interpreted as evidence for stronger ammonium limitation in multi-bacterial communities. Growth of *R. pomeroyi*'s *glnD* mutant was especially affected when *V. hepatarius* was a member of the community (>3-fold greater fitness change compared to *Rp+M*) (Table 2.1; Dataset S2.1). Genomic analysis revealed that all three strains harbor genes to assimilate ammonium (which was not a component of the medium, and thus was available in the cultures only via regeneration). However, assimilation of nitrate (provided in excess in the culture medium) was possible only for *M. donghaensis* (Table S2.1), decreasing its reliance on ammonium. These nitrogen uptake phenotype predictions were experimentally confirmed in growth assays with either ammonium or nitrate as the nitrogen source (Fig. 2.3d). A second *R. pomeroyi* nitrogen mutant was disrupted in an allophanate hydrolase gene, making it unable to release ammonium from urea. The decreased fitness of this mutant is consistent with stronger nitrogen limitation in the multi-bacterial communities. Nitrate was used as the nitrogen source for these model systems because it fuels most natural diatom blooms (30) and differences in genetic capabilities for nitrogen acquisition are known to affect marine bacterial success (31, 32).

Competition for phosphorus was indicated by two mutants in phosphate acquisition and utilization. Despite the phosphate-replete medium, fitness decrease of a phosphonate utilization mutant (*phnM*) suggested an increased reliance on dissolved organic phosphate. Genomic analysis indicated that *R. pomeroyi* is the only bacterium in the model phycosphere communities with a broad-specificity C-P lyase, suggesting another niche dimension that could decrease direct competition (33) (Table S2.1). Fitness decreases in multispecies communities were observed for mutants of polyphosphate kinase (*ppk*) which are unable to utilize stored polyphosphate, an energetically economical source of phosphorous for ATP (34). Considering the total suite of 26 competition mutants, managing options for carbon, nitrogen, and phosphorous procurement was key to the competitive success of phycosphere bacteria, most likely outweighing the associated energetic costs of regulation (4, 20, 35).

Cross-feeding. Twenty-four mutants with significant fitness differences had non-functional genes in anabolic pathways (Table 2.2). All had higher fitness in multi-bacterial treatments (above the 1:1 line in Fig. 2.2a) with an average increase of 2.8-fold over the single-bacterial treatment (Dataset S2.1). This category included mutants with disruptions in the biosynthesis of purines (four genes), pyrimidines (two genes), essential amino acids (14 genes), vitamins B_5 and B_{12} (two genes), and molybdopterin (two genes) (Table 2.2). The latter two categories represent metabolic cofactors that are energetically expensive to synthesize yet known to be released exogenously by some members of microbial communities, referred to as ‘public goods’ (36-38). Mutant rescue could have resulted from metabolite export from the other species, as reported previously for a marine *Vibrio* species (39), or from release by stressed or dying cells (40, 41) during *V. hepatarius* or *M. donghaensis* cell density decreases (Fig. 2.1b). In either case, fitness increases indicated resources release at levels sufficient to rescue auxotrophs.

This hypothesis of cross-feeding was tested by inoculating *R. pomeroyi* mutants disrupted in purine biosynthesis gene (*purF, purN*) into spent medium from all three species. Medium from *V. hepatarius* cultures rescued growth of the purine mutants, while medium from *M. donghaensis* and *R. pomeroyi* cultures did not, consistent with the interpretation of cross-feeding dominated by metabolites from *Vibrio* (Table 2.2; Fig. 2.3e). Nucleotide cross-feeding among bacterial species has been found previously; for example, *Escherichia coli* purine auxotrophs were recused when co-cultured with *Rhodopseudomonas palustris* (42) and dissolved free nucleotides have been documented in natural seawater and shown to be readily assimilated by bacterial communities (43). Metabolite exchange between co-isolated strains (44) and predictions from genome-scale metabolic models (45-47) suggest that cross-feeding is a common feature of microbial communities. Here, fitness outcomes revealed metabolite exchange between phycosphere bacteria that at a minimum includes amino acids, nucleobases, and co-factors.

Chemically mediated interactions. Fitness changes in mutants that were disrupted in the synthesis or efflux of secondary metabolites pointed to potential bacterial interactions via ecological signaling molecules (5). The nine *R. pomeroyi* mutants in this category had disruptions in secretion and efflux systems, and in the synthesis of exogenous signaling compounds (Table 2.3), and these experienced either increases or decreases in fitness. For example, increased fitness of a type I secretion system mutant suggested that *R. pomeroyi* benefitted from avoiding the cost of toxin production or export, potentially because the excreted antimicrobial was ineffective against *V. hepatarius* and *M. donghaensis* or the other populations of *R. pomeroyi* mutants synthesized the toxin and provided protection. Decreased fitness of a type II secretion system (Table 2.3) suggested that *R. pomeroyi* was disadvantaged if unable to export accumulated toxins. Observations that the decline in *V. hepatarius* and *M. donghaensis*

populations in the multi-bacterial communities (Fig. 2.1b) did not occur when the bacteria were grown in single-species culture with the diatom (Fig. S2.2), support the hypothesized antagonism via antimicrobials. Further, agar plate assays demonstrated that *V. hepatarius* has the potential to inhibit growth of *R. pomeroyi* (Fig. S2.4) consistent with antimicrobial activity being a component of phycosphere ecology.

Altered environment. Mutants in this category had disruptions in genes that respond, directly or indirectly, to environmental conditions external to the cell that are hypothesized to be changed by the presence of other bacteria; these experienced either increases or decreases in fitness. Mutations in genes synthesizing the aa3-type cytochrome oxidase of the aerobic respiratory electron transport chain (four genes; Table 2.4) and nitric oxide reductase resulted in higher fitness, while those encoding alternative cytochromes such as c-554, P450 and the nitrite reductase cd1 resulted in lower fitness (three genes). Collectively, these suggest intensified daily dynamics in oxygen availability in the multi-species phycospheres to the point where bacterial fitness is impacted. Because our experimental systems were established with cell density and metabolite release rates comparable to those in surface seawater, these results should be relevant for natural phycospheres. Ephemeral oxygen depletion has been reported for marine particles such as microbial aggregates and fecal pellets (48), including photosynthetically active microenvironments (49, 50). Indeed, a flexible respiratory system to adjust to dynamic oxygen fluctuations has been proposed as a key trait for bacteria associating with marine phytoplankton (19, 51, 52), with which fitness outcomes of *R. pomeroyi* mutants concur.

Higher fitness of mutants unable to synthesize superoxide dismutase (*sodB*) pointed to a reduced need to protect against this reactive oxygen species when sharing the phycosphere (Table 2.4). Superoxide is involved in cellular stress, signaling, and redox cycling of metals (53).

While both *T. pseudonana* (54) and *R. pomeroyi* (55) release superoxide extracellularly, net production by *T. pseudonana* is three orders of magnitude greater than *R. pomeroyi* (54, 55) and other marine bacteria (56), and phytoplankton-produced superoxide can reach levels inhibitory to bacteria (57). The *sodB* mutant rescue is thus interpreted here as an indication of "public goods" provided by bacteria that scavenge superoxide radicals in the mixed-species communities.

In what may be a general response to the challenges of multi-species environments, *R. pomeroyi* mutants with disrupted rRNA genes, ribosomal protein genes, and regulatory genes for transcription and translation had higher fitness in multi-bacterial communities (seven genes). Accordingly, we hypothesize that maximally functioning protein translation machinery is less beneficial when other bacteria share the phycosphere. Bacteria respond to changes in external resource availability by altering their proteome partitioning (58, 59), and under conditions in which nutrient or substrate availability limits growth, decreased need for ribosome-related proteins has been observed (60). Consistent with this, *R. pomeroyi* had fewer generations in multi-bacterial communities (e.g., 4.4 in the *Rp+V+M* treatment compared to 6.4 in the *Rp* treatment; Table S2.2). Mutants in *pntAB*, which mediates conversion of NADH to NADPH (61) (Table 2.4), also exhibited higher fitness in multi-bacterial communities, consistent with presumed lower demand for this anabolic energy molecule.

Similar to observations of mycobacteria enduring hypoxia and slowed growth under carbon starvation, decreased fitness of two *R. pomeroyi* carbon monoxide (CO) dehydrogenase mutants suggested a potential reliance on alternative electron donors to remain energized (63). CO oxidation does not provide enough energy to support growth or alter intracellular metabolite pools in *R. pomeroyi* (63). Nonetheless, increased synthesis of CO enzymes has been observed under carbon starvation (64) and would allow the bacterium to exploit CO for cellular

maintenance (65). Slowed growth of *R. pomeroyi* as other bacterial species assemble into the phycosphere may increase the fitness benefits of a functioning CO oxidation pathway.

Conclusions

Direct fitness measures of single-gene mutants in a model ocean hot-spot revealed how growth and activity of a focal bacterium were affected by community members. Apportionment of the available labile organic matter was governed by two factors: the bacterium's ability to compete for communal substrates, and its capacity to utilize those less commonplace. The latter has been proposed to lay the groundwork for evolution of mutualistic relationships between marine phytoplankton and bacterial lineages (35, 66). Cross-feeding in bacterial communities is controversial regarding its extent and ecological relevance (44, 67). Here, *R. pomeroyi* fitness benefitted from ~13 central metabolites (amino acids, purines, pyrimidines, and co-factors) available in the multispecies communities in amounts sufficient to rescue auxotrophs. The general importance of metabolites produced by species sharing a phycosphere, regardless of the mechanism by which they are released, was underscored by 1.7-fold higher fitness gains among mutants disrupted in anabolic genes relative to those disrupted in catabolic genes or transporters (Fig. S2.5). Nonetheless, the *R. pomeroyi* mutant pool achieved 30% fewer generations when other species shared the phycosphere, indicating an overall growth cost to life in a community.

Identification of authentic bacteria-bacteria interactions is challenging when experimental systems have substrate concentrations and bacterial growth rates considerably higher than those in natural ecosystems. By provisioning our model systems with exometabolites from co-growing diatom cells, we achieved an environment with high fidelity to a phycosphere hot-spot in terms

of substrate composition, substrate supply rate, microbial density, and spatial organization. In support of this, diatom and bacterial cell abundances in the model systems were consistent with those in natural diatom blooms (15, 68, 69), and *R. pomeroyi* growth rate in the model systems (0.95 d^{-1} for the first 4 d of the study and 0.31 d^{-1} for the 8 d average) fell within the range reported for Rhodobacteraceae in natural marine systems (70). The importance of interactions among bacteria that share ocean hot-spots is underscored by the >200 *R. pomeroyi* genes with measurable effects in multispecies communities. Among the changes predicted to occur in the surface ocean environment during the coming decades, decreased nutrient supply (71-73), may intensify competition for phycosphere nitrogen and phosphorus, and altered phytoplankton community composition may affect organic carbon available to bacteria (74, 75, 76). Such changes to the arena of bacterial competition have the potential to impact carbon and nutrient biogeochemistry in the surface ocean.

Methods

Transposon library generation. Competent *Ruegeria pomeroyi* DSS-3 cells were prepared according to Sebastián & Ammerman (2011). Briefly, cells were grown at 20°C in YTSS (4 g/L yeast, 2.5g/L tryptone, 20 g/L sea salts) with the addition of 40 mM sucrose to 0.4 OD_{600}. Cells were washed three times with ice-cold 10% glycerol, resuspended 1:1000 of the original culture volume in 10% glycerol, and divided into 100 µl aliquots for electroporation. A 1 µl aliquot of Ez-Tn5 <R6Kyori/KAN-2>Tn Transposome (Lucigen) was added to 100 µl of competent cells just prior to electroporation. Cells were electro-transformed in a 2 mm electrode gap cuvette using a Bio-Rad GenePulser II (Hercules, CA) set to 1.8 kV, 25 mF, and 200 V, and then immediately recovered in 1 ml of YTSS at 30°C for 2 h. Recovered cells were plated on YTSS+25 µg ml^{-1} kanamycin (KAN) agar and incubated at 30°C for up to 72 h. Mutant colonies

were counted and washed from plates using Marine Basal Medium (77), and added to glycerol at a final concentration of 20% (Fig S2.1). Aliquots were stored at -80°C.

Model phycospheres. Ruegeria pomeroyi DSS-3, *Vibrio hepatarius* HF70 and *Marivivens donghaensis* HF1 were selected for this study because they were the three most abundant members of a phycosphere enrichment culture; further, they had 16S rRNA sequences with >95% identity to bacteria known to associate with marine phytoplankton (14, 21) and survive in co-culture with phytoplankton. Prior to experimentation, *V. hepatarius* and *M. donghaensis* were inoculated into YTSS medium from isolated colonies and grown overnight at 30°C and 200 RPM. A concentrated *R. pomeroyi* mutant library cryostock was thawed on ice and inoculated at ~0.2 OD_{600} into YTSS+KAN medium and grown for ~6 h, resulting in two doubling periods. At the same time, *V. hepatarius* and *M. donghaensis* were sub-cultured and grown to exponential phase (0.4 – 0.6 OD_{600}). Cells were pelleted at 4000 x g, washed three times, and resuspended to ~$5x10^7$ cells ml^{-1} in 0.2 µm filter-sterilized artificial seawater (ASW). Four aliquots of washed transposon mutants were stored at -80°C; these were used to determine the mutant library composition prior to selection.

Thalassiosira pseudonana CCMP 1335 (National Center for Marine Algae and Microbiota) was maintained in exponential growth by diluting into fresh L1+Si ASW (78) every four days to a starting density of ~10^4 cells ml^{-1} for three consecutive transfers at 20°C with a 16h:8h light:dark cycle prior to experimentation. Diatom cultures were inoculated into 24 x 300 cm^3 vented polystyrene tissue culture flasks with 500 ml L1+Si ASW, and seeded with bacteria at ~10^5 cells ml^{-1} each to establish four treatments: *R. pomeroyi* single-bacterial culture (*Rp*), *R. pomeroyi* plus *V. hepatarius* (*Rp+V*), *R. pomeroyi* plus *M. donghaensis* (*Rp+M*), and *R. pomeroyi* plus *V. hepatarius* and *M. donghaensis* (*Rp+V+M*) (n=4) (Fig. S2.1).

Cell enumeration. Bacterial abundance was determined for each species based on visually distinct colony forming units (CFUs) on YTSS and YTSS+KAN plates on days 0, 4, and 8. Diatom abundance and combined bacterial abundance was determined by flow cytometry on a Beckman Coulter CyAn ADP (Beckman Coulter, Hialeah, Florida) on days 0, 2, 4, 6, 8. Samples were fixed with a final concentration of 1% paraformaldehyde in the dark at room temperature for 15 min before storing at -80°C. Samples were diluted in 0.2 µm filter-sterilized ASW, stained with 1X SYBR Green I (Thermo), and AccuCount Fluorescent particles were added as a standard. Total bacteria and phytoplankton cells were enumerated with side scatter and green and red fluorescence by a 488 nm laser applying a FL-530/30 bandpass filter and a FL4-680/30 bandpass filter. Data were analyzed in FlowJo v10.2 (Ashland, OR: Becton, Dickinson and Company; 2019) and corrected based on fluorescent particle counts as per the manufacturer's instructions.

Bacterial inorganic nitrogen utilization profiles and substrate tests. Wild-type *R. pomeroyi, V. hepatarius*, and *M. donghaensis* were inoculated into YTSS medium and grown overnight as above. Cells were washed and transferred as monocultures supplemented with glucose (5 mM) and either ammonium (1 mM) or nitrate (1 mM), or with no nitrogen source, and grown in a 24-well plate in a Synergy H1 microplate reader (BioTek) at 30°C with constant shaking. OD_{600} was measured every 15 min until stationary phase at approximately 60 h. Substrate tests were performed similarly, using Marine Basal Medium supplemented with ammonium and substrates glycolate, DMSP, glutamate, glutamine, asparagine, or aspartate at 12 mM carbon for 20 h.

Validation of purine crossfeeding. Washed cells from an overnight culture of WT *R. pomeroyi, V. hepatarius*, and *M. donghaensis* were washed, transferred to L1 ASW

supplemented with glucose (1 mM) and ammonium (0.5 mM), and grown to stationary phase. Cultures were centrifuged (4000 x g, 5 min), and supernatant was filtered (0.2 µm) and stored at 4°C as cell-free spent medium. *R. pomeroyi* mutants for *de novo* purine synthesis (Δ*purF,* Δ*purN*) generated through transposon mutagenesis (courtesy of Dr. Christopher Reisch, University of Florida) were inoculated into YTSS and grown overnight. Cells were washed and transferred to L1 ASW supplemented with glucose (1 mM) and ammonium (0.5 mM) and six treatments were established with addition of an equal volume of cell-free spent medium of *V. hepatarius, M. donghaensis,* or wild-type *R. pomeroyi* pre-grown in L1 supplemented with glucose (1 mM), an equal volume of ASW, an equal volume of ASW containing dNTPs (0.1 mM), or an equal volume of ASW containing adenosine (0.1 mM). Cells were grown in a 96-well plate in a Synergy H1 microplate reader (BioTek) at 30°C with constant shaking, and OD_{600} was measured every 30 min for 40 h.

*DNA extraction, sequencing, and bioinformatic analysis***.** After 8 d, DNA was extracted from each model phycosphere and from aliquots of the initial mutant library inoculum (n=4) using the ZymoBIOMICS DNA Miniprep Kit (D4300) according to manufacturer's instructions. Library preparation and sequencing was performed at the Georgia Genomics and Bioinformatics Core facility using custom PCR oligomers consisting of a region complementary to the transposon sequence with a 6 bp random heterogeneity spacer (5'ATGATACGGCGACCACCGAGATCTACACTCTTTCCCTACACGACGCTCTTCCGATCTNNNNNNGACCTGCAGGCATGCAAGCTTCAG). Transposon specific sequencing was run on an Illumina NextSeq using a single-end 75 bp high output flow cell.

Amplified sequences were trimmed and mapped using TPP as part of TRANSIT v3.0.2 (79). In short, transposon genome junctions were identified by the sequence

AGATGTGTATAAGAGACAG in the first 60 bp and trimmed to ~22 bp beginning at the site of transposon insertion. Trimmed reads were mapped to the *R. pomeroyi* DSS-3 genome (GenBank accession NC_003911) with BWA (80) in 'aln' mode allowing for one mismatch, and a wig formatted file was generated indicating each site of insertion and the number of reads that mapped to it (https://doi.org/10.5281/zenodo.7489904). Wig files were combined in TRANSIT using the combine wig tool. Genome sites with no insertional mutants were excluded. The transposon mutant library was composed of 83,647 unique mutants, curated to 64,365 that fell within the central 90% of a protein coding region, resulting in an average of 15 mutant strains per gene (one mutation every 50 base pairs). Reads were normalized by scaling the read count in each sample to the grand mean across all samples (Dataset S2.2).

Fitness analysis. Relative mutant fitness (*W*) was determined following van Opijnen (2009) with some alterations. Reads mapping to each unique transposon insertion were summed within a gene, averaging 423 reads per gene. Relative fitness (*W*) of mutants was calculated using the equation:

$$W = \frac{\ln\left[N(t2) * \frac{d}{N(t1)} + 1\right]}{\ln\left[(1 - N(t2)) * \frac{d}{\left(1 - N(t1)\right)} + 1\right]}$$

Where N(t1) and N(t2) are the frequencies of a mutant in the pool at the start and end of the experiment, and d (expansion factor) represents the fold change of the total mutant pool during the 8-d growth period. Expansion factors and generation times were calculated based on flow cytometry data (cells ml^{-1}), using CFU data to determine the proportion of *R. pomeroyi* in the bacterial community. Mutants with <10 average reads between the initial and final time points were removed from analysis.

Mean relative fitness for 3,748 out of 4,293 coding regions (Dataset S2.3) was determined from four replicate measurements of fitness. Fitness differences were calculated as:

$$log_2(\frac{W_{multi-bacteria} + \Psi}{W_{Rp} + \Psi})$$

where Ψ is a small number (0.01) to prevent a zero or non-integer. Statistical significance of fitness differences was determined by randomization tests (81) with 10,000 permutations using a custom script (82), and p-values were adjusted for multiple comparisons using the Benjamini-Hochberg procedure within the stats (v3.6.2) package in R. Mutant fitness analysis assumed that phytoplankton growth and release of photosynthate was independent of bacterial strains present, consistent with similar diatom growth (Fig. 1b) and comparable photosynthetic physiology (Fig. S2.2) in all treatments.

All plots and statistical analyses were performed in R v4.0.1 (83) using the packages tidyverse (84) and data.table (85). Figures were generated in R and Adobe Illustrator 2020.

Author Contributions: JES and MAM conceived the study, JES and CBS performed the study, JES and TRI analyzed the data, and JES and MAM wrote the paper.

Acknowledgements

We thank F. X. Ferrer González, W. F. Schroer, M. Uchimiya, H. Fu, M. Powers, M. Olofsson, M. M. Hamilton, Z. S. Cooper, B. Nowinski and K. G. Ross for helpful suggestions, S. E. Brown and N. M. Wood for experimental support, H. J. Schreier for providing expertise on nitrogen assimilation, J. Nelson at the UGA CTEGD Cytometry Shared Resource Lab provided guidance on flow cytometry protocols, and T. J. Simmonds and N. Workman at the UGA GGBC prepared libraries for sequencing. This work was supported by Simons Foundation grant 542391 to MAM within the Principles of Microbial Ecosystems Collaborative, and NSF Graduate

Research Fellowship Program award GRFP-1445117 to JES. This is the NSF Center for Chemical Currencies of a Microbial Planet (C-CoMP) publication #015.

Competing Interests

The authors declare no competing interests

Data availability

The authors declare that the data supporting the findings of this study were deposited at NCBI (Accession: PRJNA910220) and are available in the Supplementary Information files and a GitHub repository at github.com/jschreie/TnSeq_Phycosphere_Interactions.

Code availability

Code for analyzing data is available at github.com/jschreie/TnSeq_Phycosphere_Interactions

References:

1. M. J. Behrenfeld, E. Boss, D. A. Siegel, D. M. Shea, Carbon-based ocean productivity and phytoplankton physiology from space. *Glob. Biogeochem. Cycles* **19** (2005).

2. M. A. Moran *et al.*, The ocean's labile DOC supply chain. *Limnol Oceanogr* **67**, 1007-1021 (2022).

3. D. A. Hansell, Recalcitrant dissolved organic carbon fractions. *Ann Rev Mar Sci* **5**, 421-445 (2013).

4. F. Azam, F. Malfatti, Microbial structuring of marine ecosystems. *Nat Rev Microbiol* **5**, 782-791 (2007).

5. M. A. Moran *et al.*, Microbial metabolites in the marine carbon cycle. *Nat Microbiol* **7**, 508-523 (2022).

6. W. Bell, R. Mitchell, Chemotactic and growth responses of marine bacteria to algal extracellular products. *Biol. Bull.* **143**, 265-277 (1972).

7. J. R. Seymour, S. A. Amin, J. B. Raina, R. Stocker, Zooming in on the phycosphere: the ecological interface for phytoplankton-bacteria relationships. *Nat Microbiol* **2**, 17065 (2017).

8. S. A. Amin, M. S. Parker, E. V. Armbrust, Interactions between diatoms and bacteria. *Microbiol. Mol. Biol. Rev.* **76**, 667-684 (2012).

9. M. Landa *et al.*, Sulfur metabolites that facilitate oceanic phytoplankton-bacteria carbon flux. *ISME J* **13**, 2536-2550 (2019).

10. A. A. Shibl *et al.*, Diatom modulation of select bacteria through use of two unique secondary metabolites. *Proc Natl Acad Sci U S A* **117**, 27445-27455 (2020).

11. H. P. Grossart, F. Levold, M. Allgaier, M. Simon, T. Brinkhoff, Marine diatom species harbour distinct bacterial communities. *Environ Microbiol* **7**, 860-873 (2005).

12. G. Behringer *et al.*, Bacterial communities of diatoms display strong conservation across strains and time. *Front Microbiol* **9**, 659 (2018).

13. M. M. Barreto Filho, M. Walker, M. P. Ashworth, J. J. Morris, Structure and long-term stability of the microbiome in diverse diatom cultures. *Microbiol Spectr* **9**, e00269-00221 (2021).

14. H. Fu, M. Uchimiya, J. Gore, M. A. Moran, Ecological drivers of bacterial community assembly in synthetic phycospheres. *Proc Natl Acad Sci U.S.A.* **117**, 3656-3662 (2020).

15. H. Teeling *et al.*, Substrate-controlled succession of marine bacterioplankton populations induced by a phytoplankton bloom. *Science* **336**, 608-611 (2012).

16. K. Krüger *et al.*, In marine *Bacteroidetes* the bulk of glycan degradation during algae blooms is mediated by few clades using a restricted set of genes. *ISME J* **13**, 2800-2816 (2019).

17. D. M. Needham, J. A. Fuhrman, Pronounced daily succession of phytoplankton, archaea and bacteria following a spring bloom. *Nat Microbiol* **1**, 1-7 (2016).

18. A. M. Martin-Platero *et al.*, High resolution time series reveals cohesive but short-lived communities in coastal plankton. *Nat Commun* **9**, 1-11 (2018).

19. A. Buchan, G. R. LeCleir, C. A. Gulvik, J. M. González, Master recyclers: features and functions of bacteria associated with phytoplankton blooms. *Nat Rev Microbiol* **12**, 686-698 (2014).

20. R. Stocker, Marine microbes see a sea of gradients. *Science* **338**, 628-633 (2012).

21. H. Fu, C. B. Smith, S. Sharma, M. A. Moran, Genome sequences and metagenome-assembled genome sequences of microbial communities enriched on phytoplankton exometabolites. *Microbiol Resour Announc* **9,** e00724-24 (2020).

22. J. M. González, R. P. Kiene, M. A. Moran, Transformation of sulfur compounds by an abundant lineage of marine bacteria in the α-subclass of the class proteobacteria. *Appl Environ Microbiol* **65**, 3810-3819 (1999).

23. M. Sebastián, J. Ammerman, Role of the phosphatase PhoX in the phosphorus metabolism of the marine bacterium *Ruegeria pomeroyi* DSS-3. *Environ Microbiol Rep* **3**, 535-542 (2011).

24. G. C. Sharpe, S. M. Gifford, A. N. Septer, A model roseobacter, *Ruegeria pomeroyi* DSS-3, employs a diffusible killing mechanism to eliminate competitors. *mSystems* **5**, e00443-00420 (2020).

25. M. C. Chao, S. Abel, B. M. Davis, M. K. Waldor, The design and analysis of transposon insertion sequencing experiments. *Nat Rev Microbiol* **14**, 119-128 (2016).

26. T. van Opijnen, K. L. Bodi, A. Camilli, Tn-seq: high-throughput parallel sequencing for fitness and genetic interaction studies in microorganisms. *Nat Methods* **6**, 767-772 (2009).

27. T. R. Ioerger, Analysis of gene essentiality from TnSeq data using transit. *Methods Mol Biol* **2377,** 391-421 (2022).

28. M. A. Moran *et al.*, Genome sequence of *Silicibacter pomeroyi* reveals adaptations to the marine environment. *Nature* **432**, 910-913 (2004).

29. L. Reitzer, Nitrogen assimilation and global regulation in *Escherichia coli*. *Annu Rev Microbiol* **57**, 155-176 (2003).

30. P. M. Glibert *et al.*, Pluses and minuses of ammonium and nitrate uptake and assimilation by phytoplankton and implications for productivity and community composition, with emphasis on nitrogen-enriched conditions. *Limnol Oceanogr* **61**, 165-197 (2016).

31. A. E. Allen *et al.*, Diversity and detection of nitrate assimilation genes in marine bacteria. *Appl Environ Microbiol* **67**, 5343-5348 (2001).

32. D. L. Kirchman, P. A. Wheeler, Uptake of ammonium and nitrate by heterotrophic bacteria and phytoplankton in the sub-Arctic Pacific. *Deep Sea Res Part I Oceanogr Res Pap* **45**, 347-365 (1998).

33. S. Lockwood, C. Greening, F. Baltar, S. E. Morales, Global and seasonal variation of marine phosphonate metabolism. *ISME J* **16**, 2198-2212 (2022).

34. K. Ishige, H. Zhang, A. Kornberg, Polyphosphate kinase (PPK2), a potent, polyphosphate-driven generator of GTP. *Proc Natl Acad Sci USA* **99**, 16684-16688 (2002).

35. H. Luo, M. A. Moran, How do divergent ecological strategies emerge among marine bacterioplankton lineages? *Trends Microbiol* **23**, 577-584 (2015).

36. Ö. Özkaya, K. B. Xavier, F. Dionisio, R. Balbontín, Maintenance of microbial cooperation mediated by public goods in single-and multiple-trait scenarios. *J Bacteriol* **199**, e00297-00217 (2017).

37. S. A. Sañudo-Wilhelmy *et al.*, Multiple B-vitamin depletion in large areas of the coastal ocean. *Proc Natl Acad Sci U S A* **109**, 14041-14045 (2012).

38. L. Gómez-Consarnau *et al.*, Mosaic patterns of B-vitamin synthesis and utilization in a natural marine microbial community. *Environ Microbiol* **20**, 2809-2823 (2018).

39. S. Pontrelli *et al.*, Hierarchical control of microbial community assembly. *bioRxiv* [Preprint] (2021). https://doi.org/10.1101/2021.06.22.449372 (accessed November 2022).

40. G. D'Souza *et al.*, Ecology and evolution of metabolic cross-feeding interactions in bacteria. *Nat Prod Rep* **35**, 455-488 (2018).

41. K. Amarnath *et al.*, Dynamic metabolic exchanges between complementary bacterial types provide collaborative stress resistance. *bioRxiv* [Preprint] (2021). https://doi.org/10.1101/2021.06.24.449802 (accessed November 2022).

42. B. LaSarre, A. M. Deutschbauer, C. E. Love, J. B. McKinlay, Covert cross-feeding revealed by genome-wide analysis of fitness determinants in a synthetic bacterial mutualism. *Appl Environ Microbiol* **86** (2020).

43. M. D. Linney, C. R. Schvarcz, G. F. Steward, E. F. DeLong, D. M. Karl, A method for characterizing dissolved DNA and its application to the North Pacific Subtropical Gyre. *Limnol Oceanogr Methods* **19**, 210-221 (2021).

44. J. Kehe *et al.*, Positive interactions are common among culturable bacteria. *Sci Adv* **7**, eabi7159 (2020).

45. A. Zelezniak *et al.*, Metabolic dependencies drive species co-occurrence in diverse microbial communities. *Proc Natl Acad Sci USA* **112**, 6449-6454 (2015).

46. G. D'Souza *et al.*, Less is more: selective advantages can explain the prevalent loss of biosynthetic genes in bacteria. *Evolution* **68**, 2559-2570 (2014).

47. J. E. Goldford *et al.*, Emergent simplicity in microbial community assembly. *Science* **361**, 469-474 (2018).

48. H. Ploug, M. Kühl, B. Buchholz-Cleven, B. B. Jørgensen, Anoxic aggregates-an ephemeral phenomenon in the pelagic environment? *Aquat Microb Ecol* **13**, 285-294 (1997).

49. I. Klawonn, S. Bonaglia, V. Brüchert, H. Ploug, Aerobic and anaerobic nitrogen transformation processes in N_2-fixing cyanobacterial aggregates. *ISME J* **9**, 1456-1466 (2015).

50. A. L. Alldredge, Y. Cohen, Can microscale chemical patches persist in the sea? Microelectrode study of marine snow, fecal pellets. *Science* **235**, 689-691 (1987).

51. I. Wagner-Döbler, H. Biebl, Environmental biology of the marine *Roseobacter* lineage. *Annu Rev Microbiol* **60**, 255-280 (2006).

52. R. J. Newton *et al.*, Genome characteristics of a generalist marine bacterial lineage. *ISME J* **4**, 784-798 (2010).

53. E. R. Zinser, The microbial contribution to reactive oxygen species dynamics in marine ecosystems. *Environ Microbiol Rep* **10**, 412-427 (2018).

54. J. M. Diaz, S. Plummer, Production of extracellular reactive oxygen species by phytoplankton: past and future directions. *J Plankton Res* **40**, 655-666 (2018).

55. C. M. Hansel, J. M. Diaz, S. Plummer, Tight regulation of extracellular superoxide points to its vital role in the physiology of the globally relevant Roseobacter clade. *mBio* **10**, e02668-02618 (2019).

56. J. M. Diaz *et al.*, Widespread production of extracellular superoxide by heterotrophic bacteria. *Science* **340**, 1223-1226 (2013).

57. T. Oda *et al.*, Generation of reactive oxygen species by raphidophycean phytoplankton. *Biosci* **61**, 1658-1662 (1997).

58. M. Scott, S. Klumpp, E. M. Mateescu, T. Hwa, Emergence of robust growth laws from optimal regulation of ribosome synthesis. *Mol Syst Biol* **10**, 747 (2014).

59. S. Klumpp, M. Scott, S. Pedersen, T. Hwa, Molecular crowding limits translation and cell growth. *Proc Natl Acad Sci USA* **110**, 16754-16759 (2013).

60. E. Bosdriesz, D. Molenaar, B. Teusink, F. J. Bruggeman, How fast-growing bacteria robustly tune their ribosome concentration to approximate growth-rate maximization. *FEBS J* **282**, 2029-2044 (2015).

61. U. Sauer, F. Canonaco, S. Heri, A. Perrenoud, E. Fischer, The soluble and membrane-bound transhydrogenases UdhA and PntAB have divergent functions in NADPH metabolism of *Escherichia coli*. *J Biol Chem* **279**, 6613-6619 (2004).

62. G. M. Cook, K. Hards, C. Vilchèze, T. Hartman, M. Berney, Energetics of respiration and oxidative phosphorylation in mycobacteria. *Microbiol Spectr* **2**, 2.3. 06 (2014).

63. M. Cunliffe, Physiological and metabolic effects of carbon monoxide oxidation in the model marine bacterioplankton *Ruegeria pomeroyi* DSS-3. *Appl Environ Microbiol* **79**, 738-740 (2013).

64. J. A. Christie-Oleza, B. Fernandez, B. Nogales, R. Bosch, J. Armengaud, Proteomic insights into the lifestyle of an environmentally relevant marine bacterium. *ISME J* **6**, 124-135 (2012).

65. P. R. Cordero *et al.,* Atmospheric carbon monoxide oxidation is a widespread mechanism supporting microbial survival. *ISME J* **13**, 2868-2881 (2019).

66. E. Kazamia, K. E. Helliwell, S. Purton, A. G. Smith, How mutualisms arise in phytoplankton communities: building eco-evolutionary principles for aquatic microbes. *Ecol Lett* **19**, 810-822 (2016).

67. J. D. Palmer, K. R. Foster, Bacterial species rarely work together. *Science* **376**, 581-582 (2022).

68. L. Riemann, G. F. Steward, F. Azam, Dynamics of bacterial community composition and activity during a mesocosm diatom bloom. *Appl Environ Microbiol* **66**, 578-587 (2000).

69. B. Norrman, U. L. Zwelfel, C. S. Hopkinson Jr, F. Brian, Production and utilization of dissolved organic carbon during an experimental diatom bloom. *Limnol Oceanogr* **40**, 898-907 (1995).

70. S. M. Gifford, S. Sharma, M. Booth, M. A. Moran, Expression patterns reveal niche diversification in a marine microbial assemblage. *ISME J* **7**, 281-298 (2013).

71. P. W. Boyd *et al.,* Biological responses to environmental heterogeneity under future ocean conditions. *Glob Chang Biol* **22**, 2633-2650 (2016).

72. J. Beardall, S. Stojkovic, S. Larsen, Living in a high CO_2 world: impacts of global climate change on marine phytoplankton. *Plant Ecol Divers* **2**, 191-205 (2009).

73. K. Gao, E. W. Helbling, D.-P. Häder, D. A. Hutchins, Responses of marine primary producers to interactions between ocean acidification, solar radiation, and warming. *Mar Ecol Prog Ser* **470**, 167-189 (2012).

74. D. B. Van de Waal, E. Litchman, Multiple global change stressor effects on phytoplankton nutrient acquisition in a future ocean. *Philos Trans R Soc Lond B Biol Sci* **375**, 20190706 (2020).

75. J. A. Hellebust, Excretion of some organic compounds by marine phytoplankton. *Limnol Oceanogr* **10**, 192-206 (1965).

76. D. C. O. Thornton, Dissolved organic matter (DOM) release by phytoplankton in the contemporary and future ocean. *Eur J Phycol* **49**, 20-46 (2014).

77. P. Baumann, "The marine gram negative eubacteria: genera *Photobacterium*, *Benekea*, *Alteromonas*, *Pseudomonsa* and *Alcaligenes*" in The prokaryotes. M. P., Stolp, H., Trüper, H. G., Balows, A., Schlegel, H. G. Eds. (Springer-Verlag, 1981), pp.1302-1331.

78. J. A. Berges, D. J. Franklin, P. J. Harrison, Evolution of an artificial seawater medium: improvements in enriched seawater, artificial water over the last two decades. *J Phycol* **37**, 1138-1145 (2001).

79. M. A. DeJesus, C. Ambadipudi, R. Baker, C. Sassetti, T. R. Ioerger, TRANSIT—a software tool for himar1 TnSeq analysis. *PloS Comput Biol* **11**, e1004401 (2015).

80. H. Li, R. Durbin, Fast and accurate short read alignment with Burrows–Wheeler transform. *Bioinformatics* **25**, 1754-1760 (2009).

81. P. H. Crowley, Resampling methods for computation-intensive data analysis in ecology and evolution. *Annu Rev Ecol Evol Syst*, 405-447 (1992).

82. S. Holland (Resampling Methods. In *Data Analysis in the Geosciences* (http://strata.uga.edu/8370/lecturenotes).

83. R Core Team, R: A language and environment for statistical computing. R Foundation for Statistical Computing. https://www.R-project.org/ (2019).

84. H. Wickham, The tidyverse. *R package ver* **1**, 836 (2017).

85. M. Dowle *et al.*, Package 'data. Table' extension of 'data. Frame'. R (>= 3.1.0), MPL–2.0 | file LICENSE (2019).

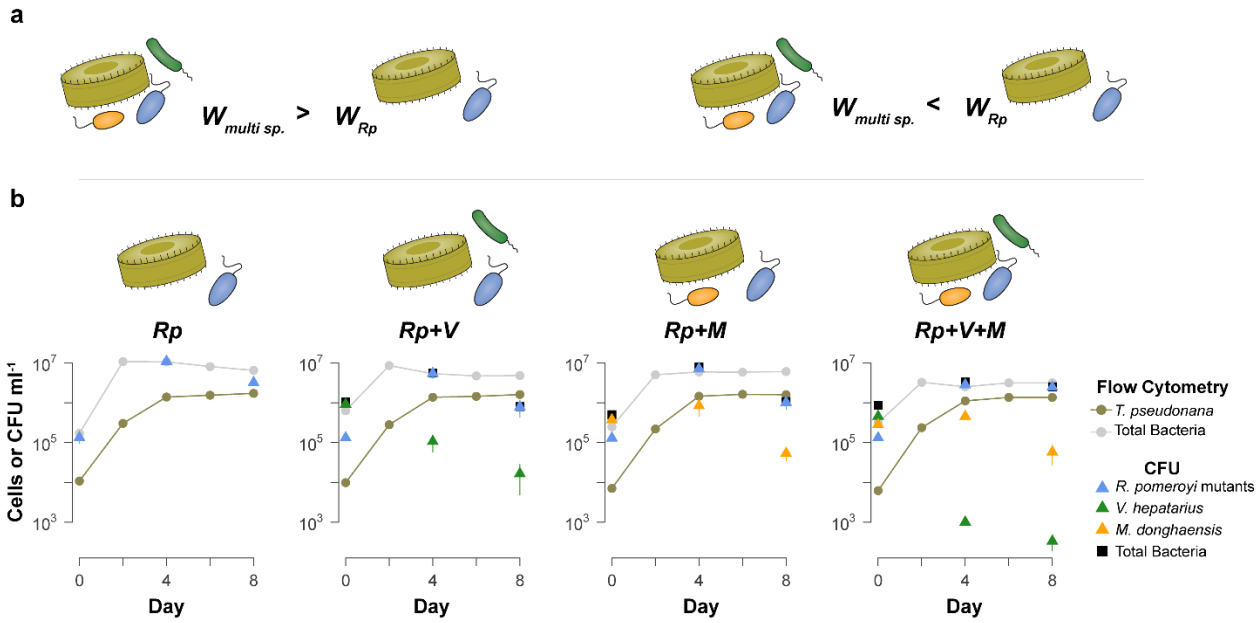

Figure 2.1. Overview of the model phycosphere experiment. **a.** Fitness of *R. pomeroyi* mutants in multi-bacterial communities (*Rp+V*; *Rp+M*; *Rp+V+M*) was compared to fitness in single-bacterial cultures (*Rp*). Higher fitness ($W_{multi\ sp.} > W_{Rp}$) indicated that the missing function was rescued or superfluous when growing with other species, for example through cross-feeding. Lower fitness ($W_{multi\ sp.} < W_{Rp}$) indicated that the missing function would have been beneficial when growing with other species, for example, by increasing competitiveness. **b.** Growth of community members over 8 d. Standard error of the mean (n=4) is displayed for all points; some fall within the symbols. Solid lines indicate diatom and bacterial density based on flow cytometric analysis (cells ml^{-1}). Triangles indicate abundance of individual bacterial species, and squares represent abundance of all bacteria (CFU ml^{-1}) at 3 time points.

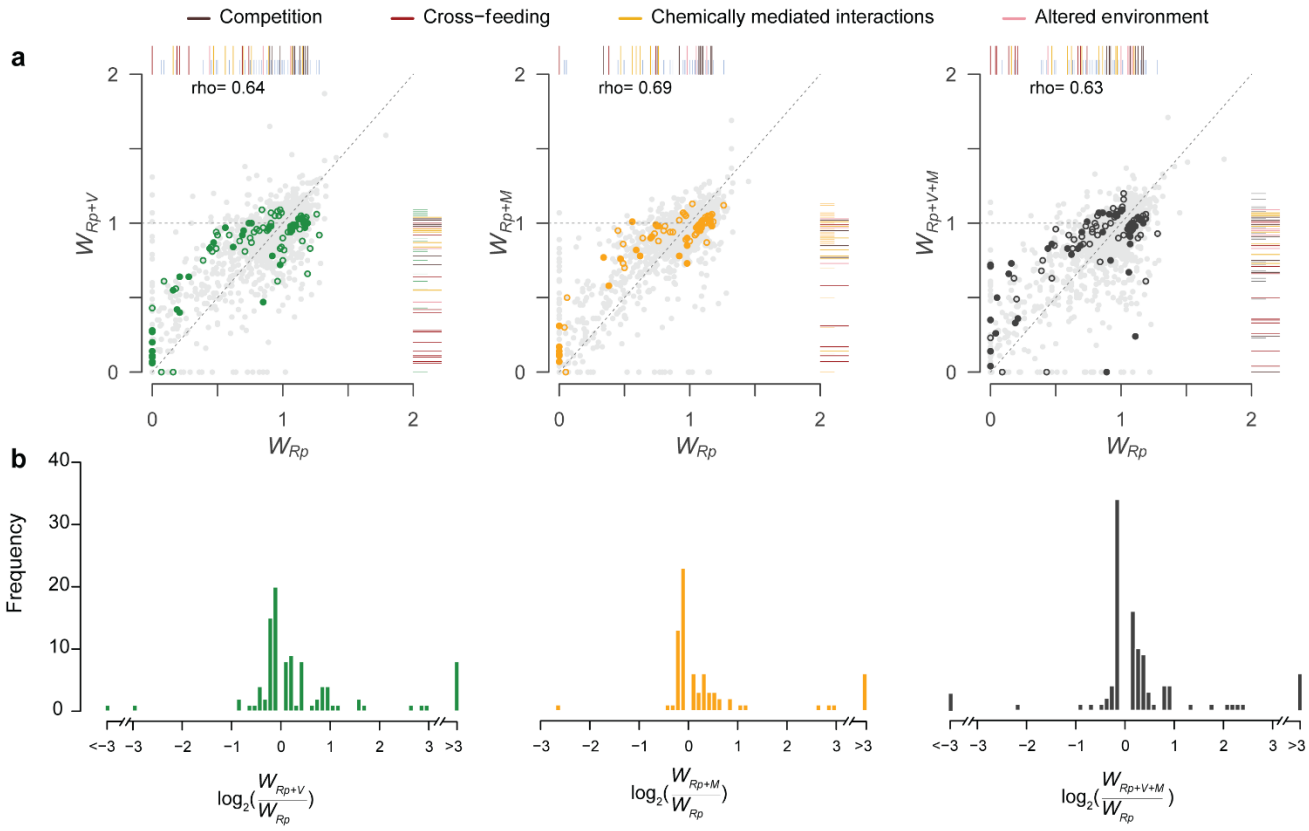

Figure 2.2. Effect of multi-bacterial communities on *R. pomeroyi* mutant fitness. **a.** Correlation between mutant fitness (*W*) in multi- (y-axis) versus single- (x-axis) bacterial treatments (Spearman's rho, $p < 0.05$ for all). Dashed lines indicate a 1:1 relationship. Mutants cover 86% of protein encoding genes, with most genes missing from the mutant pool mediating functions essential for cell viability. Symbols with color indicate significantly different fitness for mutants in multi-bacterial treatments versus the single-bacterial treatment based on Benjamini-Hochberg adjusted *p* values from randomization tests of the $\log_2$ fold-change of fitness (*p-adj* < 0.05). Colored symbols that are also filled are included in Tables 1 – 4. Rug plots on the right and top of plots show the distribution of *W* for mutants with significantly different fitness; longer rug markers are colored to represent the four ecological modes of interaction. Colored points close to the 1:1 line have small but statistically significant fitness differences. **b.** Distribution of the $\log_2$ fold-change of fitness for multi-bacteria treatments compared to the single-bacterial (*Rp*)

treatment. Positive values indicate mutant fitness increases in multi-species communities; negative values indicate fitness decreases. Mutants with fitness changes greater than |3| were binned.

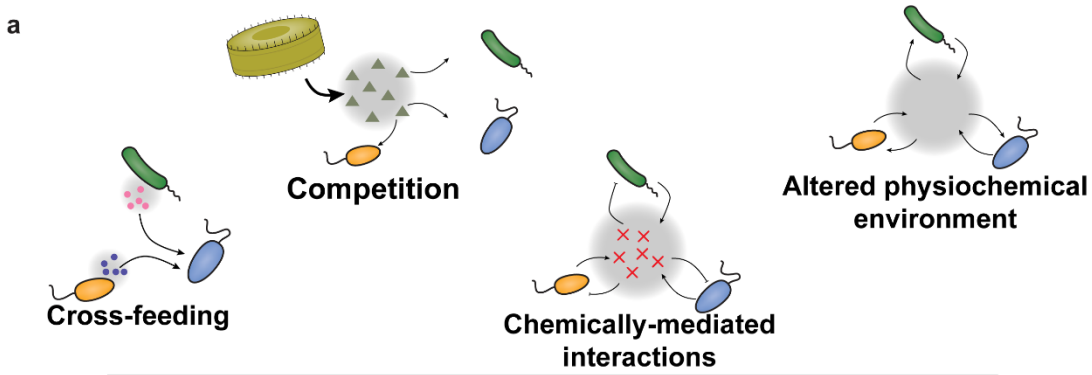
a
Competition
Cross-feeding
Chemically-mediated interactions
Altered physiochemical environment

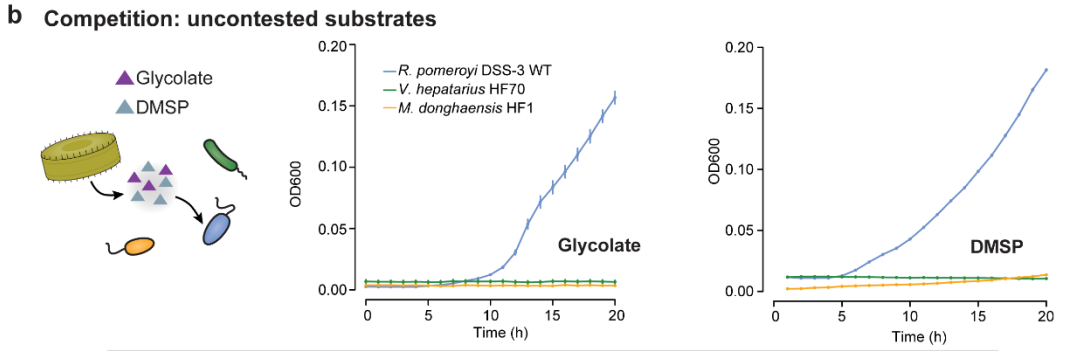
b
Competition: uncontested substrates
Glycolate
DMSP
R. pomeroyi DSS-3 WT
V. hepatarius HF70
M. donghaensis HF1
OD600
Time (h)
Glycolate
DMSP

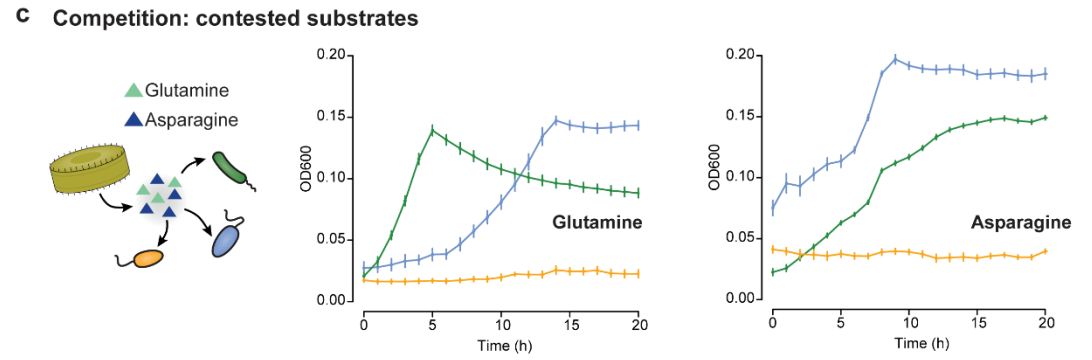
c
Competition: contested substrates
Glutamine
Asparagine
OD600
Time (h)
Glutamine
Asparagine

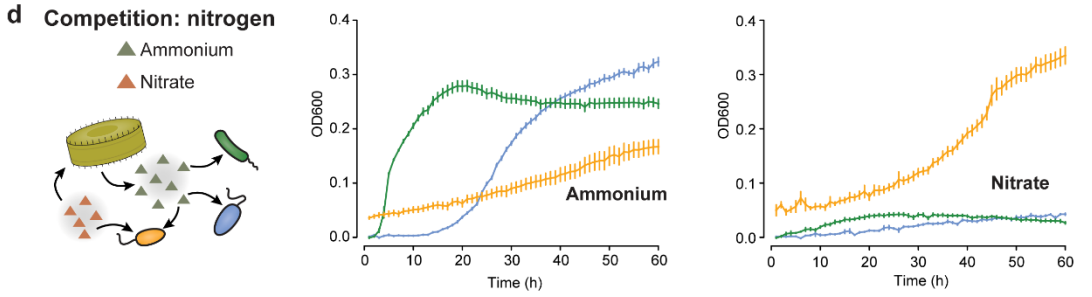
d
Competition: nitrogen
Ammonium
Nitrate
OD600
Time (h)
Ammonium
Nitrate

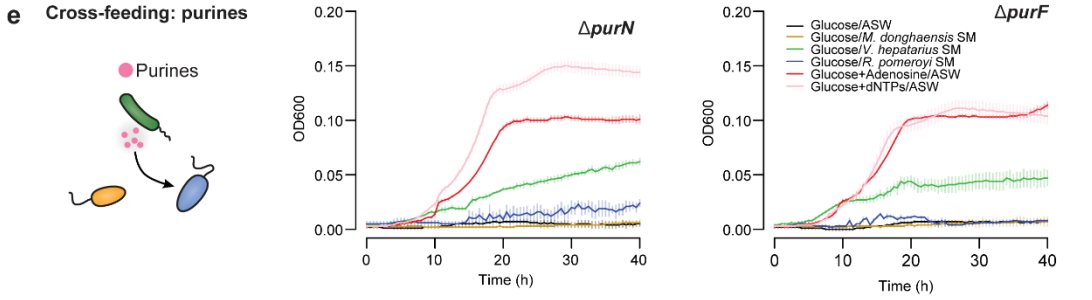
e
Cross-feeding: purines
Purines
ΔpurN
ΔpurF
OD600
Time (h)
Glucose/ASW
Glucose/M. donghaensis SM
Glucose/V. hepatarius SM
Glucose/R. pomeroyi SM
Glucose+Adenosine/ASW
Glucose+dNTPs/ASW

Figure 2.3. Experimental tests of bacterial interaction hypotheses. **a.** Four categories of bacterial interactions implicated by phycosphere mutant fitness assays. **b.** Minimal medium with glycolate or DMSP (12 mM carbon) as the sole carbon source supported strong growth only of *R. pomeroyi,* suggestive of increased importance of a non-contested resource. **c.** Minimal medium with glutamine or asparagine (12 mM carbon) as the sole carbon source supported growth of both *V. hepatarius* and *R. pomeroyi,* suggestive of a communal carbon source**. d.** Minimal glucose medium with ammonium or nitrate as the inorganic nitrogen source. Only *M. donghaensis* can assimilate nitrate, consistent with exploitative competition for ammonium observed only between *R. pomeroyi* and *V. hepatarius*. **e.** Growth of isolated mutants *purN* and *purF* in minimal glucose medium amended witheither spent medium, adenosine, or dNTPs. Mutant auxotrophy is confirmed by lack of growth in glucose alone. Rescue of auxotrophy is demonstrated by addition of adenosine, dNTPs, or *Vibrio* spent medium, supporting the hypothesis of purine cross-feeding.

Table 2.1. Fitness differences (log_2-fold) of selected mutants involved in competition whose growth was significantly influenced in the multi-bacterial treatments. Empty cells represent fitness changes that were not significantly different based on randomization tests.

Gene	Protein Name (Gene Symbol)	Function	Rp+V	Rp+M	Rp+V+M
SPO3479	glycolate oxidase (*glcE)*	Carbon source - Glycolate	-0.44		
SPO3805	Methylthioacryloyl-CoA hydratase (*dmdD*)	Carbon source - DMSP		-0.11	
SPO2708	carnitine dehydratase	Carbon/nitrogen source - carnitine	-0.16		
SPO1586	N-methylglutamate dehydrogenase (*mgdC*)	Carbon/nitrogen source - methylamine		-0.18	
SPO3360	2-amino-3-ketobutyrate co-A ligase (*kbl*)	Carbon/nitrogen source - threonine			-0.12
SPO0673	taurine--pyruvate aminotransferase (*tpa*)	Carbon/nitrogen source - taurine		-0.2	
SPO0397	protein-P-II uridylyltransferase (*glnD*)	Nitrogen acquisition			-6.5
SPO3661	allophanate hydrolase family protein	Nitrogen acquisition	-0.24	-0.24	-0.29
SPO0891	alkylphosphonate utilization protein (*phnM*)	Phosphate acquisition		-0.11	

SPO1727	polyphosphate kinase 2, putative	Phosphate storage			-2.2
SPO1213	oligopeptide ABC transporter, ATP-binding	Transporter - peptide		-0.12	
SPO2815	peptide/nickel/opine ABC transporter, permease	Transporter	-0.12		
SPO2816	peptide/nickel/opine ABC transporter, permease	Transporter	-0.14		
SPO1814	TRAP dicarboxylate transporter (*dctP*)	Transporter - organic acid	-0.21	-0.2	-0.18
SPO1816	TRAP dicarboxylate transporter (*dctM*)	Transporter - organic acid		-0.17	-0.18
SPO2626	TRAP transporter (*dctM*)	Transporter - organic acid	-0.13		-0.12
SPO2627	C4 dicarbodylateTRAP transporter (*dctQ*)	Transporter - organic acid	-0.17		-0.65
SPO2630	C4-dicarboxylate TRAP regulatory protein	Transporter - organic acid	-0.25		
SPOA0238	TRAP dicarboxylate transporter (*dctP*)	Transporter - organic acid	-0.18	-0.2	-0.18
SPOA0240	TRAP transporter (*dctM*)	Transporter - organic acid	-0.14	-0.14	-0.14
SPOA0237	C4-dicarboxylate transport transcriptional regulatory protein (*dctD*-2)	Transporter - organic acid	-0.27	-0.25	-0.22

SPO0521	glutamate/glutamine/aspartate/asparagine ABC transporter, permease	Transporter - N-rich amino acid			0.22
SPO0715	phosphocarrier protein HPr	Transporter - sugar		1.2	
SPOA0249	TRAP dicarboxylate transporter (*dctP*)	Transporter - organic acid			0.13
SPO1496	ABC transporter, permease	Transporter		0.38	
SPOA0367	ABC transporter, permease	Transporter	0.12		

Table 2.2. Fitness differences (log_2-fold) of selected mutants involved in cross-feeding whose growth was significantly influenced in the multi-bacterial treatments. Empty cells represent fitness changes that were not significantly different based on randomization tests.

Gene	**Protein Name (Gene Symbol)**	**Function**	**Rp+V**	**Rp+M**	**Rp+V+M**
SPO0018	argininosuccinate synthase (*argG*)	Arginine	3.5	3	
SPO0332	argininosuccinate lyase (*argH*)	Arginine	2.8		
SPO0422	2-isopropylmalate synthase (*leuA*)	Leucine		0.6	
SPO0210	3-isopropylmalate dehydrogenase (*leuB*)	Leucine			2.4

SPO0215	3-isopropylmalate dehydratase (*leuD*-1)	Leucine	1.1		0.77
SPO1351	O-succinylhomoserine sulfhydrylase (*metZ*)	Homocysteine	3		
SPO1734	homoserine dehydrogenase (*hom*)	Homoserine		5	
SPO1884	S-methyltransferase component of split *metH*	Methionine			3.9
SPO1973	3-dehydroquinate dehydratase, type II (*aroQ*)	Aromatic amino acids	3.9		
SPO2150	anthranilate phosphoribosyltransferase (*trpD*)	Tryptophan	3.6		2.3
SPO2151	indole-3-glycerol phosphate synthase (*trpC*)	Tryptophan	4.4		
SPO3768	glutamate synthase (*gltB*)	Glutamate	0.9		0.75
SPO2634	sulfite reductase	Amino acid - sulfur assimilation	4.8		
SPO2635	phosophoadenylyl-sulfate reductase (*cysH*)	Amino acid - sulfur assimilation		4.2	
SPO0102	3-methyl-2-oxobutanoate hydroxymethyltransferase (*panB*)	Vitamin B5	0.43	0.42	0.44
SPO3224	cobalamin biosynthetic protein (*cobC*)	Vitamin B12			6.2

SPO3633	molybdopterin converting factor, subunit 2	Molybdopterin	0.41		0.3
SPO3634	molybdopterin converting factor, subunit 1 (*moaD*)	Molybdopterin			0.3
SPO0284	dihydroorotase, multifunctional complex	Pyrimidine			2.2
SPO2654	orotate phosphoribosyltransferase (*pyrE*)	Pyrimidine	4.9		
SPO1318	adenylosuccinate synthetase (*purA*)	Purine		3.6	5.2
SPO1870	phosphoribosylformylglycinamidine synthase II (*purL*)	Purine			3.1
SPO2168	phosphoribosylglycinamide formyltransferase (*purN)*	Purine	1.6		
SPO2677	amidophosphoribosyltransferase (*purF*)	Purine	1.2		

Table 2.3. Fitness differences (log_2-fold) of selected mutants involved in chemically-mediated interactions whose growth was significantly influenced in the multi-bacterial treatments. Empty cells represent fitness changes that were not significantly different based on randomization tests.

Gene	Protein Name (Gene Symbol)	Function	Rp+V	Rp+M	Rp+V+M
SPO1240	type I secretion outer membrane protein (*tolC*)	Antimicrobial/Efflux	0.9		0.9
SPO1928	Tat (twin-arginine translocation) pathway signal sequence domain protein	Antimicrobial/Efflux		-0.13	
SPO3091	type II secretion system protein F (*gspF*)	Antimicrobial/Efflux		-0.11	-0.13
SPO1757	capsular polysaccharide export protein (*kpsS*)	Efflux			-0.18
SPO2713	Protein translocase subunit SecA 2 (*secA*2)	Efflux		-0.42	
SPO2251	gene transfer agent (*orfg*14)	Gene transfer	-0.84		
SPO0071	competence protein F, putative	Gene transfer	-0.13		-0.2
SPOA0111	indolepyruvate oxidoreductase (*iorA*)	Signaling - auxin			-0.12
SPO2287	autoinducer synthesis protein	Signaling			0.12

Table 2.4. Fitness differences (log_2-fold) of selected mutants indicative of an altered environment whose growth was significantly influenced in the multi-bacterial treatments. Empty cells represent fitness changes that were not significantly different based on randomization tests.

Gene	Protein Name (Gene Symbol)	Function	Rp+V	Rp+M	Rp+V+M
SPO3073	cytochrome c oxidase, subunit III (*ctaE*)	Aerobic respiration	0.43	0.33	
SPO3075	Protoheme IX farnesyltransferase (*ctaB*)	Aerobic respiration	0.87	0.68	0.86
SPO3076	cytochrome c oxidase, subunit II (*ctaC*)	Aerobic respiration		0.47	0.49
SPO1383	cytochrome c oxidase, aa3-type, subunit I (*ctaD*)	Aerobic respiration	0.43		
SPOA0212	nitric oxide reductase F protein	Respiration			0.31
SPO2099	cytochrome c-554 (*cycF*)	Respiration	-0.15		
SPO1898	cytochrome P450 family protein	Respiration	-0.14		
SPOA0223	cytochrome cd1 nitrite reductase (*nirF*)	Respiration	-0.17		
SPO0935	nitroreductase family protein	Respiration			-0.17
SPO2340	superoxide dismutase, Fe (*sodB*)	Reactive oxygen species	1.7		2.1

SPO_Sp16SA	16S rRNA	Cell cycle/Growth			0.11
SPO_Sp16SB	16S rRNA	Cell cycle/Growth			0.13
SPO_Sp16SC	16S rRNA	Cell cycle/Growth			0.14
SPO0503	ribosomal protein L30 (*rpmD)*	Cell cycle/Growth			0.34
SPO1443	ATP-dependent RNA helicase RhlE (*rhlE*)	Cell cycle/Growth	0.44	0.36	0.42
SPO3256	ribosomal protein L31 (*rpmE*)	Cell cycle/Growth		3.9	
SPO0691	GTP-binding protein Era (*era*)	Cell cycle/Growth	0.78	0.84	
SPO2819	NAD(P)+ transhydrogenase, beta (*pntB*)	Energy	0.39	0.36	
SPO2820	NAD(P) transhydrogenase, alpha (*pntA*)	Energy			0.36
SPO0095	nicotinate phosphoribosyltransferase (*pncB*)	Energy	0.11		
SPO1519	carbon monoxide dehydrogenase, large subunit (*coxL*-1)	Energy - carbon monoxide	-0.17		-0.23
SPO3901	carbon monoxide dehydrogenase G protein, putative	Energy - carbon monoxide			-0.31

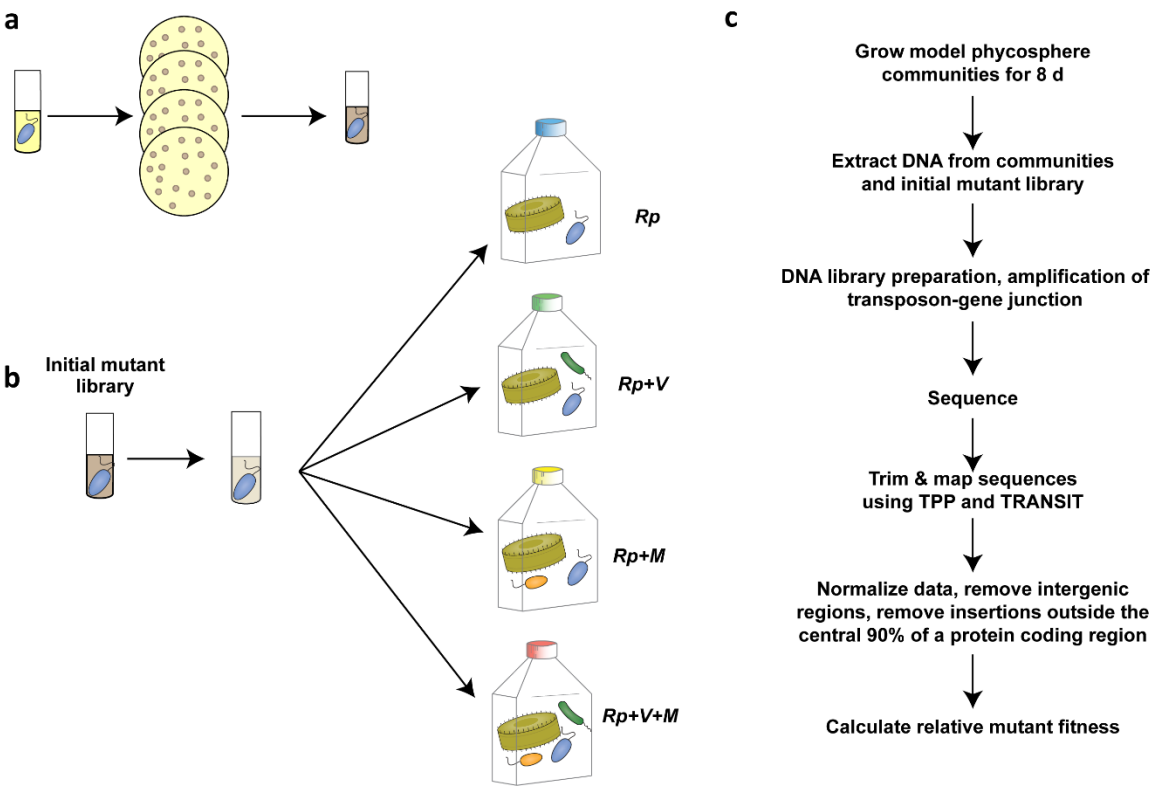

Supplemental Figure S2.1. Graphical explanation of transposon mutant library generation, model phycosphere assay, and data processing. **a**. Generation of a Tn5 transposon mutant library in *Ruegeria pomeroyi* DSS-3. Electrocompetent cells were transformed with Tn5 transposome, recovered in rich medium, and plated and incubated on selective (kanamycin) medium. Colonies were washed from the plates and added to glycerol to generate a saturated transposon mutant library. **b**. Model phycosphere set-up. The saturated transposon mutant library of *R. pomeroyi* was inoculated into selective liquid medium, grown, washed, and resuspended to ~$5x10^7$ cells ml^{-1} to generate the initial mutant library, which was inoculated into diatom cultures to establish four treatments: *R. pomeroyi* single-bacterial culture (*Rp*), *R. pomeroyi* plus *Vibrio hepatarius* HF70 (*Rp+V*), *R.pomeroyi* plus *Marivivens donghaensis* HF1 (*Rp+M*), and *R. pomeroyi* plus *V. hepatarius* plus *M. donghaensis* (*Rp+V+M*) (n=4). **c**. Data generation and processing. Model phycosphere communities were grown for 8 d. Cultures were pelleted, and DNA was extracted

from each community and the initial mutant library. DNA libraries were prepared for transposon sequencing, and subsequently processed to calculate relative mutant fitness.

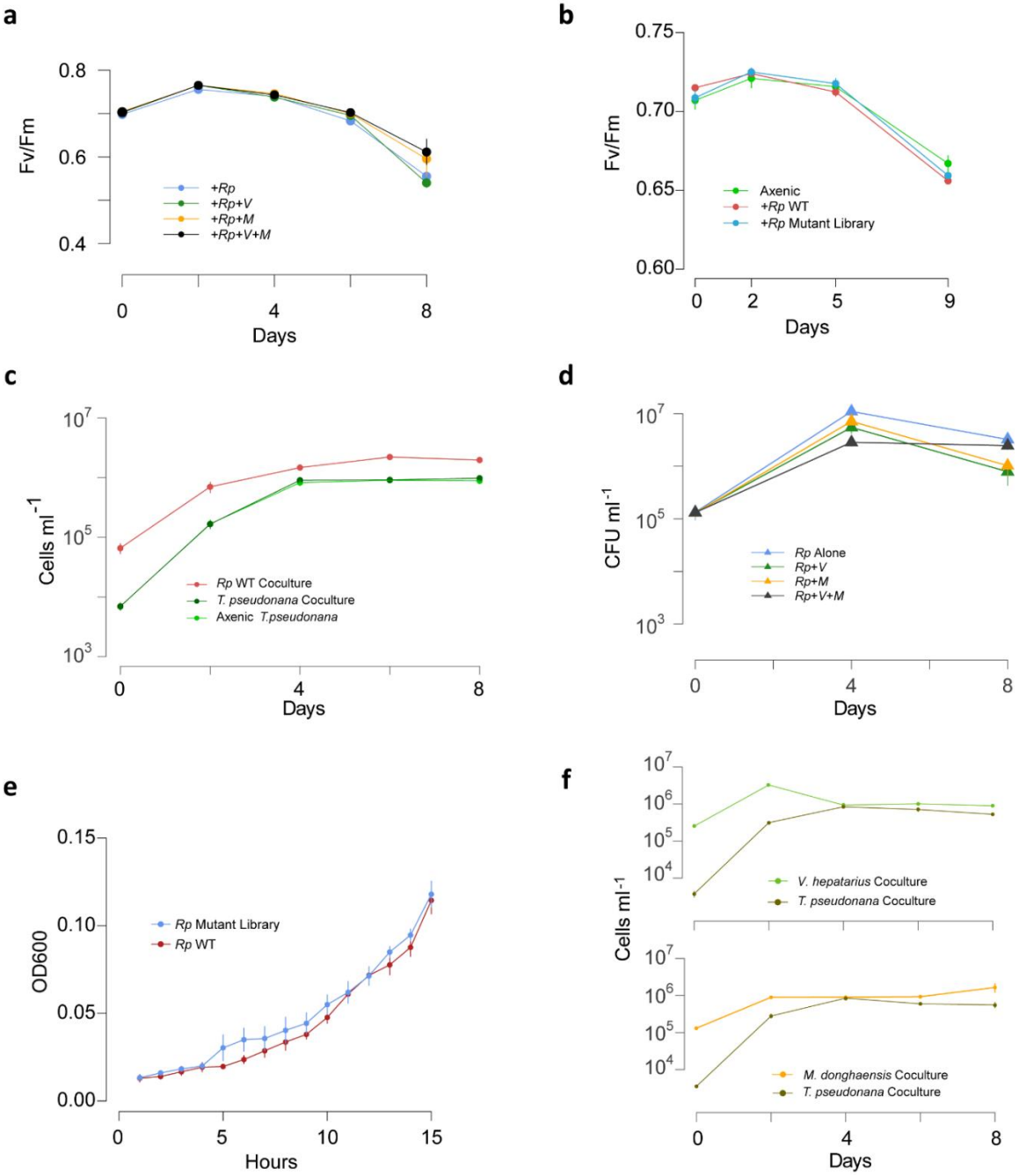

Supplemental Figure S2.2. Microbial growth and physiology. Diatom photosynthetic efficiency (Fv/Fm) measured by a Satlantic FIRe Fluorometer. **a**. Mean Fv/Fm measured for model phycosphere communities and **(b)** communities containing axenic diatoms or co-cultures with wild-type *R. pomeroyi* or the mutant library. Mean Fv/Fm at the final time points are statistically

indistinguishable (a; F=1.7, df=3, p=0.22. b; F=3.1, df=2, p=0.12). **(c)** Growth of *T. pseudonana* in coculture with wild-type *R. pomeroyi* and axenic (n=3). **(d)** Growth of the *R. pomeroyi* mutant library in each of the four model phycosphere communities from Figure 1b. **(e)** Similarity of mutant library and wild-type *R.pomeroyi* growth on ectoine (1.25 mM carbon) (n=3). **(f)** Cocultures of *T. pseudonana* with *V. hepatarius* (top) *or M. donghaensis* (bottom) demonstrating growth of these bacteria in the absence of *R. pomeroyi* (n=3). Some standard error bars fall within the symbol. Rp=*Ruegeria pomeroyi*, V=*Vibrio hepatarius* HF70, M=*Marivivens donghaensis* HF1.

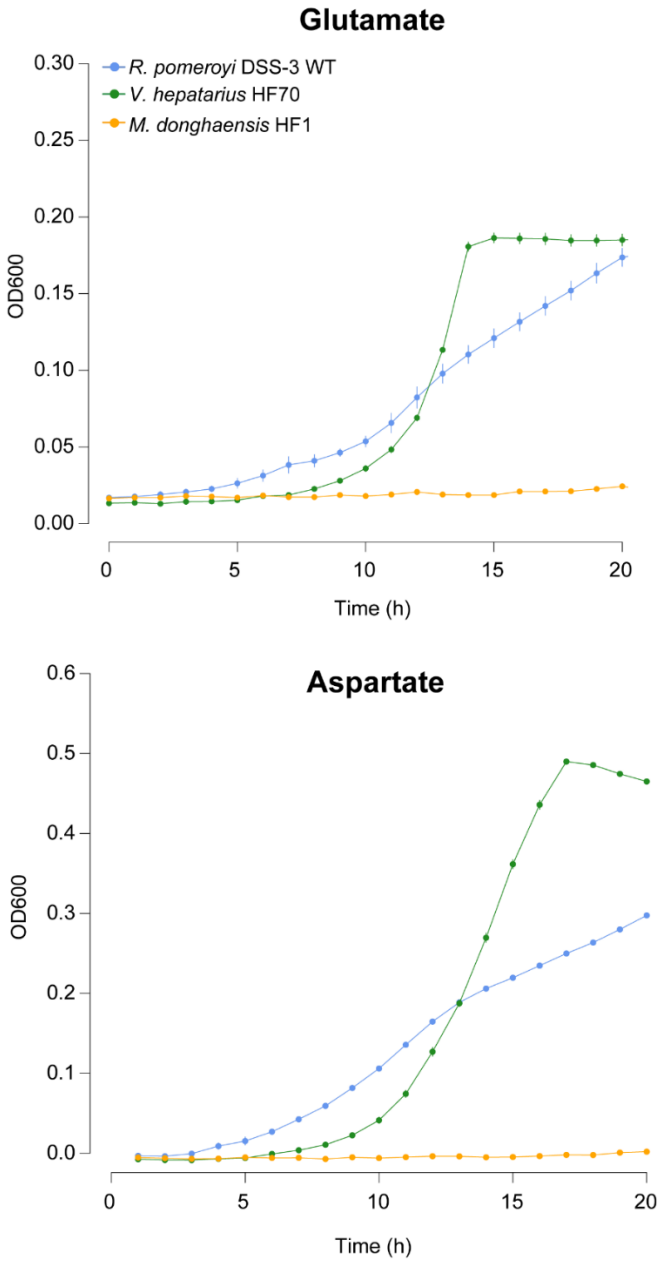

Supplemental Figure S2.3. Growth of monocultures in minimal medium with either glutamate or aspartate (12 mM carbon) as the sole source of carbon (n=3-6).

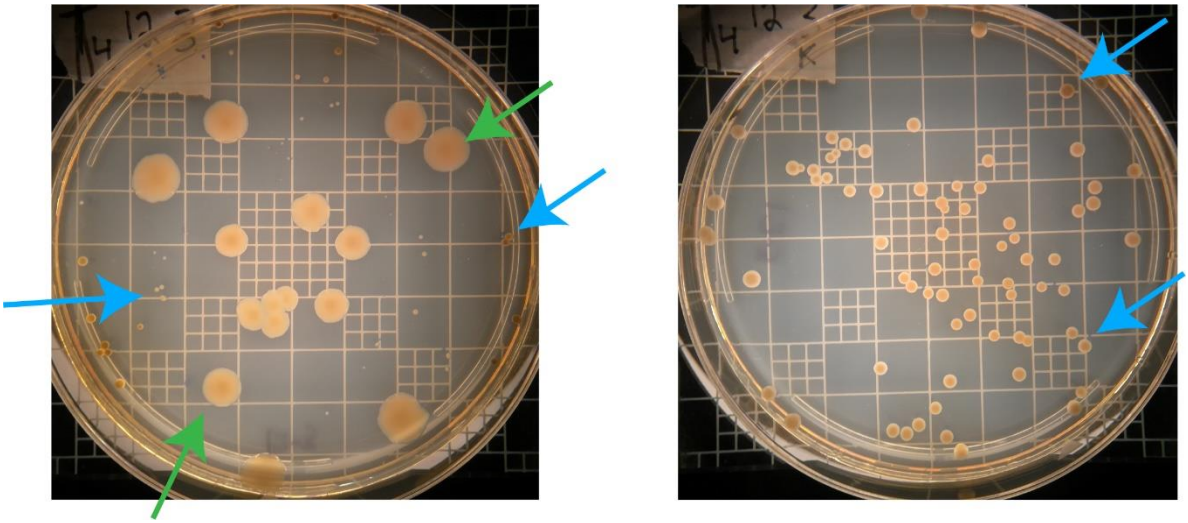

Supplemental Figure S2.4. Examples of non-selective (left) and selective (right, kanamycin) agar plates with CFUs of *R. pomeroyi* (blue arrows) and *V. hepatarius* (green arrows). *V. hepatarius* inhibits the growth of *R. pomeroyi* on solid medium, as seen by the clear zone of inhibition around *V. hepatarius* colonies. *M. donghaensis* does not inhibit, and is not inhibited by, other strains on solid medium.

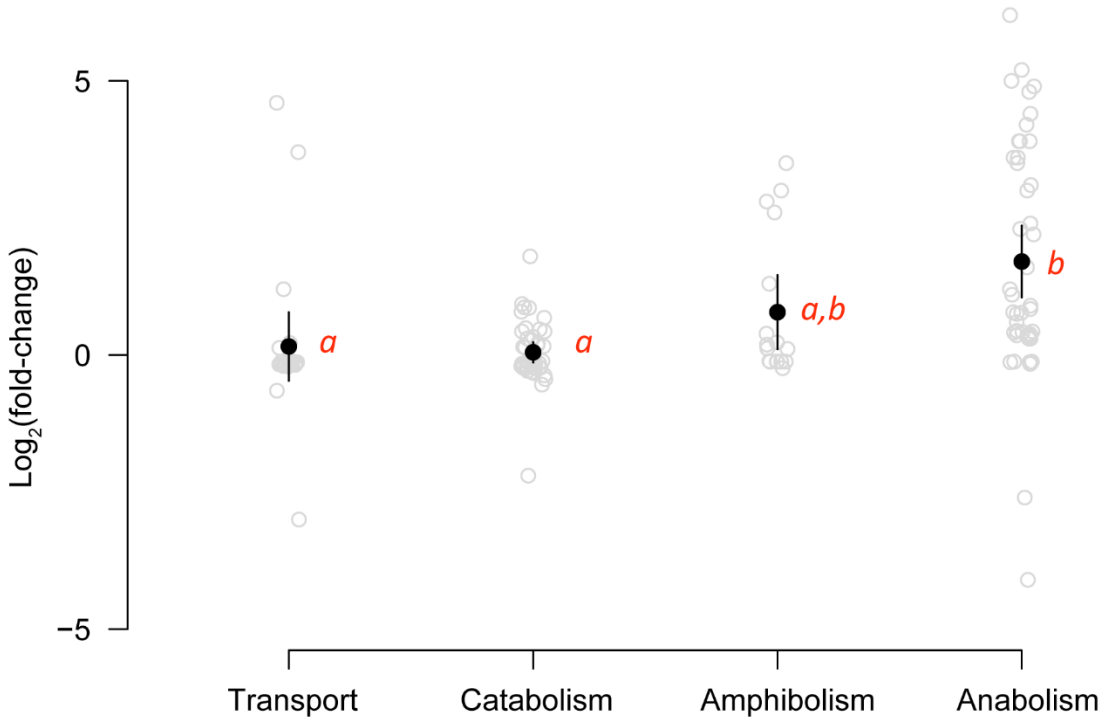

Supplemental Figure S2.5. Fitness differences for *R. pomeroyi* mutants with COG classifications that function in transport, catabolism, amphibolism (both catabolism and anabolism), or anabolism. Gray points are significant fitness changes in multi-bacterial communities; black points indicate the mean of significant fitness differences with 95% confidence intervals. Significant differences between categories are indicated by red letters *a* and *b*.

Table S2.1. IMG search results for metabolic potential of *M. donghaensis*, *V. hepatarius*, and *R. pomeroyi.*

Metabolic Process	**Gene ID**	**Locus Tag**	**Gene Product Name**	**Genome Name**
Assimilatory nitrate reduction	2889571834	Ga0440170_01_84031_86631	assimilatory nitrate reductase catalytic subunit	*Marivivens donghaensis* HF1
Nitrate/nitrite transport	2889571837	Ga0440170_01_89404_91083	nitrate/nitrite transport system ATP-binding protein	*Marivivens donghaensis* HF1
Nitrate/nitrite transport	2889571838	Ga0440170_01_91089_92171	nitrate/nitrite transport system permease protein	*Marivivens donghaensis* HF1
Nitrate/nitrite transport	2889571839	Ga0440170_01_92231_93598	nitrate/nitrite transport system substrate-binding protein	*Marivivens donghaensis* HF1
Ammonium assimilation	2889571852	Ga0440170_01_105083_106435	glutamine synthetase	*Marivivens donghaensis* HF1
Ammonium assimilation	2889573122	Ga0440170_17_148076_149503	glutamate synthase (NADPH/NADH) small chain	*Marivivens donghaensis* HF1
Ammonium assimilation	2889573124	Ga0440170_17_150233_154774	glutamate synthase (NADPH/NADH) large chain	*Marivivens donghaensis* HF1

Ammonium assimilation	2889572678	Ga0440170_11_280636_282021	glutamate dehydrogenase (NAD(P)+)	*Marivivens donghaensis* HF1
Dissimilatory nitrate reduction	2916743923	Ga0481171_06_79626_79805	nitrate reductase NapE	*Vibrio hepatarius* HF70
Ammonium assimilation	2916743332	Ga0481171_01_155577_156986	glutamine synthetase	*Vibrio hepatarius* HF70
Ammonium assimilation	2916743504	Ga0481171_03_38999_43462	glutamate synthase (NADPH/NADH) large chain	*Vibrio hepatarius* HF70
Ammonium assimilation	2916743505	Ga0481171_03_43483_44895	glutamate synthase (NADPH/NADH) small chain	*Vibrio hepatarius* HF70
Ammonium assimilation	2916745099	Ga0481171_17_51425_56266	glutamate dehydrogenase	*Vibrio hepatarius* HF70
Ammonium assimilation	637289773	SPO2295	L-glutamine synthetase (EC 6.3.1.2)	*Ruegeria pomeroyi* DSS-3
Ammonium assimilation	637289224	SPO1743	glutamate dehydrogenase	*Ruegeria pomeroyi* DSS-3

Ammonium assimilation	637291236	SPO3768	glutamate synthase (NADPH) large subunit (EC 1.4.1.13)	*Ruegeria pomeroyi* DSS-3
Ammonium assimilation	637291238	SPO3770	glutamate synthase (NADPH) small subunit (EC 1.4.1.13)	*Ruegeria pomeroyi* DSS-3
C-P lyase: substrate specific	2889572014	Ga0440170_03_48139_48480	protein PhnA	*Marivivens donghaensis* HF1
C-P lyase: substrate specific	2889572397	Ga0440170_11_12863_13279	PhnB protein	*Marivivens donghaensis* HF1
C-P lyase: substrate specific	2916743366	Ga0481171_02_22514_23629	2-aminoethylphosphonate-pyruvate transaminase	*Vibrio hepatarius* HF70
C-P lyase: broad specificity	637287960	SPO0468	alkylphosphonate utilization protein PhnG	*Ruegeria pomeroyi* DSS-3
C-P lyase: broad specificity	637287961	SPO0469	alkylphosphonate utilization protein PhnH	*Ruegeria pomeroyi* DSS-3
C-P lyase: broad specificity	637287962	SPO0470	alkylphosphonate utilization protein PhnI	*Ruegeria pomeroyi* DSS-3

C-P lyase: broad specificity	637287963	SPO0471	alkylphosphonate utilization protein PhnJ	*Ruegeria pomeroyi* DSS-3
C-P lyase: broad specificity	637287964	SPO0472	alkylphosphonate utilization protein PhnK	*Ruegeria pomeroyi* DSS-3
C-P lyase: broad specificity	637287965	SPO0473	alkylphosphonate utilization protein PhnL	*Ruegeria pomeroyi* DSS-3
C-P lyase: broad specificity	637287966	SPO0474	alkylphosphonate utilization protein PhnN	*Ruegeria pomeroyi* DSS-3
C-P lyase: broad specificity	637287968	SPO0476	alkylphosphonate utilization protein PhnM	*Ruegeria pomeroyi* DSS-3
C-P lyase: broad specificity	637288378	SPO0891	alkylphosphonate utilization protein PhnM, putative	*Ruegeria pomeroyi* DSS-3

Table S2.2. Mean generations of *R. pomeroyi* realized over the first 4 days of culture

Community	**Generations over 4 days**	**standard deviation**
Rp	6.4	0.13
Rp+V	5.4	0.12
Rp+M	5.8	0.06
Rp+V+M	4.4	0.09

Table S2.3. Statistics associated with transposon insertion reads that were trimmed and mapped to the *R. pomeroyi* genome from TRANSIT TPP output

Condition	**Rep**	**Total Reads**	**Trimmed Reads**	**Mapped Reads**	**Percent Mapped**	**Insertion Sites**
Initial Library	1	11273142	4360270	3857733	0.8847	49548
Initial Library	2	8118575	3620276	3161913	0.8734	52877
Initial Library	3	6893616	3030343	2626152	0.8666	55549
Initial Library	4	8915564	4357750	3780643	0.8676	59618
Rp	1	10970318	812423	683144	0.8409	46549
Rp	2	11962253	3513203	2942767	0.8376	50647
Rp	3	8166359	2380137	1957370	0.8224	51329
Rp	4	8683279	1822029	1544658	0.8478	45396
Rp+V	1	12039463	2386758	2094851	0.8777	47374
Rp+V	2	12488290	3063769	2681615	0.8753	49295
Rp+V	3	11230683	2336137	2035010	0.8711	47213
Rp+V	4	15247311	2809497	2458482	0.8751	48850
Rp+M	1	12035705	2706510	2340246	0.8647	49335
Rp+M	2	14060261	3623641	3133965	0.8649	52420
Rp+M	3	9409195	3318129	2788195	0.8403	54893

Rp+M	4	14070202	3475382	3047851	0.877	49675
Rp+V+M	1	4762902	810063	742781	0.9169	45144
Rp+V+M	2	8278437	1786446	1640589	0.9184	44020
Rp+V+M	3	6359470	1413777	1264975	0.8947	46895
Rp+V+M	4	14212015	2929608	2582185	0.8814	48619

CHAPTER 3

BACTERIAL GENE FITNESS IN INCREASINGLY COMPLEX COMMUNITIES [1]

[1] Schreier, JE, Brown, SE, Uchimiya, M, Schroer, WF, Smith, CB, Moran, MA. To be submitted to *FEMS Microbiology Ecology*.

Abstract

Phytoplankton exude labile dissolved organic matter providing a shared pool of resources for the heterotrophic bacteria that live in their vicinity, creating a dense network of interactions. Bacteria associated with phytoplankton and their organic matter are consistently and reproducibly dominated by a few phylogenetic groups, suggesting that there are ecological factors guiding community assembly. Understanding the interactions between these bacterial taxa remain challenging as they are largely driven by exchange of and competition for metabolites. Here, we use the diatom *Thalassiosira pseudonana* CCMP13356 to generate model phycosphere communities with up to nine heterotrophic bacteria assembled in a hierarchical pattern. Direct fitness of genes that mediate bacterial interactions in increasingly species-rich communities were identified using a transposon mutant library of copiotrophic bacterium *Ruegeria pomeroyi* DSS-3 present in all communities. We find strong higher-order interactions present in communities of low and intermediate species richness, that weaken at high levels of species richness. Our findings demonstrate that fitness is largely driven by changes in the competition landscape determined by the number and types of bacteria that are added to the communities.

Introduction

The surface ocean microbiome is home to a dense network of coexisting taxa performing a multitude of functions (1, 2), culminating in one of the largest annual fluxes of carbon on Earth. Theory and empirical evidence demonstrate that ecosystem function, such as remineralization of labile organic matter by heterotrophic bacteria, can saturate with increasing biodiversity (3). Underlying this are interactions within bacterial communities that are

heightened by the combined effects of the metabolic dissimilarity, due to diverse community members, and the complexity/supply rate of the resource pool (4-6). Increasing metabolic dissimilarity can shift interactions between coexisting taxa from negative (e.g. competition, antagonism) to positive (e.g. niche partitioning, cross-feeding) (3, 4) due to a decrease in direct competition for resources and an increase in the chance that functions will be complementary. The complexity of resources available can create more niche space for taxa to coexist (7), while the flux of resources controls bacterial productivity, triggering density-dependent mechanisms such as production of allelopathic compounds (8). These influences are intertwined, and it is their net effect that guides bacterial community function (3, 4, 6, 7, 9-12).

In nutrient-rich coastal oceans, diatoms contribute up to 75% of primary production annually (13). A portion of fixed carbon is exuded or lost as labile dissolved organic matter, creating a phycosphere; the fundamental ecological interface between phytoplankton and the heterotrophic bacterial community forming around them (14, 15). Across diatom phycospheres, a functional and taxonomic diversity of heterotrophic bacterial members have been identified, and each phycosphere supports from few to many coexisting bacterial species (16-18). Observation of dominance by a few phylogenetic groups of heterotrophic bacteria (Alphaproteobacteria, Gammaproteobacteria, Bacteroidetes) (19) suggests that there are likely ecological factors guiding community assembly (20).

Disentangling the network of interactions between these bacterial taxa remains challenging. Model phycosphere communities are investigated using either a bottom-up design (pairing an axenic phytoplankton with one to a few bacterial isolates) (9, 21) or a top-down design (isolating a phytoplankton along with its native phycosphere community or seeding an axenic phytoplankton with a seawater inoculum) (22, 23). In this study, we use a bottom-up

design with the model diatom *Thalassiosira pseudonana* to create a model phycosphere with substrate supply rate and microbial density with high fidelity to environmental conditions. We inoculated the diatom model system with up to nine heterotrophic bacteria in a hierarchical pattern that allowed a comparison of more species-rich communities to their simpler component parts. One bacterium, *Ruegeria pomeroyi,* was present in all communities and inoculated in the form of a transposon mutant library. Differences in the success of individual *R. pomeroyi* mutants, assessed as growth rate over 8 days, provided insights into the benefits and challenges of living in increasingly species-rich communities. The genetic concept of epistasis was applied to determine the non-linear effects of increasingly complex communities, providing a metric of higher-order interactions. We find that coalescence of phycosphere communities of low and intermediate richness alters the competition for diatom derived organic matter in a non-linear manner, indicative of higher-order interaction. Yet competition occurring in coalescence of the most complex phycosphere community could be approximated as the mean of the fitness effects of the simple component communities. Nonetheless, strong interactions for diatom-derived organic matter were observed at every complexity level of the coalesced communities. We find that resource acquisition by *R. pomeroyi* is an emergent property of communities of low and intermediate richness due to high-order interactions that, surprisingly, weaken with increasing species richness.

Results

*Phycosphere Communities***.** We established 15 model phycosphere communities with varied bacterial taxonomic composition and richness that were reliant on photosynthate released by the co-cultured diatom *Thalassiosira pseudonana.* The communities were established in a

hierarchical manner to enable comparison of higher-order communities to their simpler components. *Ruegeria pomeroyi*, a marine bacterium cultured from coastal seawater (24), served as the focal bacterium, inoculated in the form of a randomly barcoded transposon mutant pool. From one to eight additional heterotrophic bacteria isolated from coastal seawater that had been enriched with phytoplankton-derived metabolites (25) were added: Alphaproteobacteria genera *Marivivens*, *Thalassospira*, *Phaeobacter*, *Pseudooceanicola*, *Celeribacter* and Gammaproteobacteria genera *Vibrio* and *Pseudoalteromonas* (26). The hierarchical communities consisted of *R. pomeroyi* plus one additional bacterium (*Rp*+1; 8 communities), two additional bacteria (*Rp*+2; 4 communities), four additional bacteria (*Rp*+4; 2 communities), and eight additional bacteria (*Rp*+8) (Fig. 3.1A). Bacteria were inoculated as a 1:1 mixture of the *R. pomeroyi* mutant pool and the sum of the other bacteria. Thus, the same number of *R. pomeroyi* mutants were inoculated into all communities to establish an equal initial mutant diversity and proportion in each community (e.g. *Rp*+2 inoculum consisted of ~$5x10^4$ cells ml^{-1} *R. pomeroyi*, $2.5x10^4$ cells ml^{-1} bacterium X, and $2.5x10^4$ cells ml^{-1} bacterium Y).

The final cell abundance in the total community (cells ml^{-1}_{final}) and final cell yield (cells ml^{-1}_{final} - cells $ml^{-1}_{initial}$) did not change with species richness, likely reflecting a limitation by the available diatom exudates (Fig. S3.1). However, the yield of *R. pomeroyi* cells (CFU_{final} - $CFU_{initial}$) decreased with increasing richness (Fig. 1B). In communities of low and intermediate richness (*Rp*+1, *Rp*+2, *Rp*+4), *R. pomeroyi* averaged 44% of the initial inoculum, increasing to an average of 68% of the mature community as measured by 16S rRNA amplicons (Fig. S3.2). At high species richness (*Rp*+8), *R.pomeroyi* comprised 31% of the initial inoculum, only increasing to 38% over the course of 8 days (Fig. S3.2). All inoculated bacterial species coexisted with *R. pomeroyi* throughout the 8 d experiment. These results suggest that it became

increasingly difficult for *R. pomeroyi* to obtain phytoplankton derived substrates as richness increased, possibly due to interactions between bacterial taxa such as resource competition or direct antagonism.

Mutant Fitness Overview. Fitness was determined for 2,223 single-gene *R. pomeroyi* transposon mutants (Dataset S3.1). Differences in *R. pomeroyi* mutant fitness as a function of species richness was calculated as the fold-change in fitness of each mutant in higher-order communities relative to the component communities; statistical significance at $p \leq 0.05$ was assigned by randomization tests with 10,000 permutations corrected for multiple comparisons using the Benjamini-Hochberg procedure. A significant negative fold-change represented disrupted genes that had a greater contribution to mutant fitness when *R. pomeroyi* interacted with a more complex bacterial community, whereas a positive fold-change represented disrupted genes that were more costly in more complex communities (Fig S3.3). Overall, 520 single-gene mutant fitness values were altered across at least one community coalescence, with 44% of these mutants being unique to the comparison of *Rp+2* compared to *Rp+1* (Fig 3.2A). Only 4% of significant mutants were observed at every level of richness for coalescent communities, and these included mutants for vitamin B_{12} and glutamate synthesis, urea catabolism, thymidine salvage, a type I target repeat protein secretion, four regulatory enzymes of the LysR, MerR, and GntR families, and other poorly annotated genes. These 22 phenotypes represented fitness outcomes that were significantly changed at every level of richness.

Mutants were categorized by function of the deleted gene and direction of fitness change into modes of ecological interactions such as those involved in resource acquisition (18%), crossfeeding (2%), chemically mediated interactions (2%), and adaptation to altered environmental conditions (4%). The remaining mutants had genes disrupted in central carbon

metabolism (3%), regulation (9%), and functions not well annotated, not clearly linked to bacterial interactions, or hypothetical (64%) (Dataset S3.2). The significant mutants with poorly annotated functions might reflect disrupted genes important during bacterial interactions, yet more work is required to identify the role these genes play. Based on the annotated gene categories, changes in fitness of *R. pomeroyi* in the coalescent communities were largely driven by resource competition for diatom derived organic matter, while crossfeeding and chemically mediated interactions (inclusive of 2 antagonism-related genes) each involved 9-fold fewer genes than competition.

Epistasis in communities of low and intermediate richness. The genetic concept of epistasis was applied to the statistically significant mutant phenotypes emerging in increasingly complex communities. Epistasis quantifies the effect of a gene mutation in the presence of another, asking whether or not phenotype effects are additive (27, 28). Epistasis-like patterns have been observed in microbial communities (28), for example non-additive effects of substrate combinations on microbial community composition (29) and in pairwise bacterial interactions when co-cultured with yeast (30). In our study, the epistasis null model compares a mutant's fitness in a coalescent community with the average of that mutant's fitness in the two component communities, which is the case if fitness effects are additive. Deviations from the null model indicate that higher-order interactions emerged in the multi-species communities, with positive values of epistasis occurring when a mutant's fitness is higher in a more complex community, and negative values of epistasis occurring when a mutant's fitness is lower in a more complex community.

Epistasis was calculated for all mutants that had a statistically significant fitness change in a coalescent community compared to the simpler components. Overall, mean epistasis was significantly negative suggesting that genes contributed more to fitness in the coalescent

communities compared to the simpler component communities (Fig. 3.2B). Next, we subdivided the mutants based on the categorized function of their disrupted gene to ask whether epistasis values were the same across categories (Fig. 3.2C). In comparisons of communities of *Rp*+2 relative to *Rp*+1, a negative mean epistasis value was calculated for the gene categories of resource acquisition, altered environment adaptation, and central carbon metabolism (Fig. 3.2C). In comparisons of communities *Rp*+4 relative to *Rp*+2, a positive mean epistasis value was calculated for gene categories of resource acquisition and regulation (Fig. 3.2C). Finally, in comparisons of communities of *Rp*+8 relative to *Rp*+4, a mean epistasis value that did not differ from zero was found for all gene categories. (Fig. 3.2C). Thus higher-order interactions among bacterial species appeared to play a substantial role in altering fitness of *R. pomeroyi* in a model phycosphere diatom-derived organic matter in communities of low and intermediate richness, but less so in the most complex coalescent community.

We looked deeper into the emerging interactions by focusing on genes indicative of resource acquisition, the largest category of fitness changes. Genes in the resource acquisition category include those encoding enzymes for the transport or catabolism of organic matter provided by the diatom, and therefore a possible subject of competition among the bacterial strains. An epistasis of |0.5| was set as the threshold to identify genes for which there was strong fitness alteration (i.e., a doubling or halving of predicted fitness in the coalescent communities relative to the epistasis null model); these represent 42% of resource acquisition mutants with significant fitness changes in resource allocation genes. A quarter of these mutants had strong positive epistasis in coalescent communities, indicating that the particular gene for resource acquisition contributed less to fitness than expected in coalescent communities. This included genes for acquisition of the diatom metabolites ectoine (with roles as both a substrate and osmolyte) and nitrogen-rich

organics polyamines, methylamines, and branched chain amino acids. The remaining three quarters of the mutants had strong negative epistasis in coalescent communities, indicating that particular gene contributed more to fitness than predicted by the null model. These included genes for acquisition of DMSP (with roles as both a substrate and an osmolyte), sulfur-rich organic acid cysteate, nitrogen-rich organics urea, aspartate, glutamate, arginine, C4 organic acids, and nucleic acids, and different metabolites in the methylamine and branched chain amino acids categories than found in the positive epistasis mutants; all of these contributed more to fitness in coalesced communities than expected.

Conclusion

Direct measures of mutant fitness in a model system with high fidelity to natural phycospheres revealed how species richness affected the functioning of a focal bacterium. As phycosphere communities increased in species richness, *R. pomeroyi* represented a smaller fraction of the community, and coexistence of all bacteria was maintained. A fundamental question in ecology is how diverse communities coexist in spite of competitive exclusion. Interactions between two competing species have been well studied (31, 32); in communities with more than two members, higher-order interactions are proposed to stabilize coexistence between diverse taxa, reflecting the plasticity of an organism's response (33, 34, 35). Epistasis-like measures of mutant fitness in microbial communities of increasing species richness indicated the presence of higher-order interactions in phycosphere bacterial communities. We find fitness to be largely driven by changes in the competition landscape that is determined by the number and types of bacteria that are added to the communities. Strong higher-order interactions emerged in low and intermediate richness coalescent communities over substrates of which 75%

of them are organic nitrogen, in line preferences of *R. pomeroyi* that foster niche partitioning (36). In the high richness coalescent community, strong negative epistasis was observed for acquisition of organic acids; evidence that further promotes Rhodobacterales as having preference for organic acids over sugars (37). Nonetheless, epistasis of the high richness coalescent community indicated the effects of the component communities were additive (i.e. the average of the two). Together these data suggest that during the initial colonization of a phycosphere, a focal bacterium will respond to the presence of other organisms by altering resource acquisition strategies. As more bacterial species are added to a maturing phycosphere, higher-order interactions saturate and are only weakly altered by addition of another member, as all members fit into their ecological niche. The development and life of a phycosphere provides a complex and dynamic resource pool that is altered by competition between bacteria and stabilized by higher-order interactions that maintain coexistence.

Materials and Methods

Model phycosphere communities. Bacteria selected for this study were members of the Alphaproteobacteria (*Ruegeria pomeroyi* DSS-3 [Bar-Seq library], *Marivivens donghaensis* HF1, *Thalassospira sp.* HF15, *Phaeobacter* sp. HF9A, *Pseudooceanicola* sp. HF7, *Celeribacter sp.* HF31) and Gammaproteobacteria (*Vibrio hepatarius* HF70, *Vibrio diazotrophicus* HF9B, *Pseudoalteromonas* sp. HF66) that were isolated from phycosphere enrichment cultures; these isolates have 16S rRNA sequences with >66 % average nucleotide identity to bacteria known to associate with marine phytoplankton (25, 26). Prior to experimentation, all bacteria except the *R. pomeroyi* Bar-Seq library were inoculated into ½ YTSS medium from isolated colonies and grown overnight at 30°C and 200 RPM. The concentrated Bar-Seq library cryostock was thawed

on ice and inoculated at ~0.2 OD YTSS+KAN (50 µg ml^{-1}) and grown for ~6 h resulting in one doubling period. At the same time, overnight cultures of the other bacteria were sub-cultures and grown to exponential phase (0.4 – 0.6 OD_{600}). Cells were pelleted at 8,000 x g, washed 5 times, and resuspended to 10^6 cells ml^{-1} in 0.2 µm filtered 20 ppt carbon-clean artificial seawater. All bacteria were adjusted to the same OD. Four aliquots of washed transposon mutants were stored at -80°C and were used to determine mutant composition prior to selection.

Thalassiosira pseudonana CCMP 1335 (National Center for Marine Algae and Microbiota) was maintained in exponential growth by diluting into carbon-clean fresh L1+Si in 20 ppt ASW every 4 d to a starting density of ~10^4 cells ml^{-1} for 3 consecutive transfers. Diatom cultures were inoculated into some size acid-washed, combusted glass culture tubes with 20 ml L1+Si at 20 ppt ASW, and seeded with bacteria at ~10^5 cells ml^{-1} to establish 16 communities of varying bacterial species richness. *R. pomeroyi* Bar-Seq library was added to all treatments at ~10^5 cells ml^{-1}; treatments with additional bacteria were inoculated such that half of the community was *R. pomeroyi*, while the other half of the community was either a single isolate or a mixture of isolates. Membership of communities was determined by random draw initially, and then assembled into more complex communities in a hierarchical pattern. Communities were: *Rp* (*R. pomeroyi* alone; richness of 1), *Rp* + 1 (8 treatments of *R. pomeroyi* in pairwise combination with each isolate; richness of 2), *Rp* + 2 (4 treatments of *R. pomeroyi* in combination with two isolates; richness of 3), Rp + 4 (2 treatments of *R. pomeroyi* in combination with four isolates; richness of 5), and *Rp* + All (1 treatment of *R. pomeroyi* with all eight isolates; richness of 9) (n=4).

Cell enumeration. Bacterial abundance for treatments was determined for each species based on visually distinct colony forming units (CFUs) on ½ YTSS and YTSS+KAN plates on days 0, 4, and 8. Diatom and total bacterial abundance was determined by flow cytometry on an Agilent Quanteon on days 0, 1, 2, 3, 4, 6, and 8. Samples were fixed with a final concentration of 1% paraformaldehyde in the dark at room temperature for 15 min before storing at -80°C. Samples were diluted in 0.2 µm filter-sterilized 20 ppt ASW and stained with DAPI (1 µg ml^{-1}). Total bacteria were measured by DAPI excitation/emission, whereas diatom abundance was measured using chlorophyll fluorescence, and cell counts were determined using the Agilent Quanteon software.

DNA extraction, sequencing, and bioinformatic analysis. On day 0, 4, and 8, 5 ml of culture was sequentially filtered through 25 mm 2.0 µm and 0.2 µm polycarbonate filters in acid-washed Swinnex filter units and filters were stored separately at -80°C. DNA was extracted from 0.2 µm filters using the Zymobiomic DNA miniprep kit according to manufacturer's instructions. The V4-V5 region of the 16S sequence was amplified using Quince V4V5 primers. Transposon insertion barcodes were amplified from the initial library and DNA extracted from 8 d old cultures using custom primers with internal barcodes; BarSeq amplicons were pooled equally by time point and pools were cleaned using the MAGBIO HighPrep PCR protocol for selection of DNA fragments between 100bp – 400bp. Library preparation and sequencing was performed at the Georgia Genomics and Bioinformatics Core facility.

16S amplicons were sequenced on Illumina MiSeq SE150 Flow Cell, and ASVs were assigned using DADA2 (38), and a custom blast+ script (39) was used to match ASVs to a database containing the 16S sequence of all strains used in this experiment. Only ASVs with

>99% identity to database sequences were retained for analysis. Amplicon reads were converted to relative abundance and compared to CFU data for validation.

Pooled BarSeq amplicons were sequenced on a NextSeq500 1x150bp high output flow cell, and were processed using the perl scripts (MapTnSeq.pl, DesignRandomPool.pl, and MultiCodes.pl) outlined in Wetmore (40) to obtain a table of transposon insertions matched to genome positions. The BarSeq mutant library was composed of 42,061 unique mutants, curated to 28,062 that fell within the central 90% of a protein coding region, resulting in an average of 10 mutant strains per gene. Reads were normalized by scaling the read count in each sample to the grand mean across all samples (Dataset S3.3).

Fitness analysis. Relative mutant fitness (*W*) was determined following Schreier et. al. 2023 using the following equation:

$$W = \frac{\ln\left[N(t2) * \frac{d}{N(t1)} + 1\right]}{\ln\left[(1 - N(t2)) * \frac{d}{\left(1 - N(t1)\right)} + 1\right]}$$

Where N(t1) represents the average frequency of a mutant in the population at the start of the experiment, N(t2) is the frequency of a mutant in the population at the end of the experiment, and d (expansion factor) represents the fold change of the total mutant population during the 8 d growth period. Expansion factors were calculated from CFU counts of *R. pomeroyi* mutants. Mutants with <10 average reads between the initial and final time points were removed from analysis. Null mutations from Schreier et al 2023 were used to scale the dataset; correction factors were small suggesting these mutations were null in this experiment as well.
Mean relative fitness for 2,223 out of 4,293 coding regions was determined from four replicate measurements of fitness, and fitness differences were calculated as:

$$log_2(\frac{W_{multi-bacteria} + \Psi}{W_{Rp} + \Psi})$$

where Ψ is a small number (0.01) to prevent a zero or non-integer. Statistical significance of fitness differences was determined by randomization tests (41) with 10,000 permutations using a custom script , and p-values were adjusted for multiple comparisons using the Benjamini-Hochberg procedure within the stats (v3.6.2) package in R.

All plots and statistical analyses were performed in R v4.0.1 (42) using the packages tidyverse (43) and data.table (44). Figures were generated in R and Adobe Illustrator 2020.

Author Contributions: JES and MAM conceived the study, JES, SEB, MU performed the study, JES, WFS, and MAM analyzed the data, and JES and MAM wrote the paper.

Acknowledgements

We thank F. X. Ferrer González, W. F. Schroer, M. Uchimiya, M. M. Hamilton, and Z. S. Cooper, for helpful suggestions, J. Nelson at the UGA CTEGD Cytometry Shared Resource Lab provided guidance on flow cytometry protocols, and the UGA GGBC prepared libraries for sequencing. This work was supported by Simons Foundation grant 542391 to MAM within the Principles of Microbial Ecosystems Collaborative, and NSF Graduate Research Fellowship Program award GRFP-1445117 to JES.

References:

1. G. Lima-Mendez *et al.*, Determinants of community structure in the global plankton interactome. *Science* **348**, 1262073 (2015).
2. D. M. Needham, J. A. Fuhrman, Pronounced daily succession of phytoplankton, archaea and bacteria following a spring bloom. *Nature Microbiology* **1**, 1-7 (2016).
3. X. Yu, M. F. Polz, E. J. Alm, Interactions in self-assembled microbial communities saturate with diversity. *The ISME Journal* **13**, 1602-1617 (2019).
4. A. Jousset, B. Schmid, S. Scheu, N. Eisenhauer, Genotypic richness and dissimilarity opposingly affect ecosystem functioning. *Ecology Letters* **14**, 537-545 (2011).
5. J. Kehe *et al.*, Positive interactions are common among culturable bacteria. *Science Advances* **7**, eabi7159 (2021).
6. S. Freilich *et al.*, Competitive and cooperative metabolic interactions in bacterial communities. *Nature Communications* **2**, 589 (2011).
7. M. Dal Bello, H. Lee, A. Goyal, J. Gore, Resource–diversity relationships in bacterial communities reflect the network structure of microbial metabolism. *Nature Ecology & Evolution* **5**, 1424-1434 (2021).
8. G. C. Sharpe, S. M. Gifford, A. N. Septer, A model roseobacter, *Ruegeria pomeroyi* DSS-3, employs a diffusible killing mechanism to eliminate competitors. *mSystems* **5**, e00443-00420 (2020).
9. J. E. Schreier, C. B. Smith, T. R. Ioerger, M. A. Moran, A mutant fitness assay identifies bacterial interactions in a model ocean hot spot. *Proceedings of the National Academy of Sciences* **120**, e2217200120 (2023).

10. D. W. Rivett, T. Bell, Abundance determines the functional role of bacterial phylotypes in complex communities. *Nature Microbiology* **3**, 767-772 (2018).
11. A. Pascual-Garcia, S. Bonhoeffer, T. Bell, Metabolically cohesive microbial consortia and ecosystem functioning. *Philosophical Transactions of the Royal Society B Biological Sciences* **375**, 20190245 (2020).
12. J. E. Goldford *et al.*, Emergent simplicity in microbial community assembly. *Science* **361**, 469-474 (2018).
13. D. M. Nelson, P. Tréguer, M. A. Brzezinski, A. Leynaert, B. Quéguiner, Production and dissolution of biogenic silica in the ocean: revised global estimates, comparison with regional data and relationship to biogenic sedimentation. *Global Biogeochemical Cycles* **9**, 359-372 (1995).
14. J. R. Seymour, S. A. Amin, J.-B. Raina, R. Stocker, Zooming in on the phycosphere: the ecological interface for phytoplankton–bacteria relationships. *Nature Microbiology* **2**, 1-12 (2017).
15. W. Bell, R. Mitchell, Chemotactic and growth responses of marine bacteria to algal extracellular products. *The Biological Bulletin* **143**, 265-277 (1972).
16. S. A. Amin, M. S. Parker, E. V. Armbrust, Interactions between diatoms and bacteria. *Microbiology and Molecular Biology Reviews* **76**, 667-684 (2012).
17. G. Behringer *et al.*, Bacterial communities of diatoms display strong conservation across strains and time. *Frontiers in Microbiology* **9**, 659 (2018).
18. O. N. Johansson *et al.*, Friends with benefits: Exploring the phycosphere of the marine diatom Skeletonema marinoi. *Frontiers in Microbiology* **10**, 1828 (2019).

19. K. E. Helliwell, A. A. Shibl, S. A. Amin, "The Diatom Microbiome: New Perspectives for Diatom-Bacteria Symbioses" in The Molecular Life of Diatoms. (Springer, 2022), pp. 679-712.
20. E. Kazamia, K. E. Helliwell, S. Purton, A. G. Smith, How mutualisms arise in phytoplankton communities: building eco-evolutionary principles for aquatic microbes. *Ecology Letters* **19**, 810-822 (2016).
21. B. P. Durham *et al.*, Cryptic carbon and sulfur cycling between surface ocean plankton. *Proceedings of the National Academy of Sciences* **112**, 453-457 (2015).
22. J. Mönnich *et al.*, Niche-based assembly of bacterial consortia on the diatom *Thalassiosira rotula* is stable and reproducible. *The ISME Journal* **14**, 1614-1625 (2020).
23. S. L. Jackrel, J. W. Yang, K. C. Schmidt, V. J. Denef, Host specificity of microbiome assembly and its fitness effects in phytoplankton. *The ISME Journal* **15**, 774-788 (2021).
24. J. M. González, R. P. Kiene, M. A. Moran, Transformation of sulfur compounds by an abundant lineage of marine bacteria in the α-subclass of the class Proteobacteria. *Applied and Environmental Microbiology* **65**, 3810-3819 (1999).
25. H. Fu, M. Uchimiya, J. Gore, M. A. Moran, Ecological drivers of bacterial community assembly in synthetic phycospheres. *Proceedings of the National Academy of Sciences* **117**, 3656-3662 (2020).
26. H. Fu, C. B. Smith, S. Sharma, M. A. Moran, Genome sequences and metagenome-assembled genome sequences of microbial communities enriched on phytoplankton exometabolites. *Microbiology Resource Announcements* **9**, e00724-00720 (2020).
27. D. Segrè, A. DeLuna, G. M. Church, R. Kishony, Modular epistasis in yeast metabolism. *Nature Genetics* **37**, 77-83 (2005).

28. J. Diaz-Colunga *et al.*, Global epistasis on fitness landscapes. *Philosophical Transactions of the Royal Society B* **378**, 20220053 (2023).
29. A. R. Pacheco, M. L. Osborne, D. Segrè, Non-additive microbial community responses to environmental complexity. *Nature Communications* **12**, 2365 (2021).
30. F. Senne de Oliveira Lino, D. Bajic, J. C. C. Vila, A. Sánchez, M. O. A. Sommer, Complex yeast–bacteria interactions affect the yield of industrial ethanol fermentation. *Nature Communications* **12**, 1498 (2021).
31. P. Chesson, Mechanisms of maintenance of species diversity. *Annual Review of Ecology and Systematics* **31**, 343-366 (2000).
32. J. Friedman, L. M. Higgins, J. Gore, Community structure follows simple assembly rules in microbial microcosms. *Nature Ecology & Evolution* **1**, 0109 (2017).
33. J. M. Levine, J. Bascompte, P. B. Adler, S. Allesina, Beyond pairwise mechanisms of species coexistence in complex communities. *Nature* **546**, 56-64 (2017).
34. J. Grilli, G. Barabás, M. J. Michalska-Smith, S. Allesina, Higher-order interactions stabilize dynamics in competitive network models. *Nature* **548**, 210-213 (2017).
35. T. Gibbs, S. A. Levin, J. M. Levine, Coexistence in diverse communities with higher-order interactions. *Proceedings of the National Academy of Sciences* **119**, e2205063119 (2022).
36. F. X. Ferrer-González *et al.*, Resource partitioning of phytoplankton metabolites that support bacterial heterotrophy. *The ISME Journal* **15**, 762-773 (2021).
37. M. Gralka, S. Pollak, O. X. Cordero, Fundamental metabolic strategies of heterotrophic bacteria. *bioRxiv*, 2022.2008. 2004.502823 (2022).
38. B. J. Callahan *et al.*, DADA2: High-resolution sample inference from Illumina amplicon data. *Nature Methods* **13**, 581-583 (2016).

39. C. Camacho *et al.*, BLAST+: architecture and applications. *BMC Bioinformatics* **10**, 1-9 (2009).
40. K. M. Wetmore *et al.*, Rapid quantification of mutant fitness in diverse bacteria by sequencing randomly bar-coded transposons. *mBio* **6**, e00306-00315 (2015).
41. P. H. Crowley, Resampling methods for computation-intensive data analysis in ecology and evolution. *Annual Review of Ecology and Systematics*, 405-447 (1992).
42. R. C. Team, R: A language and environment for statistical computing. (2013).
43. H. Wickham *et al.*, Welcome to the Tidyverse. *Journal of Open Source Software* **4**, 1686 (2019).
44. M. Dowle *et al.*, Package 'data. table'. Extension of 'data. frame' (2019).

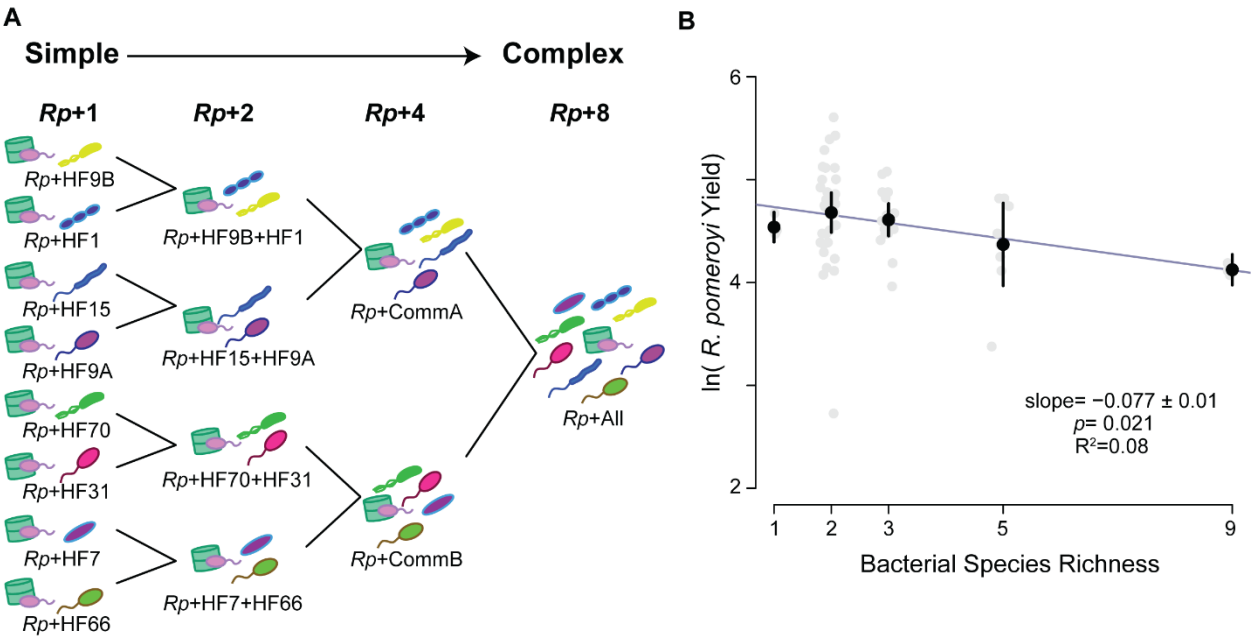

Fig 3.1. A. Schematic of the hierarchical experimental design coalescing more simple communities into more complex. **B.** *R. pomeroyi* cell yield after 8 d decreased as a function of species richness. Black symbols indicate mean cell yields and grey symbols indicate cell yields for each community and replicate.

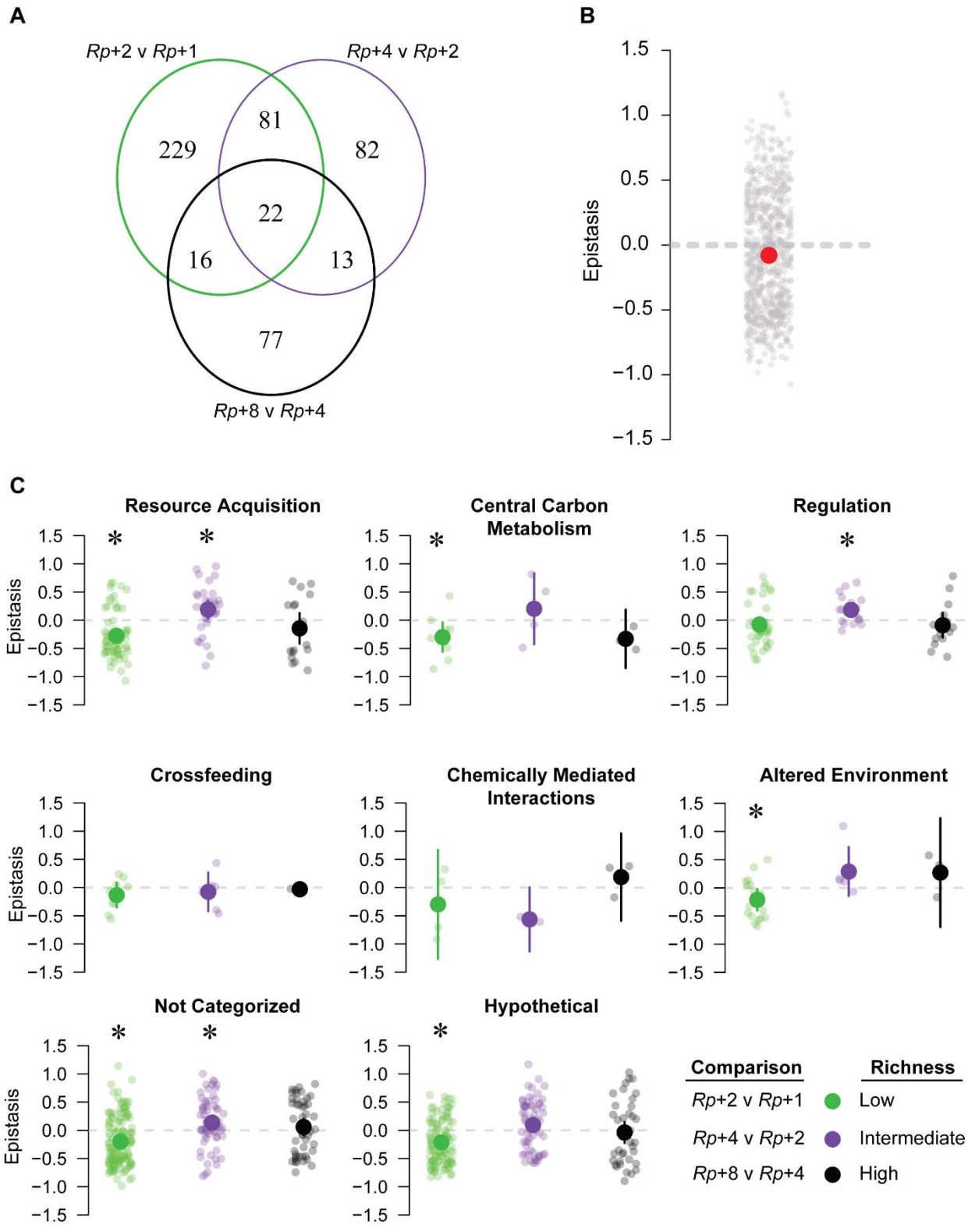

Fig 3.2. Mutant epistasis. **A.** Venn diagram displaying the number of significant phenotypes observed in each coalescent community. **B.** Epistasis for all significant phenotypes. Grey points

represent epistasis metrics for mutants that had statistically significant differences. Red point represents the mean and 95% confidence intervals. **C.** Epistasis of all significant phenotypes grouped by gene function and separated by richness of coalesced communities. Dark points represent the mean and 95% confidence intervals of epistasis and transparent points represent epistasis for individual mutants. Asterisks denote non-zero measures of mean epistasis.

A.

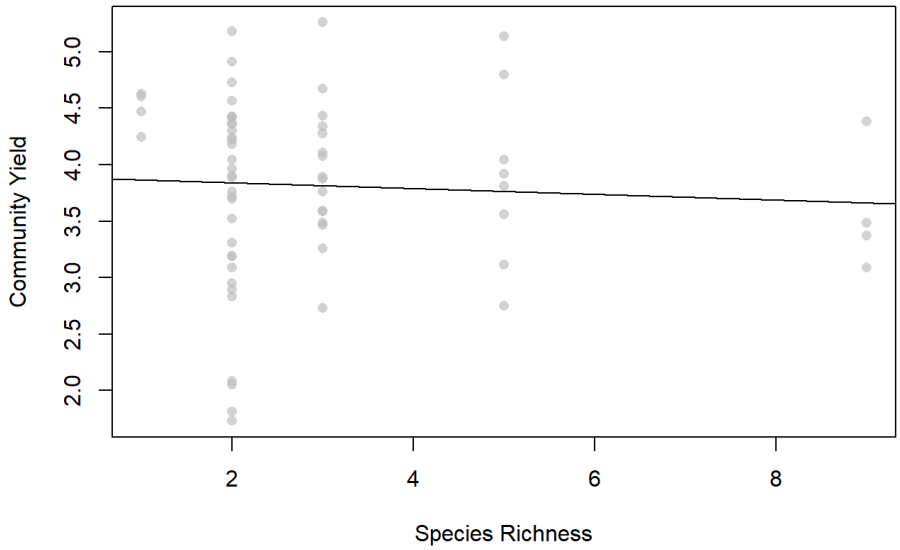

B.

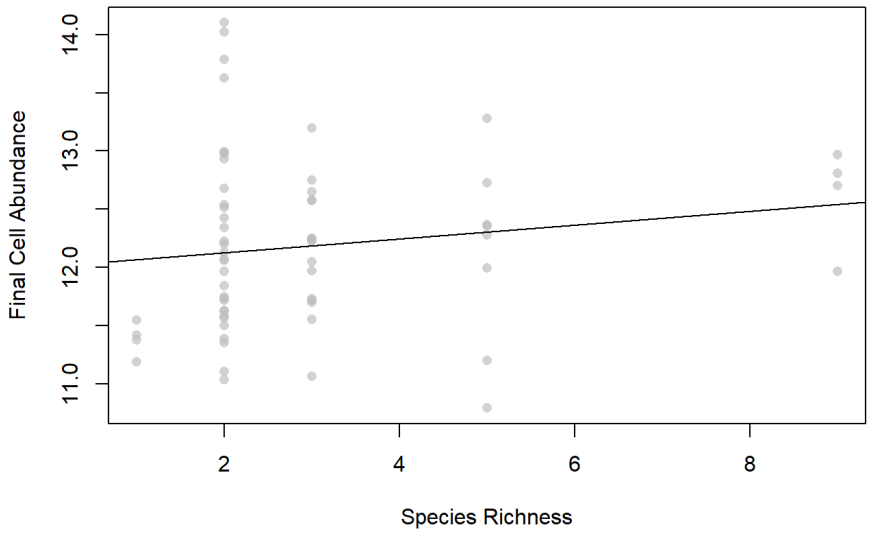

Fig S3.1 A. Yield of the bacterial community and **B.** $\log_{10}$(Final Cell Abundance) of the bacterial community. Linear regressions are not statistically significant relationships ($p > 0.05$)

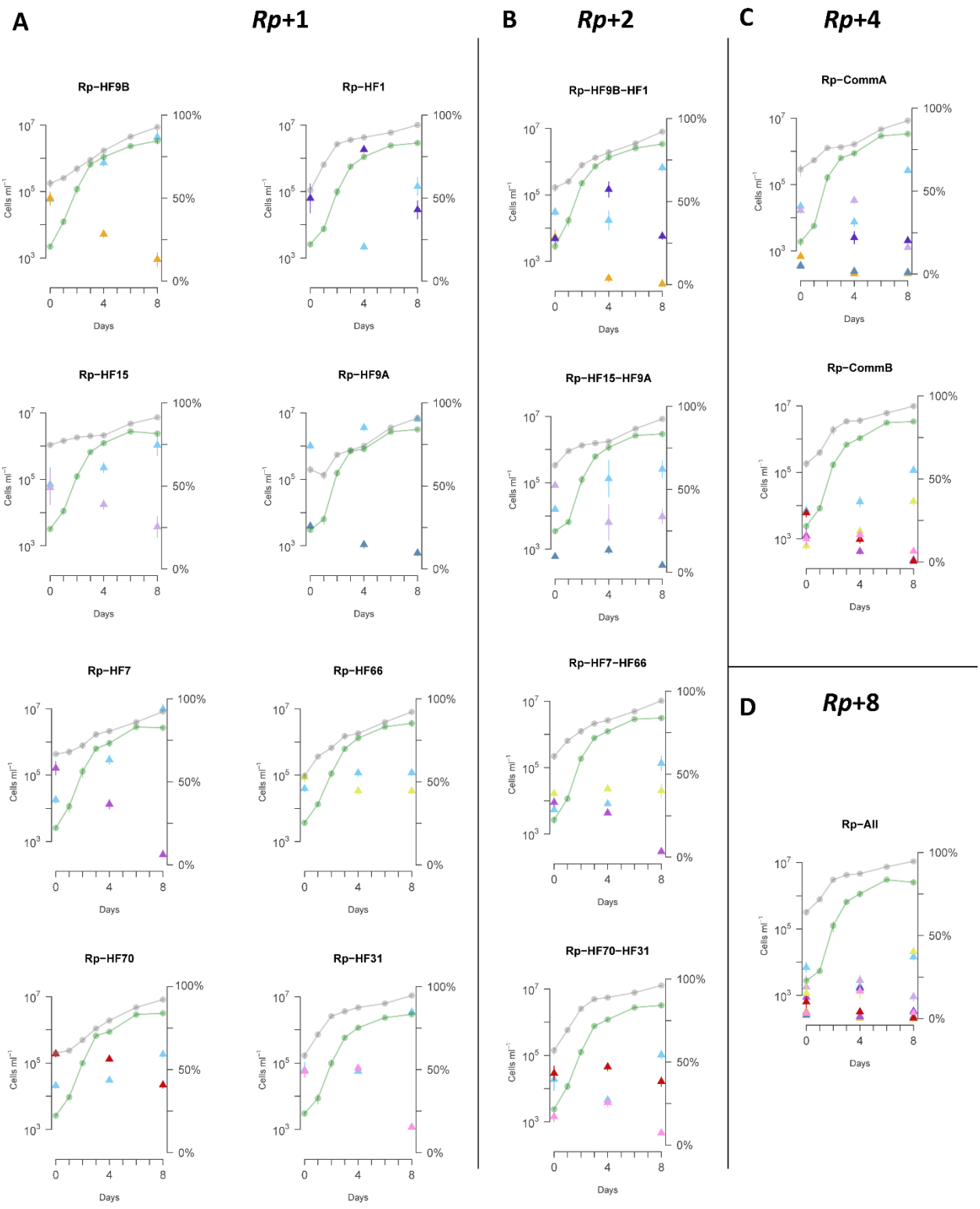

Fig S3.2. Diatom (connected green circles) and total bacterial community cell abundances (connected grey circles) and 16S relative abundances (triangles; right axes) for phycosphere

communities. *R. pomeroyi* (blue triangles) and competitor stated in the title of each plot (**A**). Color of each competitor is consistent between plots.

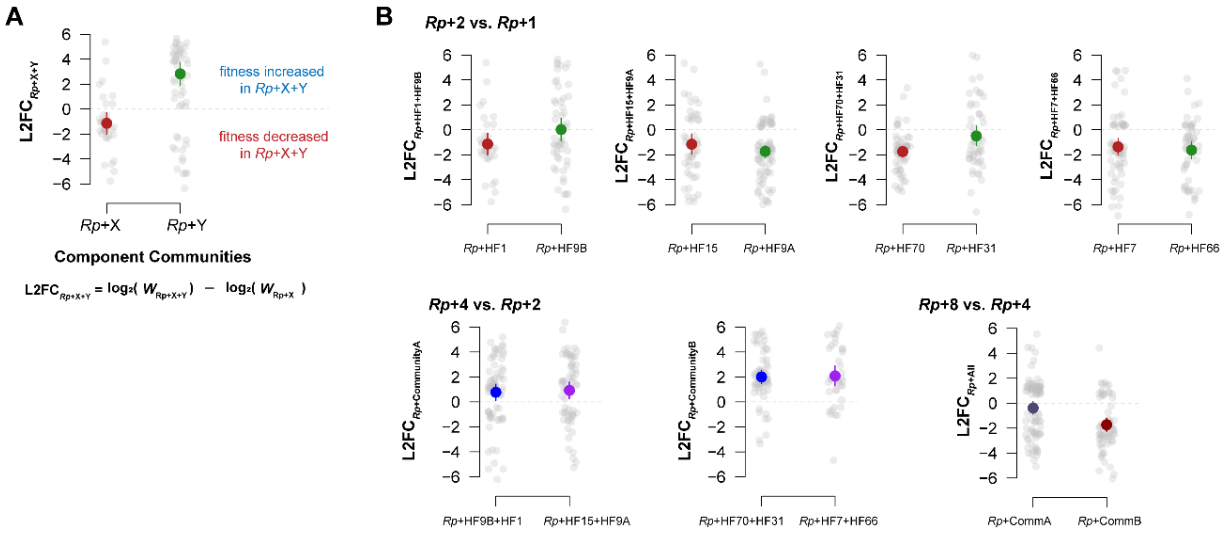

Fig S3.3. Fold-change of mutants in each community. **A.** Schematic representing calculation of fitness fold-change. Gray points represent mutants with statistically significant phenotypes and color points represent fold-change mean and 95% confidence intervals. **B.** Fold-change of significant phenotypes for each community grouped by richness of the coalescent communities.

CHAPTER 4

SIGNALS AND SUBSTRATES: THE ROLE OF CHEMOTAXIS AND GROWTH IN SHAPING MARINE BACTERIAL COMMUNITY COMPOSITION [1]

[1] Schreier, JE, Clerc, EE, Słomka, J, Smith, CB, Fu, H, Raina, JB, Moran, MA, Stocker, R. To be submitted to *The ISME Journal*.

Abstract

The surface ocean is a mosaic of exploitable hot-spots arising from organic matter released from living and senescing phytoplankton. Success of marine bacteria in navigating this patchy microscale environment relies on sensing the chemical gradients that indicate an organic matter source. After arrival at the source, robust growth on available substrates is required to maintain success. Organic compounds in hot-spots thus serve as signals directing bacterial foraging strategies, and as substrates enabling growth once there. These roles are not mutually exclusive and are likely to depend on both the metabolites available and the bacteria responding. Here, we quantitatively separate the effects of these two factors in determining the success of pairs of bacterial strains competing in a model hot spot environment. The *in situ* chemotaxis assay (ISCA) was used to test for bacterial strains' ability to locate a metabolite source, while growth assays were used to test for the strains' ability to utilize the metabolite. Our findings demonstrate that the combined effect of both factors often predicted success in the final community, but deviations from this prediction for 38% of tested pairs suggest that ecological interactions between competing bacteria also impact community assembly.

Introduction

From the perspective of a marine bacterium, the surface ocean consists of a patchwork of exploitable substrate hot-spots arising from living phytoplankton and other suspended or sinking organic matter (1, 2). One way to navigate this patchwork is through directed motion via chemotaxis, in which the bacterium senses a chemical gradient leading to a source of organic matter (3, 4). When living phytoplankton cells are the organic matter source, chemotaxis also

allows bacteria to maintain close spatial associations to this relatively long-lived nutrient hot-spot (5-7).

Success of a foraging bacterium relies not only on finding a source of organic matter, but also the ability to grow robustly on the substrates available (2). These dual roles of phytoplankton exudates, as signals influencing bacterial foraging strategy (8-10) and as substrates available for growth (11-16), are not mutually exclusive. For example, the phytoplankton metabolite dimethylsulfoniumpropionate (DMSP) has been found to function in both roles, as a signal for chemotaxis (17-19) and as a substrate supporting bacterial growth (20, 21).

Because processing of labile organic carbon by hotspot bacterial communities is a quantitatively important biogeochemical flux with the capacity to influence the ocean-atmosphere carbon balance (8, 11, 12, 22, 23), classifying the ecological effects of phytoplankton metabolites on bacteria is an important undertaking. It is also a challenging one, however, since the same compound can invoke different bacterial responses, even within members of a single bacterial taxon (9, 19). Experiments that have investigated how bacterial communities assemble on single carbon sources (24-26) have found modular assembly of many coexisting taxa, in some cases stabilized by crossfeeding of metabolic secretions. However, the roles played by microbial foraging strategies and subsequent growth capabilities in influencing community assembly have yet to be quantitatively assessed.

Here, we address how bacterial abilities to chemotax toward phytoplankton metabolites in combination with their ability to subsequently consume the metabolites influence assembly in simple two-species model communities. The study used a pairwise chemotaxis-growth competition assay to experimentally simulate bacteria arriving at a nutrient patch and remaining

for 24 h. We found that the combined measures of chemotactic ability and growth potential typically predicted success in the final community, but clear deviations from this prediction suggested that ecological interactions between pairs could impact community assembly.

Results & Discussion

Characterization of Chemotaxis and Growth in Marine Bacterial Strains. We measured the chemotactic index and growth rate of three marine Alphaproteobacteria and four marine Gammaproteobacteria in response to ten representative phytoplankton metabolites spanning chemical classes that included amino acids, amino acid derivatives, organic acids, and organic sulfur compounds (Fig. 4.1). The bacterial strains were isolated previously from bacterial enrichment communities on these same marine phytoplankton exometabolites (25), which had been identified as exometabolites of living diatoms (27-29) or dinoflagellates (28). Maximum growth rates were determined from kinetic growth assays as the slope of the linear portion of natural log transformed OD_{600} (30) and ranged from 0.024 ± 0.002 h^{-1} for *Pseudoalteromonas* HF66 (Fig. 4.1b) to 0.54 ± 0.02 h^{-1} for *Vibrio* HF9B (Fig. 4.1d). Chemotactic response of each bacterium was evaluated using the *in situ* chemotaxis assay (ISCA), a microfluidic device containing wells loaded with substrates and connected to a sterile external artificial seawater environment by a port through which metabolites diffuse out and bacteria swim in (31). The strength of the chemotactic response was defined as the chemotactic Index (I_C), representing the concentration of cells in ISCA wells filled with filtered seawater containing a single metabolite, normalized to the mean concentration of cells in wells containing filtered seawater without a metabolite. An $I_C > 1$ represents positive chemotaxis of a bacterial strain to a given metabolite. Across all bacterial isolates, I_C ranged from 0.16 ± 0.03 for *Phaeobacter* HF9A (Fig. 4.1g) to

13.71 ± 2.72 for *Pseudoalteromonas* HF66 (Fig. 4.1b). The strength of chemotactic responses observed here is similar to previously reported *in situ* chemotactic responses to phytoplankton-derived dissolved organic matter (9), polysaccharides (Clerc *et al*., in review), and rich culture medium (31).

Bacteria Vary in Their Response to the Same Metabolite. Chemical roles (classified as signal, substrate, both, or none) were identified for the set of test compounds (Fig. 4.1), and differed among strains, in agreement with previous observations (9, 19). In 12 cases out of the 70 signal/substrate assays, the metabolite played a role as both a signal for chemotaxis and a substrate for growth. In 16 cases, the metabolite functioned only as a signal, in 17 cases it functioned only as a substrate, and finally in 25 cases, it was neither a signal nor a substrate. As examples of these outcomes, trimethylamine (TMA) was never used as a substrate yet induced strong chemotaxis in *Thalassospira* HF15, *Pseudoalteromonas* HF66 and *Vibrio* HF57 (Fig. 4.1a,b,c). Conversely, xylose and isethionate were used only as substrates, and did not elicit any chemotactic response (Fig. 4.1a,b,d, g). Ectoine, glycolate, glutamate, spermidine, ribose and DMSP had roles as both substrates and/or signals, depending on the bacterial strain tested (Fig. 4.1a-g). Finally, 2,3-dihydroxypropane-1-sulfonate (DHPS) did not elicit a chemotactic response in any strain, nor did it support their growth (Fig. 4.1a-g).

Bacterial strains typically responded to or were able to grow on three or four compounds (with a variability of ± 2.5 compounds, both for chemotaxis and growth), but four showed chemotaxis to and/or growth on five or more (Fig 4.1a,b,c,d,g). *Thalassospira* HF15 was the most versatile strain, capable of chemotaxis to and growth on ectoine, glutamate, and DMSP; growth on xylose; and chemotaxis to TMA (Fig. 4.1a). Conversely, *Vibrio* HF70 did not

chemotax to any compound, yet could grow well on ectoine, glutamate, and ribose (Fig. 4.1f). *Celeribacter* HF31 demonstrated a narrow range of capabilities, only growing on glutamate and chemotaxing to ectoine (Fig. 4.1e). Gammaproteobacteria were able to chemotax to or grow in 38% of metabolite tests, while Alphaproteobacteria were able to chemotax to and grow in 26% of metabolite tests (Fig. 4.1g). Our observations converge with the commonly observed superior motility and chemotactic performance of Gammaproteobacteria relative to other bacterial phyla (9, 19, 31-33) (Clerc *et al*., in review). Taken as a whole, our assays highlight the varying functional roles of phytoplankton-derived metabolites as substrates, signals, or both for surface ocean bacteria.

Genes Repertoire is Consistent with Chemotaxis and Growth Assays. We queried the genetic potential for the strains to utilize the ten metabolites (Fig. 4.1h) using a protein database of well-annotated transport and catabolic proteins (Dataset S4.1). Proteins with homology $\geq$70% identity to our reference database were considered to have the same function, whereas proteins with homology between 50 – 70% were considered as potential matches that may have the same function (Fig. 1h, Dataset S4.2; (34)). If a bacterial strain exhibited chemotaxis to or growth on a metabolite tested, we hypothesized that it had a utilization gene. Our prediction was supported for 65% of the strain-metabolite combinations (Fig. 4.1h, Dataset S4.3) and provided further insight into our experimental observations. For example, *Vibrio* strains were chemotactic towards DMSP (Fig. 4.1c,d) but could not use DMSP as a sole carbon source (Fig. 1 c,d,f) in agreement with previous studies (19, 35). However, they harbor homologs to a transporter for DMSP uptake (35, 36) (Dataset S4.2) consistent with use of DMSP as a signal of a favorable environmental condition (37). TMA was observed only as a signal for three bacteria (Fig.

4.1a,b,c); strains, *Thalassospira* HF15 and *Pseudoalteromonas* HF66 carry homologs to catabolic enzymes that degrade TMA (Fig. 4.1h) but growth was not observed. This metabolite has not be identified as a source of carbon for biomass, and may instead serve as a source of nitrogen or energy (38).

Predictions that were not supported fell under two categories: either the bacteria lacked homologous proteins but exhibited chemotaxis or growth, or the bacteria had homologous proteins but chemotaxis or growth was not observed. The former case is likely due to the poor or missing annotations of bacterial proteins for the uptake and catabolism of metabolites. For example, *Pseudoalteromonas* HF66 could chemotax towards and metabolize spermidine, yet lacked genes with homology to reference genes in Alphaproteobacteria and Gammaproteobacteria (39). Alternatively, when a strain harbored homologous proteins but did not respond either by chemotaxis or growth to test metabolites, such as *Celeribacter* HF31 and *Phaeobacter* HF9A to xylose, this metabolite was not a signal and could likely not be used as a sole carbon source. Overall, querying the genetic potential of the strains clarified why some metabolites were only observed as signals, and highlighted the need for better annotations of pathways responsible for transport and catabolism of phytoplankton-derived metabolites.

Community Assembly Assays Isolate Separate Effects of Signals and Substrates. To explore how these dual responses of bacteria to phytoplankton metabolites influenced community assembly, we performed simple competition experiments between pairs of bacteria (Fig. S4.1). DMSP and spermidine were selected as the metabolites for this experiment because all strains except *Vibrio* HF70 and *Celeribacter* HF31 used them as a substrate and/or signal (Fig. 4.1a-g). Chemotaxis-growth competition assays were performed by pairing one of the six

strains with *Pseudoalteromonas* HF66, picked as the fixed strain due to its positive chemotaxis and growth with both DMSP and spermidine. Strain pairs were grown individually in rich medium before being inoculated together into sterile seawater containing ISCA units with wells loaded with either 1mM DMSP or spermidine (n=3) (Fig. S4.1a). After 1 h of incubation, samples of bacteria successfully reaching ISCA wells were retrieved, and a subsample was incubated at 27°C for 24 h (Fig. S4.1b) to measure growth on the ISCA metabolite. Samples collected at the time of inoculation from the filtered seawater, after chemotaxis from the ISCA wells, and after growth from the 24 h growth assay, were analyzed for bacteria cell number by flow cytometry and for community composition by 16S rRNA gene amplicon sequencing (Fig. S4.1c).

Chemotaxing Bacterial Strains Influence Each Other. We first analyzed the chemotactic indices of strain pairs relative to the component single strains to ask whether chemotaxis patterns were altered in the presence of a competitor. Strains were inoculated at equal cell numbers. After 1 h, the relative abundance of each in the ISCA community represented the contribution of each to the observed I_C (Fig. 4.2). We compared these data to predictions made by a null model of chemotaxis in which each strain behaved independently of the other (Supplementary Note 4.1) to assess whether ecological interactions may have shaped success in arriving at the synthetic hotspot. Inputs for the model included the individual strains' I_C on DMSP or spermidine (Fig. S4.2), the proportion of each strain's 16S rRNA gene in the inoculum prior to chemotaxis, and a ratio of relative motility of the strains in rich media (Supplementary Note 4.1).

Both significant increases and decreases in chemotactic ability were observed when DMSP was the chemoattractant for strain pairs. *Thalassospira* HF15 exhibited increased strength

of chemotaxis when paired with *Pseudoalteromonas* HF66, as did *Pseudoalteromonas* HF66 when paired with *Vibrio* HF70 (Fig. 4.2a). Thus, interactions can have the benefit of creating an enhanced chemotactic response. To explore the mechanism behind enhanced chemotaxis, we incubated *Pseudoalteromonas* HF66 for 1 h in seawater containing 1 mM DMSP and tested filtered spent medium as a chemoattractant for *Thalassospira* HF15 in the ISCA. We observed a chemotactic response by *Thalassospira* HF15 that was 1.4-fold stronger in the spent medium compared to DMSP itself (Fig. S4.3, t-test, $p < 0.05$). As the spent medium likely contained DMSP and DMSP-derived degradation products and/or metabolites secreted by *Pseudoalteromonas* HF66, we hypothesize these additional signals enhanced the chemotactic response.

Comparison of observed and predicted chemotactic responses revealed a lower strength of chemotaxis for most bacteria when spermidine was the metabolite tested (Fig. 4.2b). The *Pseudoalteromonas* HF66 I_C had lower than predicted chemotaxis for all paired tests on spermidine. For the strain paired with *Pseudoalteromonas* HF66, a lower observed than predicted *Ic* was found in 4 of 6 tests, suggesting that antagonistic or inhibitory interactions can develop rapidly between competitors (Fig. 4.2b). Overall, these data suggest that marine bacteria can alter the chemotactic response of competitors.

Chemotaxis Plus Growth Abilities is a Good Predictor of Community Assembly. Once bacteria position themselves favorably in a nutrient hotspot via chemotaxis, they can proliferate if substrate conditions are advantageous. To predict how growth by bacteria that successfully chemotax to hot-spots shapes community assembly, we modified the chemotaxis null model (Supplementary Note 4.1) to include growth rates of the strains on DMSP and spermidine

(Supplementary Note 4.2), calculating the percent deviation between the predicted and observed community composition (Dataset S4.4). Observed values that deviated by less than 10% from predicted were considered strong matches to the null model, indicating that success in that simple community was based on the combined effects of strength of chemotaxis and growth rate. Observed values that deviated more than 10% from predictions were considered weak matches to the null model. Overall, the null model of chemotaxis plus growth successfully predicted the final community in 63% of the assays (Fig. 4.3), demonstrating that combined knowledge of the ability of bacteria to chemotax to a metabolite hotspot and to grow at the expense of available metabolites is often sufficient to predict success in a simple assembled community.

In several cases, however, significant deviations between observed and predicted community composition occurred, suggesting interactions between the paired strains. The greatest deviation between model predictions and observed community composition was in DMSP assays between *Pseudoalteromonas* HF66 and *Thalassospira* HF15 (Fig 4.3a; Dataset S4.4). The earlier finding that *Pseudoalteromonas* HF66 spent medium positively enhanced the chemotaxis of *Thalassospira* HF15 on DMSP (Fig S4.3) likely set the stage for *Thalassospira* HF15 to account for half of the community despite being only a quarter of the inoculum (Fig 4.3a). Of the five cases where observations deviated from the null model, two were in assays with *Thalassiospira* HF15 as the paired strain, and two were in assays with *Vibrio* HF70 as the paired strain. In both instances deviations from the null model first appeared after chemotaxis and continued through growth, suggesting interactions between strains alter the trajectory of the bacterial community (Fig 4.3).

Conclusion

This study provides insights into the multifaceted roles that metabolites play in shaping bacterial community assembly in hot-spots models of phycospheres, the metabolite rich regions that form around living phytoplankton. Our findings reveal that metabolites serving as signals for the location of a hot-spot and those serving as substrates for bacteria that successfully arrive there affect the composition of bacterial communities. A single substrate can vary in whether it is an attractant or substrate for a bacterial strain, and each bacterial strain can have a different response to the same metabolite, highlighting the intricate nature of microbial foraging strategies and interactions in assembly even in very simple (two-member) communities. The composition and associated biogeochemical functions of ocean hot-spot microbiomes can be affected in the early phases of recruitment when influences from bacterial chemotaxis, substrate utilization, and interspecies interactions coalesce.

Methods

Bacterial strains. Alphaproteobacteria (*Phaeobacter* sp. HF9A, *Celeribacter* sp. HF31, *Thalassospira* sp. HF15) and Gammaproteobacteria (*Vibrio diazotrophicus* HF9B, *Vibrio* sp. HF57, *Pseudoalteromonas* sp. HF66, *Vibrio hepatarius* HF70) were isolated previously from bacterial enrichment communities used to study the effect of known marine phytoplankton exometabolites on bacterial community assembly (25), had fully sequenced genomes(40), and were observed to be motile in rich medium. Bacteria were grown from cryostocks on ½ YTSS (2.0 g yeast extract and 1.25 g tryptone prepared in artificial seawater (Instant Ocean, Spectrum Brand) agar plates at 27°C overnight. A single colony per strain was inoculated in strain-specific

media optimized to promote bacterial motility. All strains except *Vibrio* HF70 and *Thalassospira* HF15 were inoculated into 1/20 YTSS. *Vibrio* HF70 was inoculated into ½ YTSS and *Thalassospira* HF15 was inoculated in 1/10 Difco 2216 Marine Broth (BD Diagnostics). Liquid cultures were grown at 27°C for 20 h in a shaking incubator. Bacterial motility was confirmed by microscopy and a subsample was stained with SYBR Green I (ThermoFisher) to determine cell concentrations using a CytoFLEX S flow cytometer (Beckman Coulter) with side scatter and FITC fluorescence.

Chemotaxis assays. Chemotaxis was characterized using the *in situ* chemotaxis assay (ISCA; (31, 41)), a microfluidic device consisting four rows of five micro-wells (110 µl each) that were individually loaded with one of ten 0.2 µm filter sterilized chemoattractants (1 mM): dimethylsulfoniopropionate (DMSP, synthesized), spermidine (Sigma-Aldrich), ectoine (Sigma-Aldrich), 2,3-dihydroxypropane-1-sulfonate (DHPS, synthesized), trimethylamine (TMA, Sigma-Aldrich), glycolate (Sigma-Aldrich), ribose (Sigma-Aldrich), isethionate (Sigma-Aldrich), xylose (Sigma-Aldrich) and glutamate (Sigma-Aldrich). In an ISCA, each row of five wells served as technical replicates for an individual chemoattractant, which were injected into triplicate ISCAs using a sterile 1 ml syringe (Codau) and needle (27G, Henke Sass Wolf). Filtered seawater was used as a negative control in each ISCA to account for cells entering wells by random motility.

Prior to chemotaxis experiments, bacteria were grown and enumerated as above. ISCAs were incubated in artificial seawater inoculated with 10^6 bacteria ml^{-1} for 1 h. After incubation, contents of the ISCA wells were extracted using a sterile syringe and needle, and technical

replicates were pooled together. Chemotactic indices were determined by measuring cell concentrations in experimental samples relative to the filtered seawater negative control.

Substrate growth tests. Bacterial strains were individually inoculated into ½ YTSS medium and grown overnight at 30°C in a shaking incubator Cells were pelleted at 4,000 x g, washed three times, and resuspended to an OD_{600} of ~0.01 in Marine Basal Medium supplemented with 3 mM ammonium and substrate at 12 mM carbon. Cultures were grown in a 96-well plate in triplicate in a Synergy H1 microplate reader (BioTek) at 30°C with constant shaking and OD_{600} was measured every hour. Maximum growth rates were determined as the slope of the linear portion of natural log transformed of triplicate OD_{600} data (30).

Chemotaxis-growth competition assay. Bacterial strains were prepared as above for chemotaxis assays. ISCA triplicates containing 1mM DMSP or spermidine were prepared as above and were incubated for 1 h in bulk artificial seawater with *Pseudoalteromonas* HF66 and one of six other bacterial strains in an equal mixture of 10^6 total bacteria ml^{-1}. Although we aimed to inoculate each strain pair equally, the clumping phenotype of *Pseudoalteromonas* HF66 in rich medium resulted in overrepresentation of this strain relative to the competing strain at the start of this experiment. This bias was accounted for in the model predictions (Supplemental Notes). At the start of the experiment, a 200 µl sample of the bulk seawater was flash frozen in liquid nitrogen to determine the relative abundance of each strain prior to chemotaxis using 16S rRNA amplicon sequencing. Following the chemotaxis assay, samples were retrieved from the ISCA wells, and technical replicates were pooled, and each sample was split into three subsamples for 16S rRNA amplicon sequencing (200 µl), flow cytometry (50 µl), and for the

growth assay (250 µl). Subsamples for the growth assay were transferred to 15 ml tubes and incubated at 27°C in a shaking incubator. After 24 h of growth, samples were collected for flow cytometry and 16S rRNA amplicon sequencing.

DNA extraction, sequencing, and 16S amplicon analysis. Samples were collected from paired chemotaxis-growth assays from the bulk seawater prior to chemotaxis, from ISCA wells after 1 h of chemotaxis, and from cultures after the 24 h grow-out. In short, DNA was extracted using a custom physical lysis protocol optimized for small sample volumes (42). Samples were mixed with lysis buffer (potassium hydroxide + dithiothreitol) and incubated at room temperature for 10 min, at -80°C for 10 min, then at 55°C for 5 min, followed by the immediate addition of stop buffer (Tris-HCl). Extracted DNA was cleaned with AMPure beads (Beckman Coulter Inc., USA) and stored at -20°C. The 16S rRNA V4-V5 hypervariable region was amplified using primers 515F-Y/926R (43), and libraries were constructed using the KAPA Hyper Prep Kit (Kapa Biosystems, Wilmington, MA). 16S rRNA amplicons were sequenced at the Georgia Genomics and Bioinformatics core using an Illumina MiSeq paired-end 150 base pair flow cell. Forward reads of amplicon sequences were processed in R with dada2 (44) using a standard pipeline (https://benjjneb.github.io/dada2/tutorial.html).

To transform the 16S rRNA amplicon counts to cell abundances, we established three mock microbial communities by mixing different concentrations of each bacterium with known optical density (OD_{600} = 0.07) and cell counts (~$1.2x10^5$ cells). DNA was extracted, 16S rRNA amplicon libraries were constructed and sequenced as previously reported. Given the total library sizes are not equal, we normalized the total reads of each library to a million. In all seven strains, we found that the normalized counts of amplicon sequence variant (ASV) are linear (R^2>0.97) to

the cell counts. These data validated the robustness of 16S amplicon sequencing, allowing us to calculate cell abundances based on their 16S amplicon counts.

Protein homology. Reference protein databases were created using blast v.2.6.0+ (45) with experimentally verified and well-annotated transporters and catabolic enzymes for metabolites used in this study. Transporter reference protein sequences were gathered from the transporter classification database (46). UniProtKB/Swiss-Prot (47) was used to gather catabolic protein sequences, and only reviewed sequences were considered. Reference Genomes of bacterial strains used in this study were downloaded from the IMG JGI portal. Protein coding sequences determined by prodigal (48) were aligned against the reference database using blastp with a cutoff evalue of 10^{-5} and only protein sequences that had $\geq$ 50% amino acid identity were retained.

Data analysis. Statistical analyses and data display were performed in R 4.3.0 using ggplot2, vegan, ggpubr, dplyr, tidyr, data.table, and tibble, and maximum growth rates were calculated using Excel 2019.

Author Contributions: EC, JES, HF, JBR, MAM, RS conceived the experiments, EC and CBS performed the experiments, CBS and HF performed 16S amplicon sequencing and analysis, JS created the model, EC and JES analyzed the data, and EC and JES wrote and reviewed the manuscript with JBR, MAM, and RS.

Acknowledgements: This work was supported by Simons Foundation grant to MAM and RS within the Principles of Microbial Ecosystems Collaborative, and NSF Graduate Research Fellowship Program award GRFP-1445117 to JES.

References

1. T. Fenchel, Microbial behavior in a heterogeneous world. *Science* **296**, 1068-1071 (2002).
2. V. I. Fernandez, Y. Yawata, R. Stocker, A foraging mandala for aquatic microorganisms. *The ISME Journal* **13**, 563-575 (2019).
3. S. Smriga, V. I. Fernandez, J. G. Mitchell, R. Stocker, Chemotaxis toward phytoplankton drives organic matter partitioning among marine bacteria. *Proceedings of the National Academy of Sciences* **113**, 1576-1581 (2016).
4. R. Stocker, J. R. Seymour, A. Samadani, D. E. Hunt, M. F. Polz, Rapid chemotactic response enables marine bacteria to exploit ephemeral microscale nutrient patches. *Proceedings of the National Academy of Sciences* **105**, 4209-4214 (2008).
5. W. Bell, R. Mitchell, Chemotactic and growth responses of marine bacteria to algal extracellular products. *The Biological Bulletin* **143**, 265-277 (1972).
6. J. D. Bowen, K. D. Stolzenbach, S. W. Chisholm, Simulating bacterial clustering around phytoplankton cells in a turbulent ocean. *Limnology and Oceanography* **38**, 36-51 (1993).
7. J. R. Seymour, S. A. Amin, J.-B. Raina, R. Stocker, Zooming in on the phycosphere: the ecological interface for phytoplankton–bacteria relationships. *Nature Microbiology* **2**, 1-12 (2017).
8. M. A. Moran *et al.*, Microbial metabolites in the marine carbon cycle. *Nature Microbiology* **7**, 508-523 (2022).
9. J.B. Raina *et al.*, Chemotaxis shapes the microscale organization of the ocean's microbiome. *Nature* **605**, 132-138 (2022).

10. A. A. Shibl *et al.*, Diatom modulation of select bacteria through use of two unique secondary metabolites. *Proceedings of the National Academy of Sciences* **117**, 27445-27455 (2020).
11. S. B. Baines, M. L. Pace, The production of dissolved organic matter by phytoplankton and its importance to bacteria: patterns across marine and freshwater systems. *Limnology and Oceanography* **36**, 1078-1090 (1991).
12. J. J. Cole, S. Findlay, M. L. Pace, Bacterial production in fresh and saltwater ecosystems: a cross-system overview. *Marine Ecology Progress Series* **43**, 1-10 (1988).
13. B. Kieft *et al.*, Phytoplankton exudates and lysates support distinct microbial consortia with specialized metabolic and ecophysiological traits. *Proceedings of the National Academy of Sciences* **118**, e2101178118 (2021).
14. F. X. Ferrer-González *et al.*, Bacterial transcriptional response to labile exometabolites from photosynthetic picoeukaryote *Micromonas commoda*. *ISME Communications* **3**, 1-11 (2023).
15. F. X. Ferrer-González *et al.*, Resource partitioning of phytoplankton metabolites that support bacterial heterotrophy. *The ISME Journal* **15**, 762-773 (2021).
16. M. Uchimiya, W. Schroer, M. Olofsson, A. S. Edison, M. A. Moran, Diel investments in metabolite production and consumption in a model microbial system. *The ISME Journal* **16**, 1306-1317 (2022).
17. H. Bürgmann *et al.*, Transcriptional response of *Silicibacter pomeroyi* DSS-3 to dimethylsulfoniopropionate (DMSP). *Environmental Microbiology* **9**, 2742-2755 (2007).

18. W. M. Johnson, M. C. Kido Soule, E. B. Kujawinski, Evidence for quorum sensing and differential metabolite production by a marine bacterium in response to DMSP. *The ISME Journal* **10**, 2304-2316 (2016).
19. J. R. Seymour, R. Simó, T. Ahmed, R. Stocker, Chemoattraction to dimethylsulfoniopropionate throughout the marine microbial food web. *Science* **329**, 342-345 (2010).
20. R. R. Malmstrom, R. P. Kiene, D. L. Kirchman, Identification and enumeration of bacteria assimilating dimethylsulfoniopropionate (DMSP) in the North Atlantic and Gulf of Mexico. *Limnology and Oceanography* **49**, 597-606 (2004).
21. M. Vila-Costa *et al.*, Transcriptomic analysis of a marine bacterial community enriched with dimethylsulfoniopropionate. *The ISME Journal* **4**, 1410-1420 (2010).
22. T. R. Anderson, H. W. Ducklow, Microbial loop carbon cycling in ocean environments studied using a simple steady-state model. *Aquatic Microbial Ecology* **26**, 37-49 (2001).
23. M. A. Moran *et al.*, The Ocean's labile DOC supply chain. *Limnology and Oceanography* **67**, 1007-1021 (2022).
24. T. N. Enke *et al.*, Modular assembly of polysaccharide-degrading marine microbial communities. *Current Biology* **29**, 1528-1535. e1526 (2019).
25. H. Fu, M. Uchimiya, J. Gore, M. A. Moran, Ecological drivers of bacterial community assembly in synthetic phycospheres. *Proceedings of the National Academy of Sciences* **117**, 3656-3662 (2020).
26. J. E. Goldford *et al.*, Emergent simplicity in microbial community assembly. *Science* **361**, 469-474 (2018).

27. B. P. Durham *et al.*, Recognition cascade and metabolite transfer in a marine bacteria-phytoplankton model system. *Environmental Microbiology* **19**, 3500-3513 (2017).
28. M. Landa, A. S. Burns, S. J. Roth, M. A. Moran, Bacterial transcriptome remodeling during sequential co-culture with a marine dinoflagellate and diatom. *The ISME journal* **11**, 2677-2690 (2017).
29. M. Olofsson *et al.*, Growth-stage-related shifts in diatom endometabolome composition set the stage for bacterial heterotrophy. *ISME Communications* **2**, 28 (2022).
30. R. J. Allen, B. Waclaw, Bacterial growth: a statistical physicist's guide. *Reports on Progress in Physics* **82**, 016601 (2018).
31. B. S. Lambert *et al.*, A microfluidics-based in situ chemotaxis assay to study the behaviour of aquatic microbial communities. *Nature Microbiology* **2**, 1344-1349 (2017).
32. R. D. Sjoblad, R. Mitchell, Chemotactic responses of *Vibrio alginolyticus* to algal extracellular products. *Canadian Journal of Microbiology* **25**, 964-967 (1979).
33. B. Bassler, P. Gibbons, C. Yu, S. Roseman, Chitin utilization by marine bacteria. Chemotaxis to chitin oligosaccharides by Vibrio furnissii. *Journal of Biological Chemistry* **266**, 24268-24275 (1991).
34. V. Sangar, D. J. Blankenberg, N. Altman, A. M. Lesk, Quantitative sequence-function relationships in proteins based on gene ontology. *BMC Bioinformatics* **8**, 1-15 (2007).
35. G. J. Gregory, K. E. Boas, E. F. Boyd, The organosulfur compound dimethylsulfoniopropionate (DMSP) is utilized as an osmoprotectant by *Vibrio* species. *Applied and Environmental Microbiology* **87**, e02235-02220 (2021).

36. G. J. Gregory, E. F. Boyd, Stressed out: Bacterial response to high salinity using compatible solute biosynthesis and uptake systems, lessons from Vibrionaceae. *Computational and Sstructural Biotechnology Journal* **19**, 1014-1027 (2021).

37. J.B. Raina, E. A. Dinsdale, B. L. Willis, D. G. Bourne, Do the organic sulfur compounds DMSP and DMS drive coral microbial associations? *Trends in Microbiology* **18**, 101-108 (2010).

38. I. D. Lidbury, J. C. Murrell, Y. Chen, Trimethylamine and trimethylamine N-oxide are supplementary energy sources for a marine heterotrophic bacterium: implications for marine carbon and nitrogen cycling. *The ISME Journal* **9**, 760-769 (2015).

39. X. Mou *et al.*, Metatranscriptomic signature of exogenous polyamine utilization by coastal bacterioplankton. *Environmental Microbiology Reports* **3**, 798-806 (2011).

40. H. Fu, C. B. Smith, S. Sharma, M. A. Moran, Genome sequences and metagenome-assembled genome sequences of microbial communities enriched on phytoplankton exometabolites. *Microbiology Resource Announcements* **9**, e00724-00720 (2020).

41. E. E. Clerc, J.B. Raina, B. S. Lambert, J. Seymour, R. Stocker, In situ chemotaxis assay to examine microbial behavior in aquatic ecosystems. *JoVE*, e61062 (2020).

42. A. R. Bramucci *et al.*, Microvolume DNA extraction methods for microscale amplicon and metagenomic studies. *ISME Communications* **1**, 79 (2021).

43. A. E. Parada, D. M. Needham, J. A. Fuhrman, Every base matters: assessing small subunit rRNA primers for marine microbiomes with mock communities, time series and global field samples. *Environmental Microbiology* **18**, 1403-1414 (2016).

44. B. J. Callahan *et al.*, DADA2: High-resolution sample inference from Illumina amplicon data. *Nature Methods* **13**, 581-583 (2016).

45. C. Camacho *et al.*, BLAST+: architecture and applications. *BMC Bioinformatics* **10**, 1-9 (2009).

46. M. H. Saier Jr *et al.*, The transporter classification database (TCDB): 2021 update. *Nucleic Acids Research* **49**, D461-D467 (2021).

47. Anonymous, UniProt: the Universal Protein knowledgebase in 2023. *Nucleic Acids Research* **51**, D523-D531 (2023).

48. D. Hyatt *et al.*, Prodigal: prokaryotic gene recognition and translation initiation site identification. *BMC Bioinformatics* **11**, 1-11 (2010).

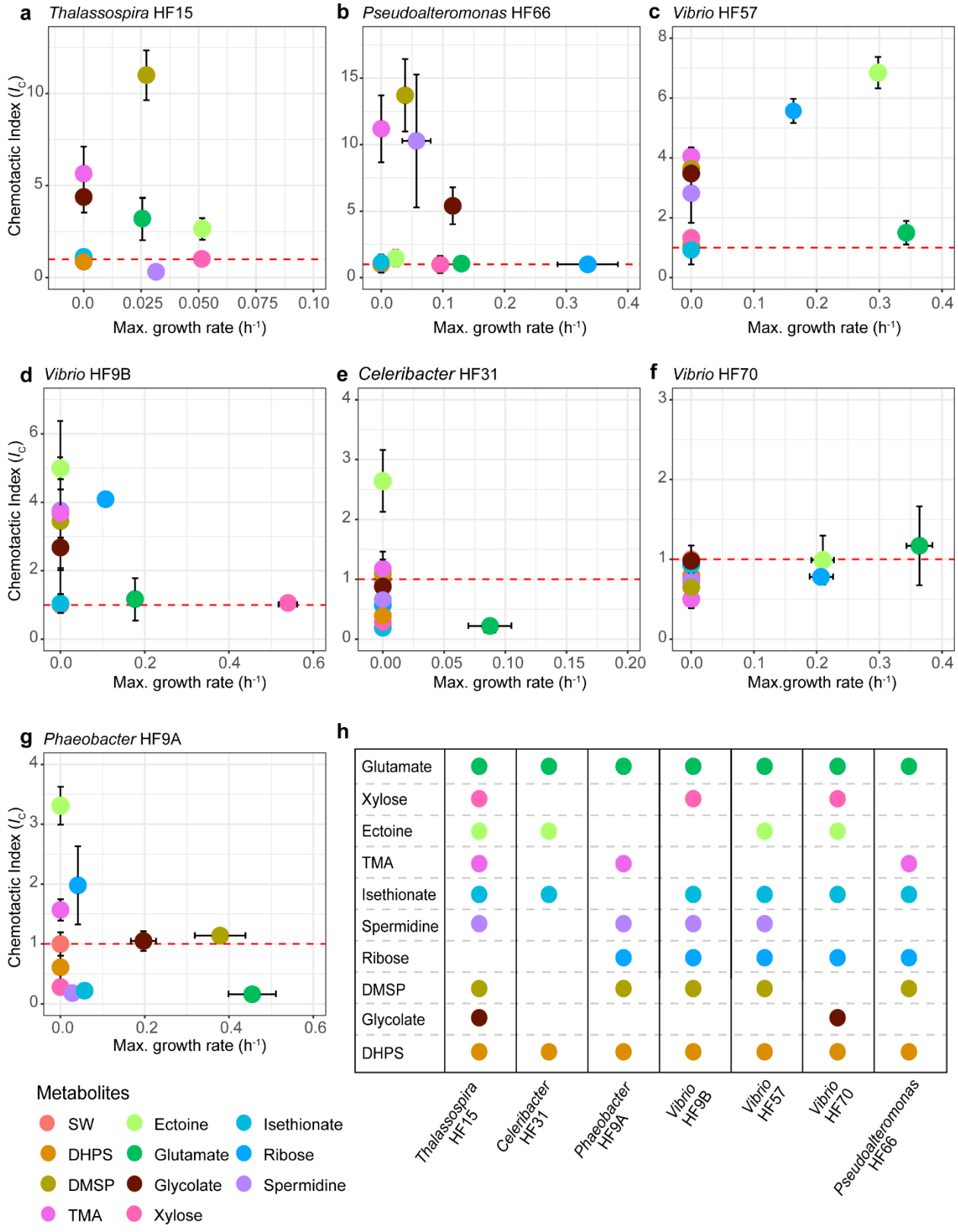
a Thalassospira HF15
b Pseudoalteromonas HF66
c Vibrio HF57
d Vibrio HF9B
e Celeribacter HF31
f Vibrio HF70
g Phaeobacter HF9A
Chemotactic Index (I_c)
Max. growth rate (h^{-1})
Max.growth rate (h^{-1})
h
Glutamate
Xylose
Ectoine
TMA
Isethionate
Spermidine
Ribose
DMSP
Glycolate
DHPS
Thalassospira HF15
Celeribacter HF31
Phaeobacter HF9A
Vibrio HF9B
Vibrio HF57
Vibrio HF70
Pseudoalteromonas HF66
Metabolites
SW
Ectoine
Isethionate
DHPS
Glutamate
Ribose
DMSP
Glycolate
Spermidine
TMA
Xylose

Figure 4.1. (a-g) Chemotactic index (I_C) and maximum growth rates of seven bacteria on ten representative phytoplankton metabolites. $I_C > 1$ represents positive chemotaxis. Standard deviations (n=3) are displayed for all points, with some falling within the symbols. (h) Genetic potential of strains to transport and catabolize metabolites that was consistent with observed chemotaxis and growth. Protein homology was determined using blast+ with a custom database containing well annotated or experimentally verified transporters and catabolic enzymes.

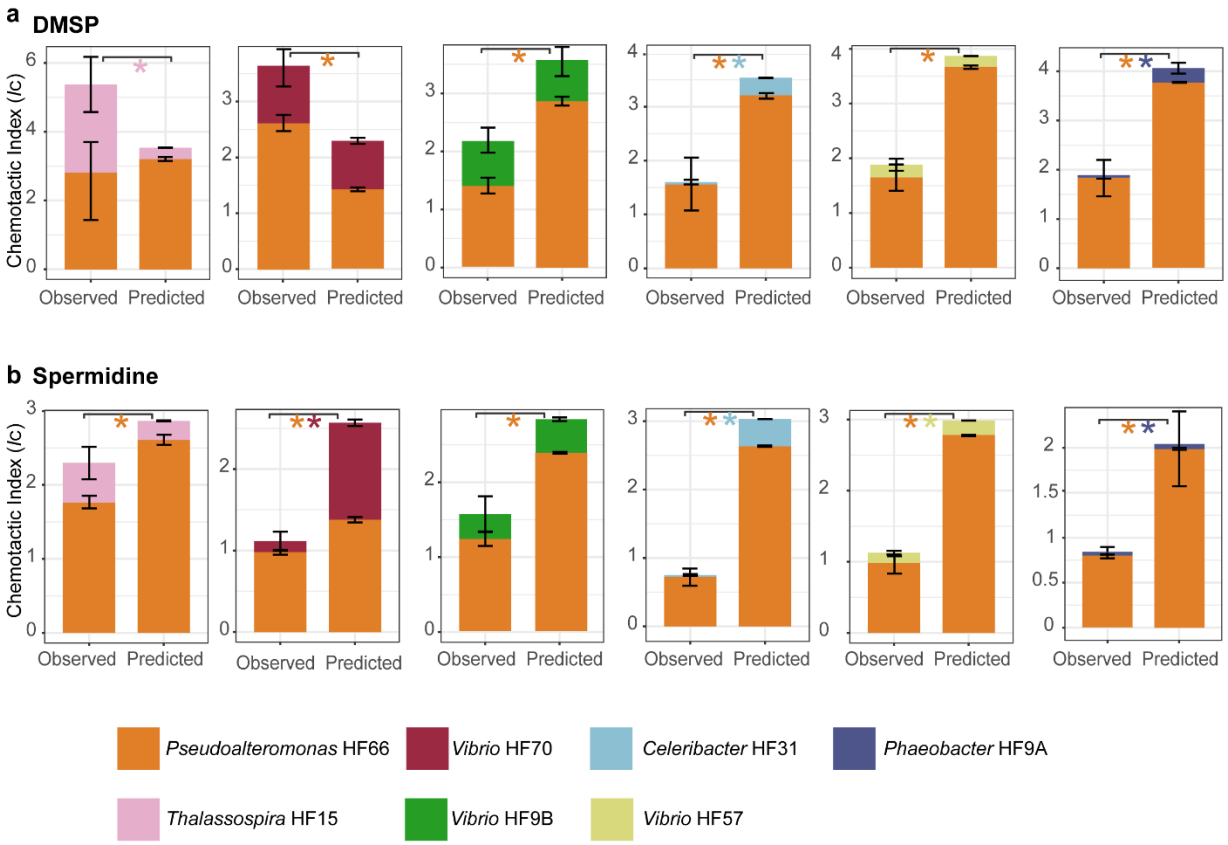

Figure 4.2. Chemotactic index (I_C) of paired strains on (a) spermidine or (b) DMSP after 1 h of incubation with standard deviation displayed (n=3). Observed I_C were decomposed into the contribution of each strain by using 16S rRNA relative abundance. Significant differences between the observed and predicted chemotactic index are indicated by the asterisk color-coded by strain (t-test, $p < 0.05$).

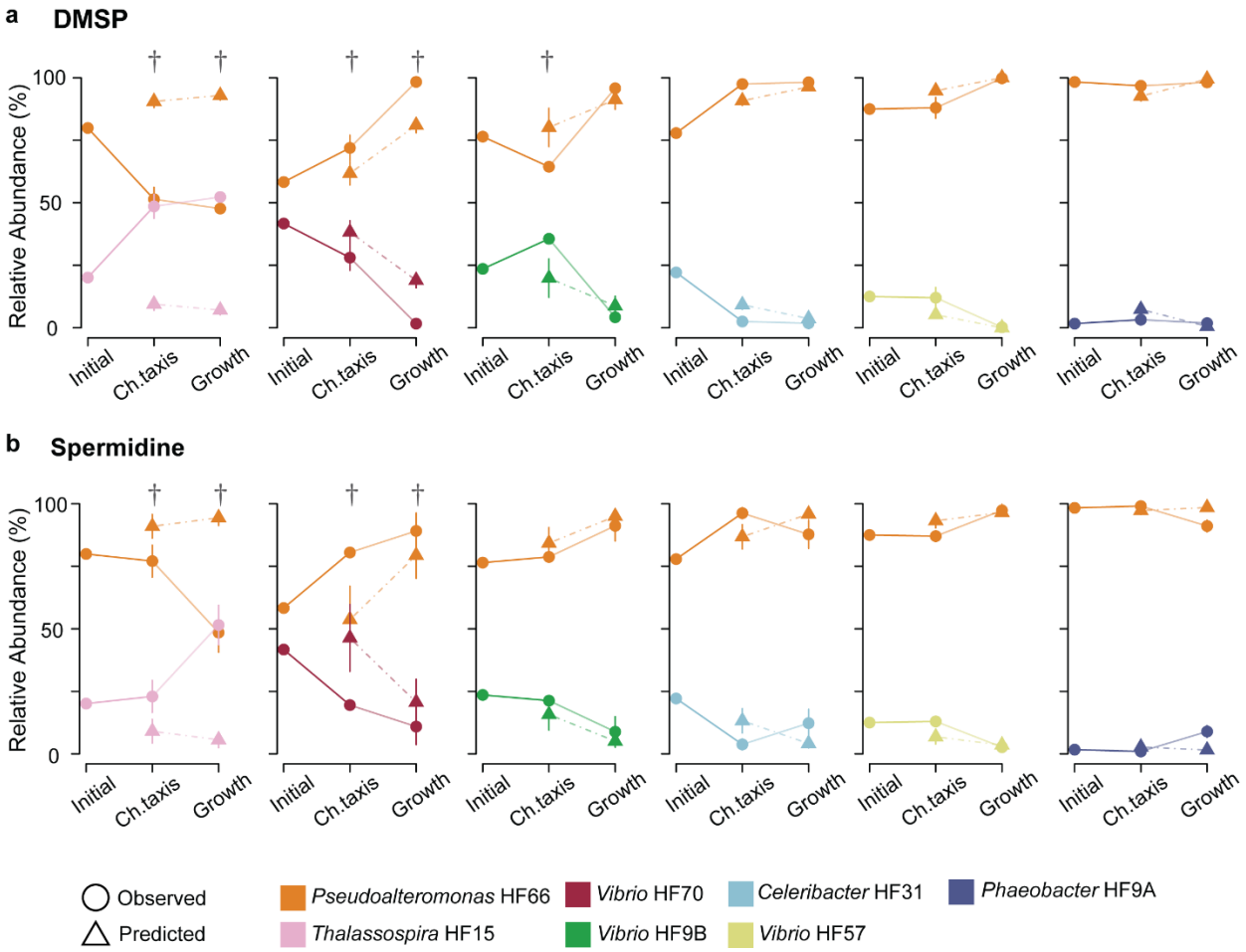

Figure 4.3. Relative abundance of the fixed strain *Pseudoalteromonas* HF66 and a competing strain in seawater at time of inoculation (Initial), after 1 h of chemotaxis (Ch.taxis), and after 24 h of growth (Growth) on DMSP or spermidine. Deviations between observed (circles) and predicted (triangles) community composition greater than 10% are indicated by dagger symbols.

Supplementary Figures

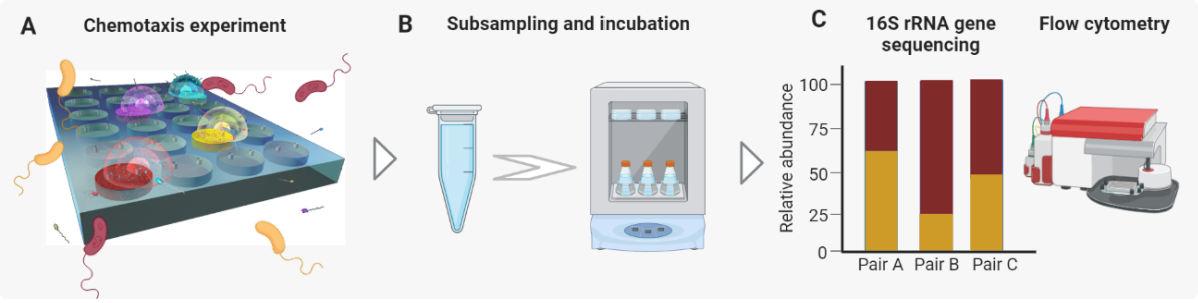

Figure S4.1. Experimental design of the chemotaxis-growth competition assays. (A) Triplicate ISCAs loaded with DMSP and spermidine were incubated for 1 h in bulk seawater containing a 1:1 mixture of HF66 paired with one of six other bacterial strains. (B) After chemotaxis, samples were retrieved from ISCA wells and were grown for 24 h. (C) Total cell abundance from the bulk seawater (prior to chemotaxis), from the ISCA wells (after chemotaxis), and from the growth assay were determined by flow cytometry, and DNA was extracted for 16S rRNA amplicon sequencing to determine relative abundance.

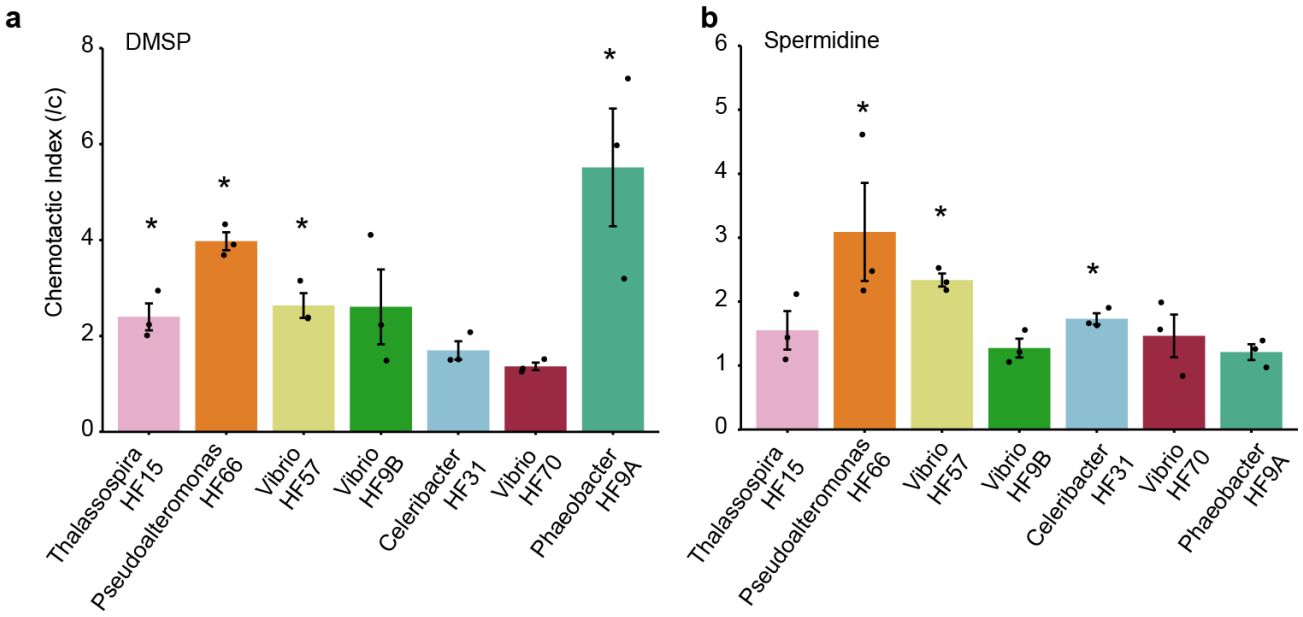

Figure S4.2. Chemotactic responses elicited by DMSP (a) and spermidine (b) in the seven bacterial strains used for model predictions. Chemotactic index (I_C) measured in response to 1 mM DMSP (a) and 1 mM spermidine (b). The chemotactic index I_C denotes the average concentration of cells in the treatment wells of the ISCA, divided by the average concentration of cells in the control wells containing filtered seawater (FSW). Each treatment was replicated across three different ISCAs ($n = 3$, individual dots). Data in panels a and b are mean ± SD. Bars marked with an asterisk denote I_C values significantly greater than the artificial seawater controls (ANOVA, $p < 0.05$).

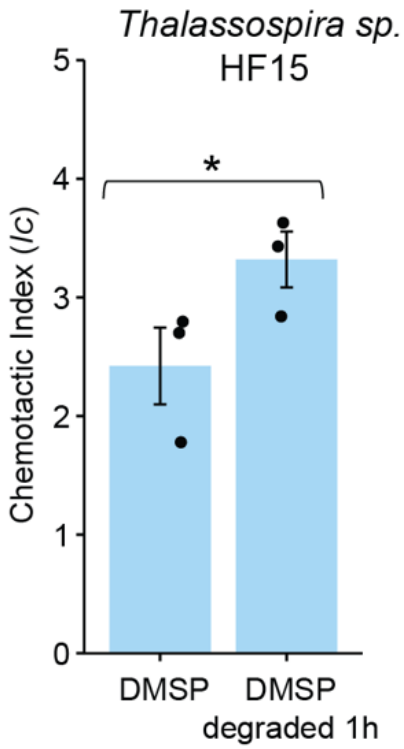

Figure S4.3. Test of synergistic interaction between *Thalassospira* sp. HF15 and *Pseudoalteromonas* HF66 on DMSP. An overnight culture of *Pseudoalteromonas* HF66 was washed twice in sterile seawater, resuspended at 10^6 cells ml^{-1} in seawater containing 1 mM DMSP, incubated at room temperature for 1 h, and then sequentially filtered through 0.2 um Sterivex filter (Millipore) and 0.02 um Anatop filter (Whatman). The resulting spent medium was used as a chemoattractant alongside DMSP (1 mM unincubated) in the ISCA, and the bulk seawater was inoculated with 10^6 cells ml^{-1} of *Thalassospira* sp. HF15. After 1 h, samples were retrieved, and cells were enumerated by flow cytometry. *Thalassospira* sp. HF15 displayed a greater chemotactic index for the spent medium of *Pseudoalteromonas* HF66 incubated with DMSP than to DMSP alone (t-test, $p < 0.05$). Each treatment was replicated across three different ISCAs ($n = 3$, individual dots). Data in panels a and b are mean ± SD. Bars marked

with an asterisk denote I_C values significantly greater than the artificial seawater controls (ANOVA, $p < 0.05$).

Supplementary Note 4.1

Null model predictions

For model predictions, we assume that:

1. The ISCA is introduced into bacterial culture at time $t = 0$. The culture contains bacteria with concentration c while the ISCA wells do not contain bacteria at $t = 0$, only substrates that diffuse outside of the ISCA and attract or repel bacteria.

2. The ISCA is exposed to the culture for time T_{exp}.

3. We count the bacteria in each chemoattractant and seawater negative control.

Assuming that experiments occur on timescales much shorter than the time needed for the concentration of bacteria in the wells to equilibrate with the outside concentration, the number of bacteria in a given well after time T_{exp} is:

$$N = \Gamma T_{\mathrm{exp}} c$$

where Γ is the collision kernel that quantifies the rate at which bacteria in the culture encounter the well. Γ depends on bacterial motility, chemotaxis strength, dimensions of the well, and external flow (if there is one).

Chemotactic index

We consider two wells: a control well filled with sea water and a well containing chemoattractant A. Assuming that the two wells are on the same ISCA, then the experiment takes the same amount of time for both wells and the bacterial concentration is the same for both wells, in which case the number of bacteria in each well is then:

$$N_{\text{control}} = \Gamma_{\text{control}} T_{\text{exp}} c, \text{ and } N_{\text{A}} = \Gamma_{\text{A}} T_{\text{exp}} c$$

The chemotactic index IC_{A} for chemical A is then defined as:

$$IC_A = \frac{N_A}{N_{\text{control}}} = \frac{\Gamma_A}{\Gamma_{\text{control}}}.$$

Chemotaxis Null model for a mixture of two strain α and β

We supposed we have two bacterial strains α and β and we measured their chemotactic indices IC_A^{α} and IC_A^{β} for chemical A. The ISCA is then placed into a bacterial culture containing both strains.

Assuming the two species do not interact, we can calculate the resulting chemotactic index $IC_A^{\alpha\beta}$ for the mixture with the following assumptions. Let $c^{\alpha\beta}$ be the concentration of the bacterial culture containing both strains. Assuming the culture contains fraction f of bacteria from strain α and fraction $1-f$ of bacteria from strain β, the concentration of strain α alone is $c^{\alpha} = fc^{\alpha\beta}$ and concentration of strain β alone is $c^{\beta} = (1-f)c^{\alpha\beta}$. Since strains do not interact, we can write down equations for each strain:

$$\begin{aligned} N_{\text{control}}^{\alpha} &= \Gamma_{\text{control}}^{\alpha} T_{\text{exp}} c^{\alpha}, \text{ and } N_{\text{A}}^{\alpha} = \Gamma_{\text{A}}^{\alpha} T_{\text{exp}} c^{\alpha} \\ N_{\text{control}}^{\beta} &= \Gamma_{\text{control}}^{\beta} T_{\text{exp}} c^{\beta}, \text{ and } N_{\text{A}}^{\beta} = \Gamma_{\text{A}}^{\beta} T_{\text{exp}} c^{\beta} \end{aligned} \quad (4)$$

In the control well, the number of cells is $N^{\alpha}_{\text{control}} + N^{\beta}_{\text{control}}$ and in the well containing chemoattractant A the number of cells is $N^{\alpha}_{\text{A}} + N^{\beta}_{\text{A}}$. The expected chemotactic index is then:

$$IC_A^{\alpha\beta} = \frac{N^{\alpha}_{\text{A}} + N^{\beta}_{\text{A}}}{N^{\alpha}_{\text{control}} + N^{\beta}_{\text{control}}} = \frac{\Gamma^{\alpha}_{\text{A}} T_{\text{exp}} c^{\alpha} + \Gamma^{\beta}_{\text{A}} T_{\text{exp}} c^{\beta}}{\Gamma^{\alpha}_{\text{control}} T_{\text{exp}} c^{\alpha} + \Gamma^{\beta}_{\text{control}} T_{\text{exp}} c^{\beta}} = \frac{\Gamma^{\alpha}_{\text{A}} c^{\alpha} + \Gamma^{\beta}_{\text{A}} c^{\beta}}{\Gamma^{\alpha}_{\text{control}} c^{\alpha} + \Gamma^{\beta}_{\text{control}} c^{\beta}}$$

Using the definitions for the chemotactic indices measured earlier $\Gamma^{\alpha}_{A} = IC^{\alpha}_{A} \Gamma^{\alpha}_{\text{control}}$ and $\Gamma^{\beta}_{A} = IC^{\beta}_{A} \Gamma^{\beta}_{\text{control}}$, as well as $c^{\alpha} = f c^{\alpha\beta}$ and $c^{\beta} = (1-f) c^{\alpha\beta}$, we obtain:

$$\boldsymbol{IC_A^{\alpha\beta} = IC_A^{\alpha} \frac{f}{f + (1-f) M^{\alpha\beta}} + IC_A^{\beta} \frac{1-f}{f/M^{\alpha\beta} + (1-f)}}$$

where we defined the motility ratio characterizing the relative motility of bacteria in the control:

$$M^{\alpha\beta} = \Gamma^{\beta}_{\text{control}} / \Gamma^{\alpha}_{\text{control}}$$

So, in the null model, the combined chemotactic index $IC_A^{\alpha\beta}$ depends on the fraction of cells from each strain as well as their relative motility. The relative motility can be related to the orginal experiments used to determine chemotactic indices of the strains separately as follows (assuming the two experiments were performed for the same amount of time):

$$M^{\alpha\beta} = \Gamma^{\beta}_{\text{control}} / \Gamma^{\alpha}_{\text{control}} = \frac{N^{\beta}_{\text{control}} / c^{\beta}}{N^{\alpha}_{\text{control}} / c^{\alpha}}$$

Note that we assume the measurements of the control for the two separate strains were performed for the same time.

Supplementary Note 4.2

Community composition null model adding growth

Equations (4) give the number of bacteria in the control and A-chemical-containing wells after time T_{exp} (typically 1 hour). We add the effect of growth for time T_{growth} (usually 24 hours), based on strain and substrate specific growth rates, called μ_{A}^{α}, the growth rate of strain α on substrate A. Assuming exponential growth, an initial number of bacteria $N(0)$ will grow to $N(0)e^{\mu_{\text{A}}^{\alpha} T_{\text{growth}}}$. Applying this to equations (4) gives:

$$N_{\text{control}}^{\alpha}\left(T_{\text{growth}}\right) = e^{\mu_{\text{A}}^{\alpha} T_{\text{growth}}}\, \Gamma_{\text{control}}^{\alpha}\, T_{\text{exp}} c^{\alpha}, \text{ and } N_{\text{A}}^{\alpha}\left(T_{\text{growth}}\right) = e^{\mu_{\text{A}}^{\alpha} T_{\text{growth}}}\, \Gamma_{\text{A}}^{\alpha} T_{\text{exp}}\, c^{\alpha},$$
$$N_{\text{control}}^{\beta}\left(T_{\text{growth}}\right) = e^{\mu_{\text{A}}^{\beta} T_{\text{growth}}}\, \Gamma_{\text{control}}^{\beta}\, T_{\text{exp}}\, c^{\beta}, \text{ and } N_{\text{A}}^{\beta}\left(T_{\text{growth}}\right) = e^{\mu_{\text{A}}^{\beta} T_{\text{growth}}}\, \Gamma_{\text{A}}^{\beta} T_{\text{exp}}\, c^{\beta}.$$

To obtain the community composition, we account for a fraction f^{α} of strain α and f^{β} of strain β (previously denoted by f and $1-f$, respectively), the final fraction F_{A}^{α} of strain α on chemical A is computed as follows:

$$\boldsymbol{F_{\text{A}}^{\alpha}} = \frac{N_{\text{A}}^{\alpha}\left(T_{\text{growth}}\right)}{N_{\text{A}}^{\alpha}\left(T_{\text{growth}}\right) + N_{\text{A}}^{\beta}\left(T_{\text{growth}}\right)} = \frac{e^{\mu_{\text{A}}^{\alpha} T_{\text{growth}}}\, \Gamma_{\text{A}}^{\alpha} T_{\text{exp}} c^{\alpha}}{e^{\mu_{\text{A}}^{\alpha} T_{\text{growth}}}\, \Gamma_{\text{A}}^{\alpha} T_{\text{exp}} c^{\alpha} + e^{\mu_{\text{A}}^{\beta} T_{\text{growth}}}\, \Gamma_{\text{A}}^{\beta} T_{\text{exp}} c^{\beta}}$$
$$= \frac{e^{\mu_{\text{A}}^{\alpha} T_{\text{growth}}}\, \Gamma_{\text{A}}^{\alpha} f^{\alpha}}{e^{\mu_{\text{A}}^{\alpha} T_{\text{growth}}}\, \Gamma_{\text{A}}^{\alpha} f^{\alpha} + e^{\mu_{\text{A}}^{\beta} T_{\text{growth}}}\, \Gamma_{\text{A}}^{\beta} f^{\beta}}$$
$$= \frac{\boldsymbol{f^{\alpha}}}{\boldsymbol{f^{\alpha} + f^{\beta} e^{\left(\mu_{\text{A}}^{\beta} - \mu_{\text{A}}^{\alpha}\right) T_{\text{growth}}} M^{\alpha\beta} IC_{\text{A}}^{\beta} / IC_{\text{A}}^{\alpha}}},$$

and for strain β, $F_{\text{A}}^{\beta} = 1 - F_{\text{A}}^{\alpha}$. Note that the final composition doesn't change, $F_{\text{A}}^{\alpha} = f^{\alpha}$, only if the following conditions hold simultaneously: the growth rates are the same, the motility ratio is

the same and the ratio of chemotactic indices are the same. If any of the three quantities deviate, the resulting composition will be different.

Calculation of uncertainty

The expressions for the chemotactic index, motility index and community composition are deterministic relations. But there is a measurement of uncertainty, which can propagate into these expressions. The fundamental quantity that is measured in the ISCA is the encounter kernel $\Gamma = N/(Tc)$, where N is the number of bacteria in a given well, T is the time of the experiment and c is the bulk concentration. Therefore, we assume that different experimental replicas are independent measurements of Γ. Assuming that the kernel Γ follows gamma distribution (rather than normal, to avoid negative values), we estimate its mean and variance using sample mean and sample variance from the replicas. Assuming further that the measurements of different Γ' s are independent from each other, we then run Monte Carlo simulations to measure the uncertainty in $IC, M^{\alpha\beta}$ and F_{A}^{α}, which all depend on the ratio of appropriate kernels.

CHAPTER 5

SUMMARY

Novel fitness and chemotaxis assays were used to determine the ecological factors driving assembly of diverse bacterial communities in ecological hotspots in the surface ocean. In chapter 2, direct fitness measures of 86% of the 4,293 total coding regions within the *R. pomeroyi* genome revealed how activity and growth of a focal bacterium were affected by community members in a model ocean hot-spot. Labile organic matter released by the diatom available for bacterial heterotrophy was partitioned by the ability of *R. pomeroyi* to compete for communal substrates and its capacity to utilize those less commonplace. The latter has been proposed to lay the groundwork for evolution of mutualistic relationships between marine phytoplankton and bacterial lineages (1). In addition to competition, we observed bacteria exchange metabolites in a process known as crossfeeding (2). *R. pomeroyi* fitness benefitted from amino acids, purines, pyrimidines, and cofactors available in the multispecies communities in concentrations sufficient to rescue auxotrophs. The importance of metabolites produced by species sharing the phycosphere, regardless of the mechanism of release, was underscored by 1.7-fold higher fitness gains among mutants disrupted in anabolic genes relative to disrupted catabolic genes or transporters. Yet, sharing the phycosphere with other species indicated an overall growth cost to life as the *R. pomeroyi* mutant pool achieved 30% fewer generations.

Finally, mutants with disruptions in genes that respond directly or indirectly to environmental conditions external to the cell with fitness altered by the presence of other bacteria highlighted the power of this assay. Changes in fitness of respiratory enzymes suggest that daily

dynamics in oxygen availability occur within phycospheres. Ephemeral oxygen depletion has been reported for photosynthetically active environments (3, 4). Ability to adjust to dynamic oxygen fluctuations is likely a key trait for bacteria associated with marine phytoplankton (5, 6), in agreement with fitness outcomes observed for *R. pomeroyi* mutants. By provisioning our model system with exometabolites from cocultures diatom cells, we achieved an environment with high fidelity to a phycosphere hot-spot in terms of substrate supply rate and composition and microbial density. The importance of interactions among bacteria that share the phycosphere was underscored by the >200 *R. pomeroyi* genes with measurable fitness effects in multispecies communities.

In chapter 3 we established 15 model phycosphere communities with varied bacterial taxonomic composition and richness reliant on photosynthate released by the cocultured diatom. The final cell abundance of the total community did not change with species richness, likely reflecting a limitation by the available diatom exudates. However, as richness increased, the total abundance of *R. pomeroyi* cells realized in these communities decreased, suggesting that it became increasingly difficult for *R. pomeroyi* to obtain phytoplankton derived substrates due to either additional resource competitors or antagonism from cocultured bacteria. Epistasis was calculated using mutants with significant fitness phenotypes between complex communities relative to component parts. Coalescence of phycosphere communities of low richness results in the non-additivity of fitness outcomes, suggesting resource acquisition is an emergent property arising from higher-order interactions between community members. Further increased richness of the communities led to additive mutant phenotypes, implying that effects on the function of *R. pomeroyi* genes are largely maintained. Underlying this finding is the alteration of competitive interactions every complexity level in the coalescent communities.

In chapter 4, we used chemotaxis and growth assays to assess how metabolites shape the composition of motile bacterial communities. All ecological roles (signal, substrate, both, or none) were identified within the set of test compounds and differed among the bacteria tested. Gammaproteobacteria were able to chemotax to or grow in 38% of metabolite tests, while Alphaproteobacteria were able to chemotax to and grow in 26% of metabolite tests. These data strongly highlight the unique roles phytoplankton-derived metabolites have for individual bacteria in the surface ocean microbiome. Artificial community-based competition experiments revealed that bacteria can alter the chemotactic response of competitors by enhancing or reducing the abundance of cells that arrive at a nutrient patch. Furthermore, growth after chemotaxis can alter the community composition through competition for a single resource. Yet, for most communities, the null model of chemotaxis and grow was able to predict 63% of observed changes in community composition demonstrating that when interactions are weak or nonexistent, knowledge of the initial community composition, and the chemotactic index, relative motility, and growth rate of individual strains can inform dynamics of community assembly. This study provides valuable insights into the multifaceted roles that phytoplankton metabolites can play in bacterial community assembly in the surface ocean.

References

1. H. Luo, M. A. Moran, How do divergent ecological strategies emerge among marine bacterioplankton lineages? *Trends in Microbiology* **23**, 577-584 (2015).
2. G. D'Souza *et al.*, Ecology and evolution of metabolic cross-feeding interactions in bacteria. *Natural Product Reports* **35**, 455-488 (2018).

3. I. Klawonn, S. Bonaglia, V. Brüchert, H. Ploug, Aerobic and anaerobic nitrogen transformation processes in N2-fixing cyanobacterial aggregates. *The ISME Journal* **9**, 1456-1466 (2015).

4. A. L. Alldredge, Y. Cohen, Can microscale chemical patches persist in the sea? Microelectrode study of marine snow, fecal pellets. *Science* **235**, 689-691 (1987).

5. I. Wagner-Döbler, H. Biebl, Environmental biology of the marine Roseobacter lineage. *Annual Reviews of Microbiology* **60**, 255-280 (2006).

6. R. J. Newton *et al.*, Genome characteristics of a generalist marine bacterial lineage. *The ISME Journal* **4**, 784-798 (2010).

APPENDIX A

CHAPTER 2 SUPPLEMENTAL MATERIAL [1]

[1] Supporting Material for: Schreier, JE, Smith, CB, Ioerger, TR, Moran, MA. 2023. *Proceedings of the National Academy of Sciences.* e2217200120. Reprinted here with permission of the publisher.

Dataset S2.1. Mutants with significant fitness differences identified from randomization tests, grouped according to function, metabolism, and direction of fitness differences. Available at: https://doi.org/10.5281/zenodo.8075804

Dataset S2.2. Normalized transposon insertions reads that are curated to the central 90% of coding regions. Available at: https://doi.org/10.5281/zenodo.8075804

Dataset S2.3. Mean relative fitness (W) of mutants from four biological replicates. P-values were calculated for 10000 permutations of randomization tests, and were adjusted using a Benjamini-Hochberg correction for multiple comparisons. Available at: https://doi.org/10.5281/zenodo.8075804

APPENDIX B

CHAPTER 3 SUPPLEMENTAL MATERIAL [1]

[1] Supporting Material for: Schreier, JE, Brown, SE, Uchimiya, M, Schroer, WF, Smith, CB, Moran, MA. To be submitted to *FEMS Microbiology Ecology*.

Dataset S3.1. Mean relative fitness of mutants in each phycosphere community. Available at: https://doi.org/10.5281/zenodo.8147725

Dataset S3.2. Mutants with significant fitness differences identified from randomization tests grouped according to function and metabolism. Available at: https://doi.org/10.5281/zenodo.8147725

Dataset S3.3. Normalized transposon insertion reads that are curated to the central 90% of coding regions. Available at: https://doi.org/10.5281/zenodo.8147725

APPENDIX C

CHAPTER 4 SUPPLEMENTAL MATERIAL [1]

[1] Supporting Material for: Schreier, JE, Clerc, EE, Słomka, J, Smith, CB, Fu, H, Raina, JB, Moran, MA, Stocker, R. To be submitted to *The ISME Journal*.

Dataset S4.1. Database of well annotated or experimentally verified transport and catabolic enzymes of Alphaproteobacteria and Gammaproteobacteria. Available at: https://doi.org/10.5281/zenodo.8148185

Dataset S4.2. Homology of bacterial strain proteins to the transport and catabolic enzyme database. Available at: https://doi.org/10.5281/zenodo.8148185

Dataset S4.3. Comparison of protein homology results to observed growth and chemotactic abilities of the bacterial strains. Available at: https://doi.org/10.5281/zenodo.8148185

Dataset S4.4. Percent deviation between predicted and observed community composition. Available at: https://doi.org/10.5281/zenodo.8148185